MnO_2 AND MnO_2/TiO_2 MEDIATED, PERSULPHATE ENHANCED PHOTOCATALYSIS FOR THE REMOVAL OF INDIGO CARMINE FROM WATER

K. P. Vidya Lekshmi,[a] Suguna Yesodharan[a] and E. P. Yesodharan[a]*

Keywords: anion effect; Indigo carmine dye; manganese dioxide; photocatalysis; titanium dioxide; persulphate.

Heterogeneous photocatalysis using UV/VIS light or natural solar radiation as the energy source is one of the most efficient advanced oxidation processes (AOP) for the removal of chemical and bacterial pollutants from water. One of the least investigated oxides in this context, i.e. MnO_2 and its combination MnO_2/TiO_2 are examined as potential photocatalysts for the removal of Indigo carmine (IC) dye pollutant from the water. The catalysts are characterized by XRD, FTIR, SEM, TEM, adsorption and surface area measurements. While MnO_2 is very efficient for the decolorization of the dye, it is not effective enough for mineralization. MnO_2 /TiO_2 as the photocatalyst at the optimized ratio of 9:1 combines the advantages of both the oxides, i.e., rapid decolorization and efficient mineralization. Persulphate ($S_2O_8^{2-}$) enhances the degradation while H_2O_2 inhibits the same. The degradation is dependent on pH with higher degradation under extremely acidic conditions. The influence of dissolved salts/anions in the water on the degradation varies from 'moderate inhibition' to 'no effect' or even 'enhancement' depending on the chemistry of the anion and reaction conditions. Effect of various parameters such as reaction time, substrate concentration, catalyst dosage, the presence of O_2, recycling of the catalyst, etc. on the efficiency of degradation is investigated. The results are critically analyzed, and a tentative mechanism is proposed.

*Corresponding author
Tel: +91 9847193695, +91 484 2604889
e-mail: epyesodharan@gmail.com
[a] School of Environmental Studies, Cochin University of Science and Technology, Kochi 682022, India.

Introduction

Heterogeneous photocatalysis mediated by semiconductor (SC) oxides is an efficient advanced oxidation process (AOP) for the decontamination of water from chemical and bacterial pollutants.[1-5] When the SC oxide is irradiated with a light energy source (UV or visible) such that hν > Eg (band gap of the SC), electron-hole pairs are created. The electrons get excited from the valence band to the conduction band leaving positively charged holes in the valence band. These holes and electrons can participate in oxidative and reductive reactions respectively. In aqueous suspensions, highly reactive OH radicals are generated, and they can promote the oxidation and eventual mineralization of the pollutant to CO_2, water, and inorganic salts.

The most widely investigated SC oxides in this respect are ZnO and TiO_2 in view of their favorable physicochemical properties, low cost, easy availability, high stability and low toxicity. The band gaps of ZnO (~3.2 eV) and TiO_2 (anatase E_{bg} = ~ 3.2 eV, rutile E_{bg} = ~3.0 eV) are fairly similar. Hence they can absorb light only below 400 nm, which is in the UV range that constitutes only <5 % of the sunlight. ZnO is relatively more active in the visible region and is hence preferred in the investigations aimed at the harnessing of solar energy.[6-9] However, it has the disadvantage of corrosion under extreme acidic and alkaline conditions as well as photocorrosion making the scope of its commercial application limited.

A number of studies have been reported on the modification of semiconductor oxides in order to extend the absorption of light to the visible range. These include dye sensitization, semiconductor coupling, impurity doping, use of coordination metal complexes and metal deposition.[4,10-14] Composites such as TiO_2/carbon have also been reported.[15] Physical modification of TiO_2 with small amounts of transition metal cations such as vanadium and chromium extends the absorption up to 550 nm and makes it active under UV as well as sunlight.[16] Deposition of noble metals such as Pt, Pd, Au, Ag etc. on TiO_2 enhances the catalytic oxidation of organic pollutants due to the increased light absorption and retardation of the recombination of photogenerated electrons and holes.[17-19]

MnO_2 is one of the least investigated SC oxides in photocatalysis in spite of its excellent semiconductivity, porosity, and mixed-valent properties. The combination of MnO_2 with TiO_2 may offer advantages of the high adsorption and reactivity of the former and photochemical property of the latter. Considering these, the application of MnO_2 and MnO_2/TiO_2 as photocatalysts for the removal of recalcitrant toxic materials is examined here. One of the widely used special application dyes Indigo Carmine (IC) is selected as the test candidate.

Indigo carmine (3,3'-dioxo-1,3,1',3'-tetrahydro-[2,2']-bi-indolylidene-5,5'-disulphonic acid disodium salt) is an important dye used for dying of clothes and also for medical diagnostic purposes. It can also help to target biopsies even better since the homogeneously stained or unstained areas can be correlated with intraepithelial neoplasia.[20] IC is highly toxic and potentially carcinogenic.[21] Extensive application of the dye leads to environmental contamination, in particular, water pollution.

The chemical structure of IC is given in Figure 1.

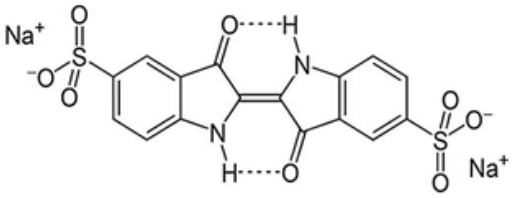

Figure 1. Chemical structure of Indigo carmine

Only a few investigations aimed at the removal IC from water have been reported.[22-26] To the best of our knowledge, the current study is the first instance of the application of MnO_2 mediated photocatalysis for the degradation/mineralization of IC from the water. The efficacy of the technique is evaluated under various reaction conditions, and the optimum parameters are identified.

Experimental

Materials

MnO_2 used in the study was supplied by Merck India Limited. The particles were approximately spherical and nonporous with > 99 % purity. The BET surface area was ~31m^2/g. The pore volume was ~ 0.05 cm^3 g^{-1}, and the average pore width was 74.2 Å. Degussa P-25 TiO_2 (> 99 % pure, average particle size ~ 15-20 µm, BET surface area ~15 m^2 g^{-1}) consisting of ~80 % anatase and ~20 % rutile was used as such without further purification.

Persulphate (PS) (purity ~99 %) and H_2O_2 (30.0 % w/v), both from Qualigen (India) and Indigo Carmine (Extra Pure Grade > 99.5 % purity) from Sisco Research Laboratories Pvt. Ltd (India) were used as such without further purification. Doubly distilled water was used in all the experiments. All other chemicals were of AnalaR Grade or equivalent.

Characterization of the catalyst

X-ray diffraction measurements were made by using Rigaku X-ray diffractometer with CuK_α radiation. Scanning Electron Microscopy (SEM) measurements were performed with JEOL Model JSM-6390LV. Diffuse Reflectance Spectra (DRS) were recorded with Varian Cary 5000 using $BaSO_4$ as the reference. Transmission electron microscopy (TEM) was done using JOEL/JEM/200; source LaB_6. FTIR spectra were recorded using Nicolet Avatar 370 instrument equipped with triglycine sulfate detector with a KBr window and a KBr beam splitter. The equipment was purged with dry air to prevent interference from atmospheric moisture. The transmission spectrum was obtained with a resolution of 4 cm^{-1} by using 32 scans in the range 400 – 4000 cm^{-1}. The powdered samples were diluted with finely ground KBr to about 5 % by weight.

Photocatalytic experiments

Photocatalytic experiments in the presence of UV were performed in a jacketed Pyrex reactor. The dye solution together with weighed amount of the catalyst and other additives as required was taken in the inner compartment and cooling water from a thermostat (27±1 ^{0}C) was circulated through the outer jacket. UV irradiation was done using a 400 W medium pressure mercury vapor lamp. The suspension was frequently stirred to ensure uniform mixing. Samples were drawn periodically, centrifuged and analyzed for the dye concentration by Spectrophotometry (608 nm). Suspension kept under identical conditions in the dark was used as the reference in each case to eliminate the contribution from adsorption towards the reduction in the dye concentration. H_2O_2 was determined by standard iodometry. Chemical oxygen demand (COD) measurements were made by the open reflux method.[27] Adsorption studies were made by the standard technique.[28]

Detection of hydroxyl radicals

The formation of ·OH radicals during the UV irradiation of the reaction system was tested by the photoluminescence (PL) technique using terephthalic acid (TPA) as the probe molecule.[29,30]

The hydroxyl radicals formed in situ in the system reacts with TPA to form the 2-hydroxyterephthalic acid (HTPA), which is a fluorescent molecule. The intensity of its PL is proportional to the concentration of in situ formed ·OH radicals in the system. MnO_2 at the standard experimental concentrations is suspended in an aqueous solution of TPA (2 x 10^{-4} M) and NaOH (2x10^{-3} M) and irradiated by UV light. The PL spectrum of the product HTPA is recorded in the range of 400 - 450 nm after every 5 minutes of irradiation. The excitation wavelength was 315 nm. The PL intensity at 425 nm corresponds to the concentration of HTPA and hence of the ·OH radicals formed in the system. Shimadzu model RF-5301PC fluorescence spectrophotometer is used for recording the spectrum.

Results and Discussions

Characterization of MnO_2

The catalysts MnO_2 and TiO_2 were characterized by XRD, SEM, TEM, Fourier transform infrared (FTIR) spectroscopy and DRS. Typical results with respect to MnO_2 are given in Figures 2 A, B, C, D and E. The characteristics of TiO_2 are same as those reported earlier.[31]

The XRD results show that the MnO_2 is amorphous in nature with weak diffraction pattern (Figure 2A). The morphology and particle size analysis were done using SEM (Figure. 2B). Particles were approximately rod-shaped with average particle size in the range of 220 nm. The characteristics of the particles are appropriate for efficient photocatalytic properties such as light absorption, diffusion as well as regeneration of the catalyst by suitable treatment.

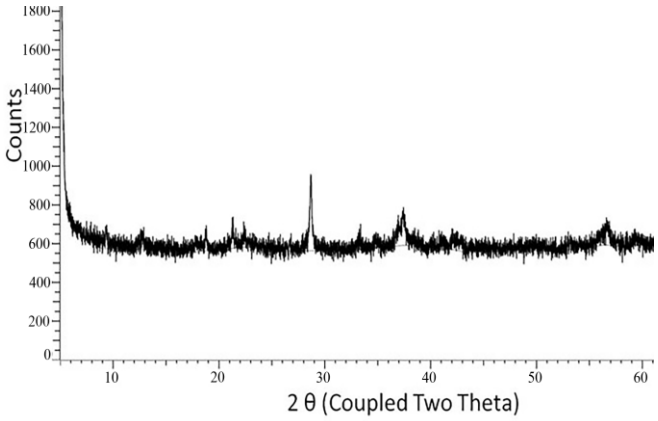

Figure 2A. XRD image of MnO_2.

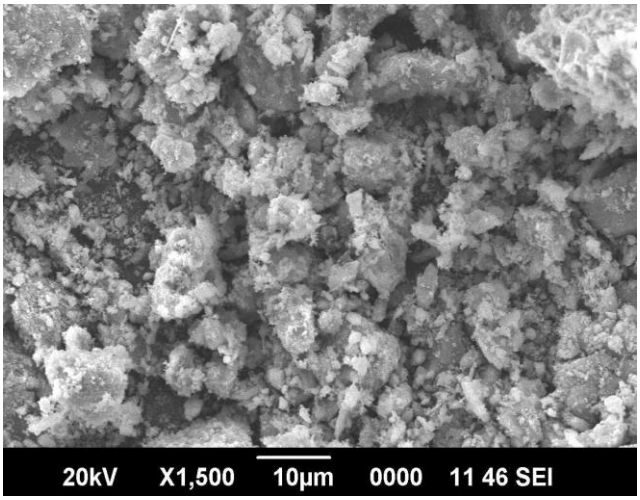

Figure 2B. SEM image of MnO_2.

The morphology and particle size are further confirmed by TEM analysis (Figure 2C) which shows platelet and rod-like structure. The FTIR pattern (Figure 2D) shows very week absorption intensity of OH (3100-3600 cm^{-1}) or H_2O (1600 and 3600 cm^{-1}). The general spectral pattern shows that MnO_2 is pure with no contamination from any of the precursors.

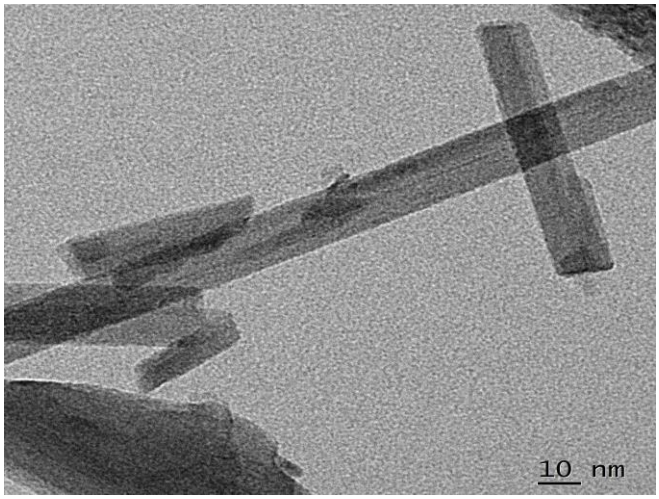

Figure 2C. TEM image of MnO_2.

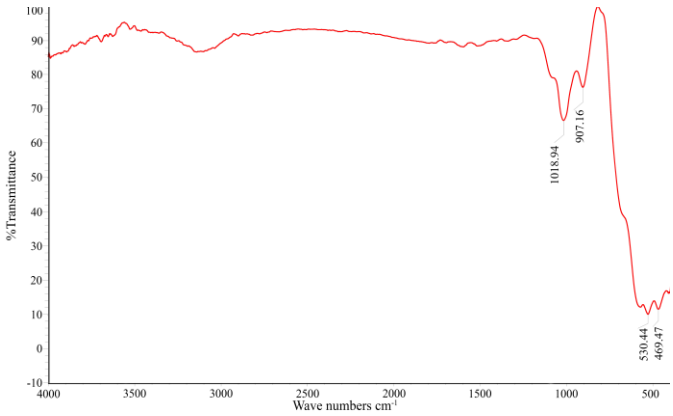

Figure 2D. FTIR spectrum of MnO_2.

Diffuse reflectance spectrum (Figure 2E) shows a sharp reflectance band between 200 and 300nm indicating that the material absorbs in the UV range. The optical absorption intensity of MnO_2 steadily increases from 300 to 800 nm with no clear band edge. This indicates that MnO_2 is not a typical semiconductor like TiO_2 or ZnO. The brown color of MnO_2 also indicates favorable absorption of visible light.[32]

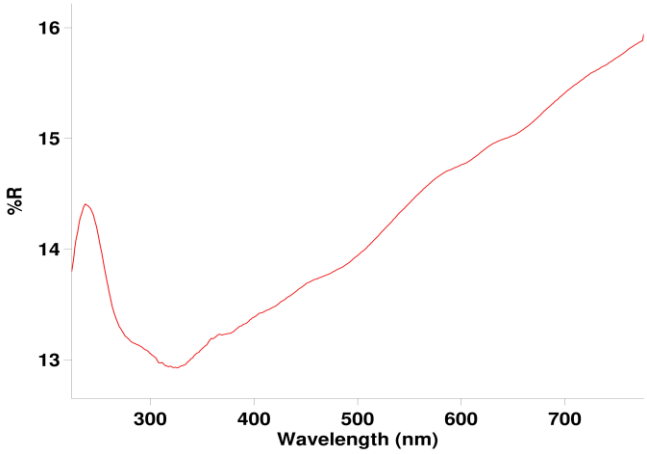

Figure 2E. DRS of MnO_2.

Photocatalytic degradation of IC on MnO_2

Photocatalytic degradation of IC in the presence of MnO_2 and UV irradiation is tested, and relevant parameters are optimized. MnO_2 is a good adsorbent of IC, and hence there is a significant decrease in the concentration of the dye initially even without irradiation. However, once the optimum adsorption under the experimental conditions is reached, no further decrease is noticed. When the suspension is exposed to UV irradiation, the concentration of IC decreases rapidly leading to eventual decolorization. In the absence of the catalyst also, moderate decolorization/degradation of the dye takes place on exposure to UV light. Preliminary results are plotted in Figure 3.

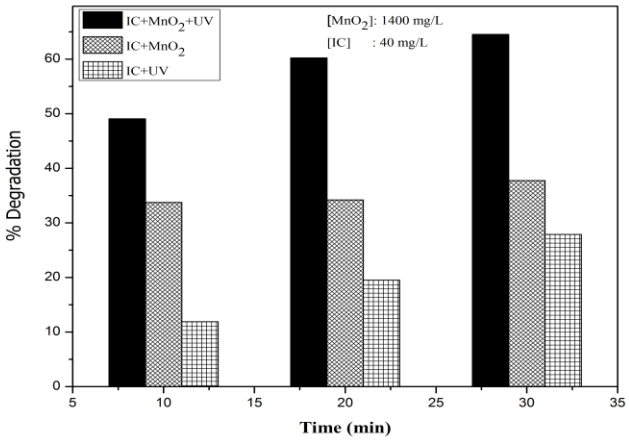

Figure 3. Photocatalytic degradation of IC in the presence of MnO2.

Effect of catalyst dosage

The effect of MnO_2 loading on the photocatalytic degradation of IC is tested by varying the dosage of MnO2, keeping other parameters constant. The results are plotted in Figure 4 which shows that the degradation of the dye increases with increase in catalyst dosage and stabilizes at 0.14 g in 100 mL under the reaction conditions.

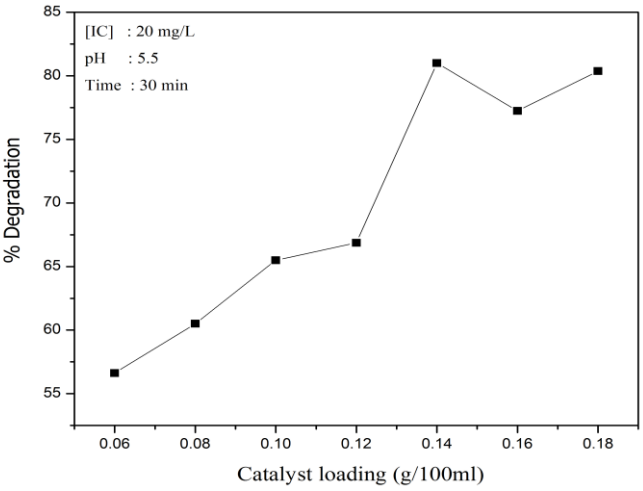

Figure 4. Effect of MnO2 dosage on the photocatalytic degradation of IC.

The enhanced degradation at higher catalyst loadings can be attributed to the increased number of adsorption and interaction sites for the IC and/or the intermediates and more effective harvesting of light. This leads to increased formation of reactive hydroxyl and other radicals which are known to be responsible for the photocatalytic degradation of organic pollutants. Any increase in catalyst concentration beyond the optimum will only result in scattering and reduced passage of light through the suspension medium. Another reason may be the aggregation of catalyst particles causing a decrease in the number of available active surface sites. Beyond a particular loading, the catalyst particles cannot be fully and effectively suspended in a particular reactor which also leads to suboptimal penetration of light and reduced adsorption of the substrate on the surface. It is also possible that at higher loading, part of the originally activated MnO_2 is deactivated through collision with ground state catalyst according to the following equation.[33]:

$$MO^* + MO \longrightarrow MO^{\#} + MO \qquad (1)$$

where MO represents MnO_2, MO* and $MO^{\#}$ are its activated and deactivated forms, respectively).

In the case of MnO_2 which is a good adsorber/absorber and reservoir for O_2, higher dosage provides more photogenerated reactive oxygen species (ROS) such as ·OH radicals. The formation of ·OH radicals in MnO_2/IC/UV is confirmed by PL spectral studies. The increase in fluorescence with irradiation time (Figure 5) corresponds to the progressive formation of ·OH radicals (See experimental section).

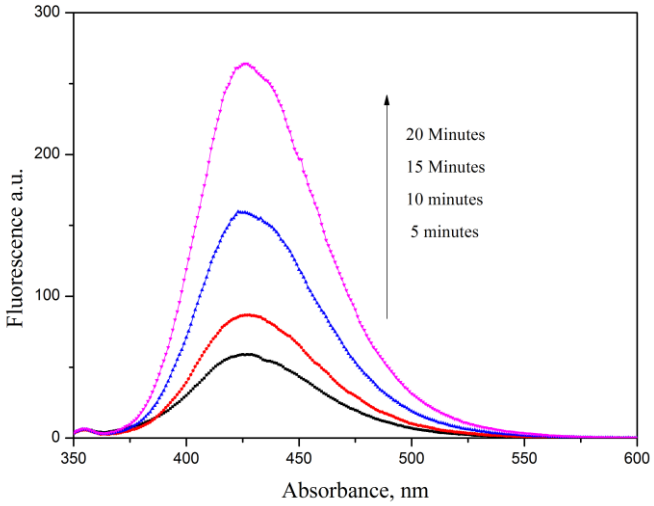

Figure 5. PL spectral changes during UV irradiation of MnO_2/terephthalic acid/NaOH.

Cao and Suib[32] suggested from binding energy calculations that MnO_2 is a mixed-valent system consisting of Mn(4+) and Mn(3+). The multiple oxidation states enable it to function as good electron donor/acceptor and hence oxidation-reduction catalyst.[34] This property favors increased photocatalytic activity with an increase in catalyst dosage. This also helps the facile regeneration of the used catalyst by replenishing the depleted oxygen. Surface and lattice oxygen species in MnO_2 are known to take part in the catalytic oxidation process. Photolysis of MnO_2 is reported to result in a five-fold increase in the surface oxygen, either by migration of oxygen to the surface or by migration of Mn to the bulk or both.[32] During the photocatalytic reaction, surface oxygen is consumed, and bulk oxygen moves to the surface. Hence, the more the catalyst dosage, the more the availability of reactive oxygen and consequently better the degradation. This can continue until other reaction parameters, as well as the size, shape, and geometry of the reactor assembly, are appropriate to facilitate the degradation process. Hence, for each reactor configuration, the optimization of catalyst dosage has to be made separately. In the present case, the optimum loading of

MnO_2 is 0.14 g in 100 mL. Hence all further studies were carried out with this loading.

Effect of concentration of IC

The effect of initial concentration of IC in the range of 10-60 mg/L in the water on its photocatalytic degradation is investigated. The percentage degradation decreases as the concentration of IC increases. In contrast, the rate of removal increases steadily and steeply with an increase in the initial concentration of IC up to 40 mg L^{-1} and stabilizes after that (Figure 6). The optimum kinetic rate of 1.9 mg L^{-1} min^{-1} is reached at 40 mg L^{-1} of IC. This is followed by a slight decrease and eventual stabilization of the rate implying gradually decreasing and eventual zero order kinetics at higher concentration of >40 mg L^{-1}.

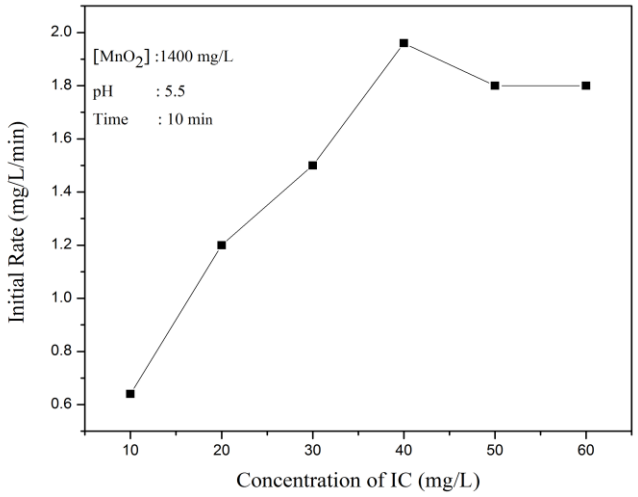

Figure 6. Effect of concentration of IC on the rate of photocatalytic degradation.

The photocatalytic degradation of many organic pollutants in water is reported to follow pseudo first order kinetics.[35-37] The increase in degradation with an increase in concentration up to 40 mg L^{-1}may is due to increase in adsorption of IC on MnO_2 which will continue until the surface is fully covered and all the active sites are occupied. Further, at higher concentration, there will be more IC molecules available in bulk as well as in the proximity of the surface which can also interact with the surface-generated active free radicals and ROS such as ·OH and H_2O_2. At higher concentration beyond the optimum, at least a part of the irradiating UV light may be blocked and/or absorbed by IC and the intermediates formed from it thereby reducing the photons available for catalyst activation. Another reason may be retardation in the penetration of light at a longer distance from the light source and consequent decrease in its path length. This results in decreased availability of photons per IC molecule in the system and hence decreased degradation.[38] As the initial concentration of IC increases, the requirement of catalyst surface needed for maintaining the corresponding rate of degradation also increases. Since illumination intensity and catalyst concentration are maintained constant, the relative number of ROS available per IC molecule is also presumably decreasing with increase in the concentration of IC.

This also leads to stabilized/ decreased rate of degradation. Once the concentration of the substrate is enough to interact with all the optimum available ROS and/or other reactive free radicals, any further increase cannot result in increased reaction, and the IC removal becomes independent of concentration. It is also possible that at higher substrate concentration, some of the reaction intermediates may get adsorbed onto the surface or remain in bulk for the relatively longer period leading to the less frequent interaction between fresh IC molecules and the ROS. At any point in time during the irradiation, there will be an optimum for the number of substrate molecules that can interact with the reactive free radicals generated in the system. This optimum will depend on some reaction parameters such as initial concentration of the substrate, pH, intensity of illumination, the wavelength of light, mass and type of photocatalyst, type and geometry of photoreactor, the presence of other contaminants, etc. Consequently, the optimization will apply only to the specific reaction conditions and cannot be generalized.

Since both catalyst and light are essential for the degradation, the negative effect of increasing concentration of IC on the rate of degradation implies that at higher concentration, the dye is inhibiting the action of the catalyst and/or light. At higher concentration, there will be better adsorption of the dye on the surface of the catalyst. This will prevent direct absorption of light by the catalyst thereby inhibiting the generation of reactive free radicals and ROS. In the absence of steady and significant degradation, the adsorbed dye will not leave the surface sites. This will prevent the adsorption of fresh dye molecules and continued degradation.

The simplest way to represent the rate of photocatalytic degradation is the Langmuir-Hinshelwood model, modified to accommodate reactions taking place at the solid-liquid interface. Accordingly, the rate of degradation is:

$$r_0 = \frac{-dC}{dt} = \frac{kKC_0}{1+KC_0} \qquad (2)$$

where

r_0 is the rate of disappearance of IC (mg L^{-1} min^{-1}),

C_0 (mg L^{-1}) is the initial concentration of the dye,

C is the concentration at time t,

K is the equilibrium adsorption coefficient (mgL^{-1}) and

k is the reaction rate constant (min^{-1}) at maximum surface coverage.

Equation 2 can be integrated and presented as

$$t = \frac{1}{kK}\ln\frac{C_0}{C} + \frac{1}{k}(C_0 - C) \qquad (3)$$

when C_0 is very small, (C_0-C) is negligible and equation (3) becomes

$$\ln \frac{C_0}{C} = kKt = k't \quad (4)$$

In the present study, the logarithmic plot of ln(C_0/C) vs. time t did not give straight lines that pass through the origin. This shows that the degradation of IC in the presence of MnO_2 does not follow the expected pseudo first order kinetics as in the case of most photocatalytic processes. The Langmuir-Hinshelwood model and the pseudo-first order kinetics underline the key role of adsorption on the rate of reaction assuming that the adsorption-desorption kinetics is faster than the photochemical reaction.[39,40] The rate of unimolecular surface reaction is proportional to the surface coverage, assuming that the reactant is more strongly adsorbed than the products on the catalyst particles.[41]

Adsorption studies of IC on MnO_2 under the reaction conditions showed that~32 % of the dye is adsorbed at the equilibrated stage. When K is large, the first term of equation (3) is negligible. i.e.

$$C_0 - C = kt \quad (5)$$

The concentration of the dye decreases with time until the optimum surface coverage is attained.

The pseudo first order kinetics, as in the case of typical semiconductor oxide photocatalysts such as ZnO (adsorption: ~11 %) and TiO_2 (adsorption: ~8 %), is not followed in the case of MnO_2 with high adsorption (~32 %). Hence it may be inferred that the degree of adsorption of the substrate on the catalyst does influence the degradation kinetics. This further indicates that the general assumptions implicit in the application of LH mechanism and related kinetic analysis are not fully applicable in the case of MnO_2 mediated photocatalysis. These assumptions are:[42]

i) The reaction of adsorbed species is the rate-determining step

ii) Fractional surface coverage (θ_A) of the reactant species is the more appropriate concentration parameter to be applied in rate laws,

iii) $\theta_A \rightarrow 1$ for saturation coverage corresponding to a monolayer of adsorbate on the surface and

iv) Langmuir adsorption isotherm type equation represents the relationship between θ_A and the activity. In the case of highly adsorbing particles such as MnO_2, there will be competition between the solvent (water) and the solute (IC) molecules for adsorption sites which can complicate the kinetics of adsorption as well as degradation.

Effect of pH

The pH of the reaction medium is known to influence the surface characteristics and adsorptive properties and consequently the photocatalytic behavior of semiconductor oxides. The effect of pH on the photodegradation of IC in the presence of MnO_2 is investigated, and the results are given in Figure 7. Maximum degradation (~97 % in 10 min) is observed at pH 2. However, under this condition, the decolorization is very facile even without UV irradiation.

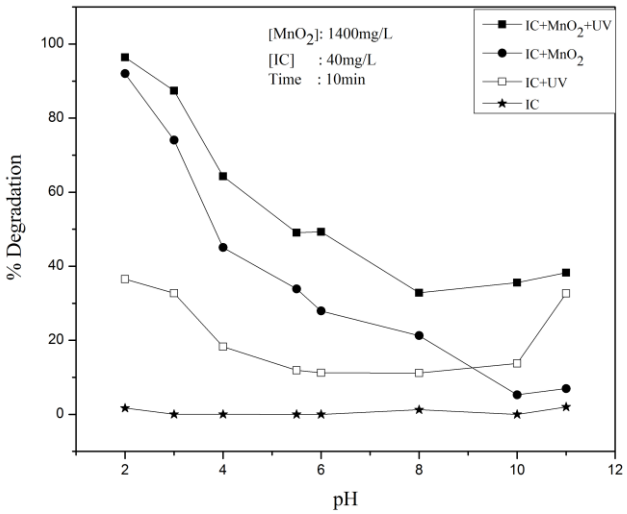

Figure 7. Effect of pH on the photocatalytic degradation of IC over MnO_2

The pH has only negligible effect on the decolorization of the dye as such (in the absence of UV and MnO_2). However, under UV, even the dye alone undergoes reasonable decolorization at various pH, the maximum being at pH 2. The degradation decreases steadily with the increase in pH up to pH 10 and increases slightly after that. The fast decolorization in the presence of MnO_2 under acidic pH, even in the absence of UV irradiation, shows that simple adsorption of IC on MnO_2 also is facilitated at acidic pH.

Similar pH effect on the adsorption of IC on TiO_2 catalyst has been reported by Barka et al.[43] pH is known to influence the surface state of the catalyst and ionization state of the dye. The point of zero charges (PZC) of MnO_2 is ~ 4.7.[26,44,45] Below this pH the surface is positively charged, and hence its oxidizing ability will be relatively higher. IC is a dianionic dye in aqueous solution, and this configuration is maintained in the pH range 3-11.[24,45] Below the PZC of MnO_2, the electrostatic interaction between the positive catalyst surface and the dianions can lead to strong interaction between them and subsequent degradation of the dye. At higher pH when the surface is negatively charged, the adsorption is less due to the electrostatic repulsion between the negatively charged surface and the dye. It is also possible that the heterogeneous degradation in the presence of MnO_2 involves the formation of precursor complex between the dye and surface bound Mn.[46] Electrons from the activated dye move to the Mn(IV) on the surface of MnO_2. Consequently, the dye undergoes oxidative degradation. The Mn(II) thus formed reductively from MnO_2 dissolves in the bulk solution. Thus MnO_2 functions both as a catalyst as well as an oxidant. The Mn(II) is oxidized to Mn(IV) oxide again by the dissolved O_2. In this respect, MnO_2 plays the role of a catalyst and dissolved O_2 acts as the oxidant. The re-adsorption of free Mn(II) ions in solution back onto MnO_2 surface is facilitated at pH beyond the PZC. At the natural pH, ~5.5 of the reaction system, the

decolorization of IC in the presence of MnO_2/UV is 50% more efficient than simple adsorption. High degradation of IC at pH ~2 shows that it is induced by extremely acidic conditions. UV irradiation and MnO_2 accelerate the degradation. The slight increase in degradation at pH~ 11 may be due to increased number of reactive ·OH radicals formed from the higher concentration of OH^- ions.

The effect of pH on the photocatalytic efficiency of a highly adsorbing and reactive oxide such as MnO_2 may not be simple or straightforward because it depends on the complex interplay of multiple factors, i.e. chemistry of the substrate and the surface, extent, and mode of adsorption (of IC as well as the numerous intermediates), concentration and nature of interactions of reactive free radicals, etc. The adsorption of the substrates is more in the acidic range while the concentration of the ·OH radical is more in the alkaline region as explained earlier. Thus the effect of pH on these two parameters, which are important for the degradation of IC, is different and opposing. As a consequence, the combined net effect need not necessarily be the same quantitatively even at the same pH at different times. Hence precise correlation of the effect of pH on the adsorption/degradation of IC with the PZC of MnO_2 will not be fully consistent. Lack of direct correlation between the PZC and the adsorption/degradation rate can also be because the PZC itself depends on some factors including the size and nature of dispersion of the particles, chemistry of substrates and the intermediates and the type of catalyst itself.

Effect of H_2O_2

H_2O_2, which is concurrently formed in many photocatalytic processes is a powerful oxidant and has been widely investigated for its potential to enhance the mineralization of organic water pollutants. The enhancement is caused by the photocatalytic generation of extra ·OH radicals as follows:

$$H_2O_2 \rightarrow 2{\cdot}OH \qquad (6)$$

In this context, the effect of externally added H_2O_2 on the photocatalytic decolorization of IC is tested under different conditions. In the absence of MnO_2, under UV irradiation, the degradation of IC increases with increase in the concentration of H_2O_2 and reaches a plateau at 50 mg L^{-1} (Figure 8A).

The initial decrease in concentration of IC in the presence of the only MnO_2 can be attributed to simple adsorption. In the presence of MnO_2 and H_2O_2 (at 10 mg L^{-1}), initially, there is inhibition in the % decolorization of IC compared to that in the presence of MnO_2 only (Figure 8A). With the increase in the concentration of H_2O_2, the net concentration of IC in the system is stabilized. This indicates that H_2O_2 is getting competitively adsorbed on the surface of MnO_2 and replacing some of the adsorbed IC molecules. Once a steady adsorption-desorption equilibrium for both IC and H_2O_2 is reached further increase in H_2O_2 does not result in enhanced adsorption of H_2O_2 or desorption of IC.

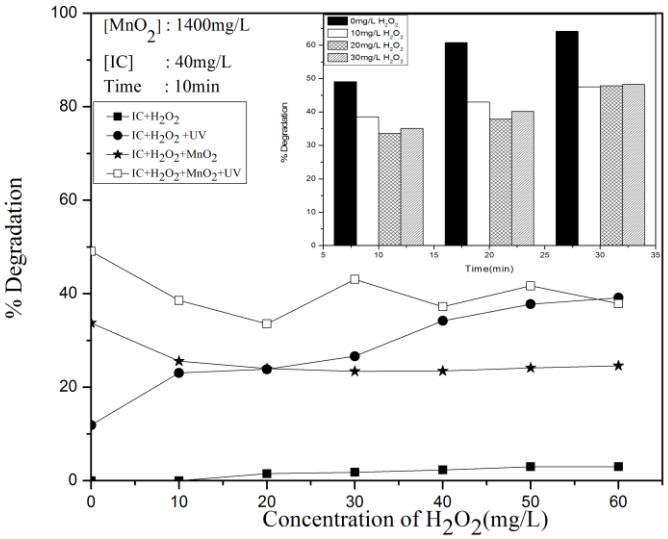

Figure 8A. Effect of added H_2O_2 on the degradation of IC (Inset: Effect of time)

In the combined presence of MnO_2 and UV irradiation, H_2O_2 inhibits the degradation initially. At the H_2O_2 concentration of ~20 mg L^{-1}, the degradation starts increasing moderately and stabilizes at ~30 mg L^{-1}. The stabilized level of degradation is almost the same as in the absence MnO_2. This shows that in the presence of H_2O_2, MnO_2 is not an effective photocatalyst for the degradation of IC. Hence MnO_2 may be simultaneously generating ·OH radicals as well as accelerating their deactivation by facilitating the interaction with H_2O_2 at the surface. The stabilization of degradation at higher concentration of H_2O_2 shows that the deactivation as well as the formation of ·OH and another ROS is more or less balanced. The stabilization is further evident from Figure 8A (inset) which shows that at later stages of the reaction when the concentration of IC becomes relatively less, the degradation remains more or less the same irrespective of the concentration of H_2O_2.

At higher concentrations of added H_2O_2 some of the reactive ·OH radicals get quenched as follows:

$$H_2O_2 + {\cdot}OH \rightarrow HO_2{\cdot} + H_2O \qquad (7)$$

Consequently, the number of ·OH radicals interacting with the substrate is less resulting in decreased degradation of IC. The quenching of the ·OH radicals (oxidation potential: 2.80 eV) results in the formation of less efficient oxidant $HO_2{\cdot}$ (1.70 eV). The decomposition of H_2O_2 into H_2O and O_2 and the recombination of $HO_2{\cdot}$ (reactions 8 and 9) are other possible reasons for the inhibition.

$$2H_2O_2 \xrightarrow{UV} 2H_2O + O_2 \qquad (8)$$

$$HO_2{\cdot} + HO_2{\cdot} \rightarrow H_2O_2 + O_2 \qquad (9)$$

Reaction 8 also results in a decrease in the UV radiation available for the catalyst which leads to decrease in the degradation of IC. Eventually, the rate of simultaneous

formation and quenching of ·OH get balanced, at least in the concentration range studied here, resulting in more or less steady degradation, i.e. no significant effect by added H_2O_2.

The initial inhibiting effect of H_2O_2 is further confirmed by addition of H_2O_2 in-between to the system in which the degradation of IC is in progress. Results are shown in Figure 8B. Every extra addition of H_2O_2 (20 min and 40 min) decreases the % degradation of IC thereby reconfirming that in the presence of MnO_2 as a catalyst, H_2O_2 functions more as an inhibitor.

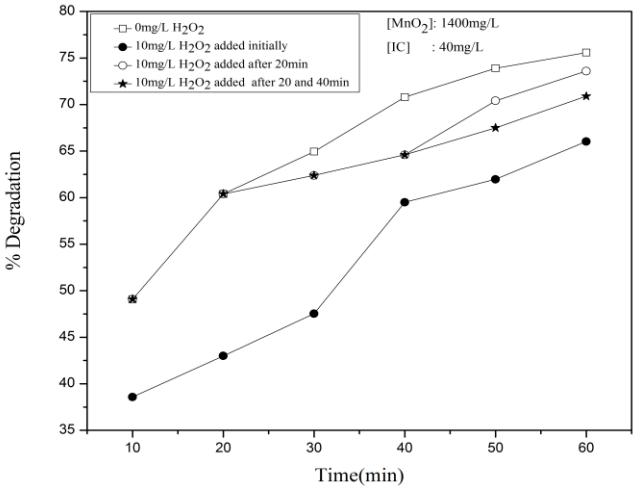

Figure 8B. Effect of in-between addition of H_2O_2 on the degradation of IC.

The effect of H_2O_2 on the adsorption of IC over MnO_2 as a possible cause of inhibition/stabilization of the degradation is tested by measuring the adsorption of the dye at various concentrations in the presence of H_2O_2. The results presented in Table 1A show that irrespective of the concentration of IC, H_2O_2 inhibits the adsorption. Similarly, experiments on the effect of increasing H_2O_2 concentration on the adsorption of IC (Table 1B), show that the adsorption decreases initially and stabilizes after that.

Table 1A. Effect of H_2O_2 on the adsorption of IC at various concentrations on MnO_2. [MnO_2]:1400 mg L^{-1}, [H_2O_2]:40 mg L^{-1}, time:30 min

[IC] mg L^{-1}	Adsorption of IC, %	
	with H_2O_2	without H_2O_2
20	23.5	40.7
30	24.4	33.5
40	22.0	33.0
50	19.5	28.9
60	17.0	27.5

Table 1B. Effect varying concentration of H_2O_2 on the adsorption of IC on MnO_2. [MnO_2]:1400 mg L^{-1}, [IC]: 40 mg L^{-1}, time: 30 min

[H_2O_2] mg L^{-1}	Adsorption of IC, %
0	33.0
10	25.5
20	24.0
30	23.5
40	22.0
50	24.2
60	24.5

Hence it is possible that in the presence of added and/or in situ formed H_2O_2, at least some of the surface sites on MnO_2 are utilized for their adsorption and/or decomposition, and this may be one of the reasons for the initial inhibition by H_2O_2. However, there is a limit to the number of sites that can be occupied by H_2O_2 at any point in time for a given amount of MnO_2. This may be a reason for the stabilization of the adsorption as well as degradation of IC beyond a particular concentration of H_2O_2.

The competition between H_2O_2 and IC for adsorption on the surface is further confirmed by using IC pre-adsorbed MnO_2 for H_2O_2 adsorption/ decomposition (IC: 60 mg L^{-1}, H_2O_2: 50 mg L^{-1}, MnO_2: 1800 mg L^{-1}). In this case, the decrease in the concentration of H_2O_2 is only ~60 % against ~ 90 % on fresh MnO_2.

Effect of persulphate (PS)

PS ($S_2O_8^{2-}$, E^0 = 2.1 V) is a powerful oxidant capable of mineralizing some recalcitrant pollutants under AOP conditions and is investigated as a potential enhancer of the photocatalytic degradation of IC. It has specific advantages such as high solubility and stability under ambient conditions. Further, the SO_4^{2-} ions, which are the major products of PS reduction are relatively harmless and considered to be environment-friendly. Preliminary experiments showed that PS as such does not cause any degradation of IC. However, irradiation by UV causes moderate degradation which increases with increase in the concentration of PS (Figure 9). The decolorization is ~35 % in the presence of MnO_2 in the absence of UV irradiation, which is due to simple adsorption and is practically unaffected by the presence of PS. This also shows that unlike in the case of H_2O_2, the adsorption of PS on MnO_2 is weak.

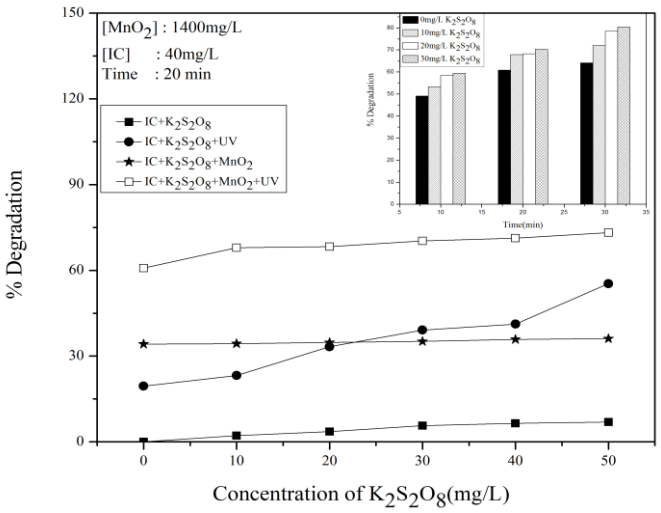

Figure 9. Effect of added $K_2S_2O_8$ on the degradation of IC (Inset: Effect of time).

PS enhances the degradation of IC moderately under MnO_2/UV in the beginning and stabilizes with an increase in the concentration of PS. The enhancement is almost ~20% with respect to the system with no added PS. The addition of PS in between to a reaction (MnO_2/IC/UV) in progress also enhances the rate of degradation of IC. Since there is no

negative effect in the presence of an excess of PS, any unused oxidant remaining in the system can be used for the treatment of fresh input of IC pollutant which is important from the angle of commercial application of the process.

The MnO_2/UV degradation of IC in the presence of the combination of H_2O_2 and PS showed that the degradation is only the average of the negative effect of H_2O_2 and the positive effect of PS. Hence this option is not pursued in detail.

PS is known to generate highly reactive $SO_4^{-\cdot}$ radical anions in situ under photocatalytic conditions. These can interact with the substrate and initiate/enhance the degradation of organics under AOPs. More $SO_4^{-\cdot}$ radicals will be formed with an increase in the concentration of PS, under UV irradiation and a series of chain reactions can follow as in equations 10-20.[47]

$$S_2O_8^{2-} \rightarrow 2SO_4^{-\cdot} \quad (10)$$

$$S_2O_8^{2-} + RH \rightarrow SO_4^{-\cdot} + HSO_4^- + R\cdot \quad (11)$$

RH: organic pollutant

$$SO_4^{-\cdot} + H_2O \rightarrow SO_4^{2-} + H^+ + \cdot OH \quad (12)$$

$$SO_4^{-\cdot} + RH \rightarrow R\cdot + HSO_4^- \quad (13)$$

$$\cdot OH + RH \rightarrow R\cdot + H_2O \quad (14)$$

$$R\cdot + \cdot OH \rightarrow \text{Intermediates} \rightarrow \text{products} \quad (15)$$

$$SO_4^{-\cdot} + R\cdot \rightarrow \text{Chain termination} \quad (16)$$

$$SO_4^{-\cdot} + \cdot OH \rightarrow \text{Chain termination} \quad (17)$$

$$2SO_4^{-\cdot} \rightarrow S_2O_8^{2-} \text{ Chain termination} \quad (18)$$

$$2 \cdot OH \rightarrow H_2O_2 \text{ Chain termination} \quad (19)$$

$$2R\cdot \rightarrow RR \text{ Chain termination/} \quad (20)$$

Various ROS such as H_2O_2, $HO_2\cdot$, $\cdot OH$ etc. and $SO_4^{-\cdot}$ formed during the irradiation interact with IC on the surface of the catalyst as well as in bulk, leading to its degradation into various intermediates and eventual mineralization. However, the degradation is not increasing with increase in the concentration of PS, after the initial enhancement. The excess of $SO_4^{-\cdot}$ radicals formed in situ at higher concentration of PS may be getting deactivated as in reactions (16) and (18). The reactive $SO_4^{-\cdot}$ radicals can also interact with PS and form less reactive $S_2O_8^{-\cdot}$ radicals as follows:

$$SO_4^{-\cdot} + S_2O_8^{2-} \rightarrow SO_4^{2-} + S_2O_8^{-\cdot} \quad (21)$$

Thus the $SO_4^{-\cdot}$ radicals which are responsible for the enhancement of the degradation of IC in the presence of PS can get deactivated by unproductive interactions. This leads to decrease/ stabilization in the rate of degradation at higher concentration of PS and with reaction time.

Effect of dissolved salts/anions

Many of the anionic contaminants which are naturally present in water inhibit the efficiency of degradation of organic pollutants under AOPs.[36,48,49] Instances of anions functioning as enhancers of the degradation of pollutants also have been reported.[50] In this context, the effect of some of the commonly occurring anions in water, i.e. SO_4^{2-}, Cl^-, PO_4^{3-}, CO_3^{2-}, HCO_3^- and NO_3^- on the efficiency of UV/MnO_2 degradation of IC is tested at various concentrations and reaction times (Figure 10A).

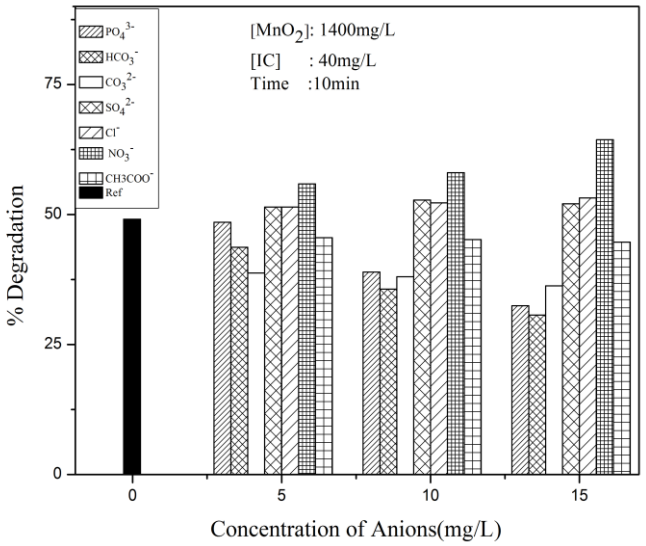

Figure 10A. Effect of concentration of anions on the photocatalytic degradation of IC.

The results showed that the anions SO_4^{2-}, Cl^- and PO_4^{3-} at lower concentrations have only negligible effect on the degradation of IC while CH_3COO^-, CO_3^{2-} and HCO_3^- inhibit the degradation at all concentrations. SO_4^{2-} and Cl^- do not influence the degradation significantly even at higher concentrations while PO_4^{3-} becomes a good inhibitor at higher concentrations. NO_3^- enhances the degradation at all concentrations.

At lower concentrations of 5 mg L^{-1}, the anion effect is less pronounced and the inhibition is in the order:

$$CO_3^{2-} \text{ (inhibition)} > HCO_3^- \text{ (inhibition)} > CH_3COO^- \text{ (inhibition)} > PO_4^{3-} \text{ (mild inhibition to no effect)} > SO_4^{2-} \text{ (no effect)} \sim Cl^- \text{ (no effect)} > NO_3^- \text{ (enhancement)} \quad (22)$$

At higher concentration of the anion (15 mg L^{-1}) where the effect is significant, the inhibition effect is in the sequence;

$$HCO_3^- \text{ (inhibition)} \geq PO_4^{3-} \text{ (inhibition)} > CO_3^{2-} \text{ (inhibition)} > CH_3COO^- \text{ (inhibition)} > SO_4^{2-} \text{ (no effect)} \sim Cl^- \text{ (no effect)} > NO_3^- \text{ (enhancement)} \quad (23)$$

The inhibiting anions become better inhibitors, and the enhancing anion becomes better enhancer with an increase in concentration. However, the comparative effect of the anions remains more or less the same irrespective of the concentration. Another parameter that can influence the effect of anions is the duration of the reaction possibly due to the increasing presence of various in-situ formed intermediates and the decreasing concentration of the substrate. The relative concentration of the ion with respect to the substrate increases progressively with time leading to more inhibition. The effect is tested at 3 different time intervals, and the results are plotted in Figure 10B.

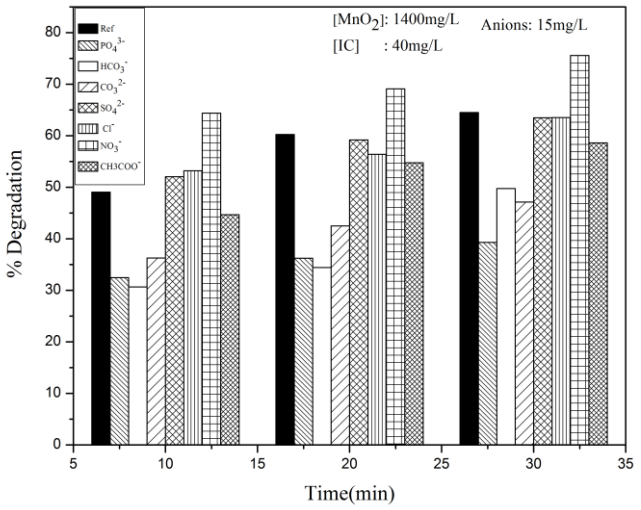

Figure 10B. Effect of reaction time on the photocatalytic degradation of IC in the presence of various anions.

The relative effect of the anions at different durations of reaction is summarized in (24) - (26).

10 min.:

HCO_3^- (inhibition) ≥ PO_4^{3-} (inhibition) > CO_3^{2-} (inhibition) > CH_3COO^- (inhibition) > SO_4^{2-} (no effect) ~ Cl^- (no effect) > NO_3^- (enhancement)

(24)

20 min.:

HCO_3^- (inhibition) ≥ PO_4^{3-} (inhibition) > CO_3^{2-} (inhibition) > CH_3COO^- (inhibition) > Cl^- (slight inhibition to no effect) ~ SO_4^{2-} (no effect) > NO_3^- (enhancement)

(25)

30 min.:

PO_4^{3-} (inhibition) > CO_3^{2-} (inhibition) ≥ HCO_3^- (inhibition) > CH_3COO^- (inhibition) > SO_4^{2-} (no effect) ~ Cl^- (no effect) > NO_3^- (enhancement)

(26)

The trend remains more or less the same irrespective of the duration of the reaction. The effect ranging from 'inhibition' to 'no effect' and 'enhancement' and the variation depending on the concentration indicate that many reaction parameters such as the characteristics of the anions, the chemistry of the substrate and the catalyst, relative concentration of different components, the nature of their interactions etc. influence the anion effect. Hence any general conclusions on the effect of anions may not be consistent.

The inhibition of the photocatalytic degradation of organics by anions/salts is often explained based on blocking of the active surface sites on the catalyst by competitive adsorption, surface layer formation and/or scavenging of reactive ·OH radicals. In this context, the adsorption of IC on MnO_2 in the presence of the anions is measured experimentally. The results are presented in Table 2.

The adsorption is the least in the presence of PO_4^{3-} followed by CO_3^{2-} and HCO_3^- while Cl^-, CH_3COO^- (Ac^-), SO_4^{2-} and NO_3^- do not influence the adsorption. The cation was kept the same in all cases, i.e., Na^+. Had competitive adsorption of the anions been the main cause, the inhibition should have been in the order:

$$PO_4^{3-} > CO_3^{2-} \geq HCO_3^- > Ac^- \sim SO_4^{2-} \geq Cl^- \sim NO_3^- \quad (27)$$

Table 2. Adsorption of IC on MnO_2 in the presence of anions. [IC] : 40 mg L^{-1}, MnO_2 : 0.14 g in 100 mL, [Anion] : 10 mg L^{-1}

Anion	Adsorption of IC, %
None	32.2
PO_4^{3-}	14.3
HCO_3^-	21.3
CO_3^{2-}	19.4
Cl^-	33.5
SO_4^{2-}	30.5
Ac^-	29.5
NO_3^-	34.7

This sequence is consistent with the experimentally observed inhibition thereby suggesting that preferential adsorption by the anion is a major cause of inhibition. The anions are also known to scavenge the ROS, especially ·OH, which also could cause the inhibition of the degradation of IC. Scavenging of the ·OH by anions would yield respective radical anion species as follows:

$$\cdot OH + HCO_3^- \rightarrow H_2O + CO_3^{\cdot -} \quad (28)$$

$$\cdot OH + CO_3^{2-} \rightarrow OH^- + CO_3^{\cdot -} \quad (29)$$

$$\cdot OH + SO_4^{2-} \rightarrow OH^- + SO_4^{\cdot -} \quad (30)$$

$$\cdot OH + NO_3^- \rightarrow OH^- + NO_3^{\cdot} \quad (31)$$

$$\cdot OH + Cl^- \rightarrow OH^- + Cl^{\cdot} \quad (32)$$

$$Cl^{\cdot} + Cl^- \rightarrow Cl_2^{\cdot -} \quad (33)$$

The radical anions are also reactive towards organic compounds, though less efficiently than ·OH.[49] Moderate degradation in the presence of the anions can also be due to the interaction of the radical anions with the substrate on the surface as well as in bulk.

The presence of anions also reduces the diffusion coefficient of the organic pollutant in the reaction medium. Consequently, the pollutant molecules will be less accessible to the reactive ·OH and this also can contribute to the inhibition. Another possible reason for the inhibition by anions is the formation of an inorganic layer on the catalyst surface. The efficiency of layer formation depends on the solubility of the salts.[51] The higher the solubility of the salt the lower will be the layer formation. The solubility of the salts (in mg/g of water at 20^0C) tested here is in the order;

$$NaNO_3\ (94.9) > CH_3COONa\ (54.6) > Na_2SO_4\ (40.8) \geq Na_2CO_3\ (39.7) > NaCl\ (36.1) > Na_3PO_4\ (16.3) > NaHCO_3\ (11.1) \quad (34)$$

Correspondingly the layer formation, if any, will be in the order:

$$HCO_3^- > PO_4^{3-} > Cl^- \geq CO_3^{2-} \geq SO_4^{2-} > Ac^- > NO_3^- \quad (35)$$

If layer formation is the major cause, the inhibition must be in the same order as in (35). The experimentally observed anion effect in the current instance is not fully consistent with equation (35). However, the trend is similar especially in the case of the maximum (HCO_3^- > PO_4^{3-}) and the minimum (NO_3^-) inhibition. Hence, the layer formation also may be contributing partially to the anion effect. However, the relative contribution of various factors towards the anion effect may vary.

The inhibitive or 'nil' effect of various anions on the photocatalytic degradation of IC in the presence of MnO_2 can be explained to a great extent by any or all of the above interpretations. However, a universally consistent explanation to account for the effect of anions in different kinds of photocatalytic systems with different catalysts, substrates and reaction conditions is not possible, and it will be more appropriate to consider individual anions to explain specific effects. In this context, two specific examples, i.e. SO_4^{2-} for 'no effect' and NO_3^- for 'enhancement' are discussed here.

The primary step in the photocatalytic process is:

$$\text{Catalyst} + h\nu \rightarrow \text{Catalyst}\ (e^-, h^+) \quad (36)$$

(Formation of electrons and holes)

$$\text{Catalyst}\ (e^-, h^+) \rightarrow \text{Catalyst} \quad (37)$$

(Recombination of electrons and holes)

In the case of SO_4^{2-} ions; they get adsorbed on the surface of the catalyst and interact with the photoproduced holes to generate sulfate radical anions as follows[52]:

$$h^+ + SO_4^{2-} \rightarrow SO_4^{\cdot-} \quad (38)$$

S is a strong oxidizing agent and hence the $SO_4^{\cdot-}$ can accelerate the degradation process according to reactions (39) and (40).

$$SO_4^{\cdot-} + \text{Pollutant} \rightarrow SO_4^{2-} + \text{Intermediate} \quad (39)$$

$$SO_4^{\cdot-} + \text{Intermediate} \rightarrow \rightarrow SO_4^{2-} + CO_2 + \text{salts} \quad (40)$$

As seen in reaction (12), the presence of $SO_4^{\cdot-}$ can lead to the formation of more reactive ·OH radicals which can accelerate the degradation of the dye. Hence, unlike in the case of other anions which scavenge the ·OH, the SO_4^{2-} anions concurrently generate them. Thus, factors leading to inhibition and enhancement of the degradation coexist in the system. Under the reaction conditions used here, they may balance, and hence the degradation is practically unaffected. It is also possible that depending on the domination of either of the effects, the net effect may be 'inhibition,' 'no effect' or 'enhancement' at any point in time during the reaction.

The enhancement in the degradation of IC in the presence of NO_3^- shows that the factors responsible for the inhibition by other anions are not significant here. Hence both the surface and bulk processes are not affected. Further, under irradiation by UV light, NO_3^- leads to the formation of reactive ·OH radicals as follows[53]:

$$NO_3^- + h\nu \rightarrow NO_2^- + O \quad (41)$$

$$NO_3^- + H_2O + h\nu \rightarrow NO_2^- + OH^- + \cdot OH \quad (42)$$

$$O + H_2O \rightarrow 2\cdot OH \quad (43)$$

The enhancement by NO_3^- can be thus attributed to the direct and indirect formation of ·OH radicals. Zepp et al.[53] suggested that nitrate-induced photooxidation is a possible transformation mechanism for trace organic pollutants in shallow clear water bodies with inputs from ground waters or other sources with higher ratios of nitrate/dissolved organic carbon concentration. Zhu et al. also reported similar findings.[54]

Chemical oxygen demand

Estimation of chemical oxygen demand (COD) of the optimized reaction system UV/MnO_2 /IC at various intervals of irradiation shows that the degradation and decolorization of IC do not lead to instant mineralization.

However, once the solution is decolorized, and the UV/MnO_2 irradiation is continued, mineralization becomes faster, and the COD reaches a stable level (Figure 11). After that, the COD decreases very slowly even on continuous UV radiation indicating that the intermediates are stable and cannot be mineralized under these conditions.

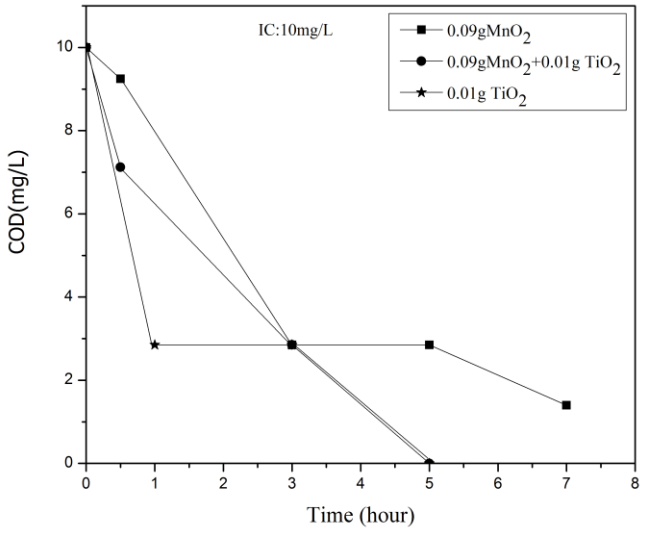

Figure 11. COD of the reaction system at different times of irradiation after decolorization of IC.

The photodegradation of IC is known to yield stable organics such as acetic acid, tartaric acid, malic acid, oxalic acid, anthranilic acid etc.[22,25] Independent experiments in our laboratory with these compounds showed that they are not mineralized under MnO_2 mediated photocatalysis (not reported here). In this context, the possibility of combining a more efficient photocatalyst such as TiO_2 with MnO_2 in order to enhance the mineralization capability is examined.

Investigations using different weight ratios of MnO_2 and TiO_2 have shown that MnO_2/TiO_2 in the ratio 9:1 is optimum for the decolorization of IC under the standardized reaction conditions. The comparative decolorization and mineralization efficiency of MnO_2, TiO_2, and MnO_2/TiO_2 for IC are evaluated. The rate of decolorization and mineralization is more in the presence of MnO_2/TiO_2 compared to individual MnO_2 or TiO_2. This is evident from the COD values in the presence of the three catalysts (Figure 11).

The complete and faster mineralization in the presence of MnO_2/TiO_2 shows clearly that the advantages of higher adsorption and oxidative properties of MnO_2 and the photocatalytic efficiency of TiO_2 can be beneficially combined for the mineralization of traces of IC in water. However, the precise mechanism of the process, as well as the nature of intermediates, may be different in the case of different catalysts, and these aspects need to be investigated in detail.

General mechanism

The primary step in semiconductor mediated heterogeneous photocatalytic processes is the formation of an electron-hole pair as in reaction (36) which may undergo concurrent recombination as in reaction (37). When the particles are small, the holes escape recombination in the bulk of the catalyst and can reach the surface. The average transit time τ_D of the charge carriers to reach the surface is calculated by Gratzel and Frank[55] as:

$$\tau_D = \frac{r^2}{\pi^2 D_c} \quad (44)$$

where

r is the radius of the particle and

D_c is the diffusion coefficient of the charge carrier.

If the photogenerated hole does not recombine with the electron, it can react with the organic pollutant (RH) or even with the solvent water as follows:

$$RH + h^+ \rightarrow {\cdot}R + H^+ aq \quad (45)$$

$$H_2O + h^+ \rightarrow {\cdot}OH + H^+ aq \quad (46)$$

The hole can also react with the OH^- ions either present in the system under alkaline conditions or formed on the surface by the dissociative adsorption of water to H^+_{ads}. and OH^-_{ads}.[56]. The OH^-_{ads} can act as traps for the holes at the surface;

$$h^+ + OH^-_{ad} \rightarrow {\cdot}OH_{ad} \quad (47)$$

$${\cdot}OH + {\cdot}OH \rightarrow H_2O_2 \quad (48)$$

H_2O_2 formed in the photocatalytic system has been proven to undergo concurrent decomposition leading to the phenomenon of oscillation in its concentration.[57] The reductive decomposition of H_2O_2 by the photogenerated electron as in (49) results in the formation of reactive ·OH radicals. This also protects the holes from recombination with the electrons.

$$H_2O_2 + e^- \rightarrow OH{\cdot} + OH^- \quad (49)$$

According to Gerischer and Heller[58] reaction (47) is more likely than reaction (46) since the availability of holes on the catalyst surface is more under photocatalysis as explained above. Further, the $\cdot OH_{ad}$ can exist as the stable product at specific surface sites. Consequently, the oxidation of organic pollutants can occur as:

$$RH + .OH_{ad} \rightarrow R{\cdot} + H_2O \quad (50)$$

The direct reaction between the organic pollutant and the hole as in reaction (45) can compete with reaction (50) if the concentration of RH is high or the RH molecules are strongly adsorbed on the surface.

If reaction (50) is the main path, the oxidation may be weaker compared to direct oxidation by holes as in reaction (45) since only some of the holes are available for the formation of $\cdot OH_{ads}$.[57] This will lead to decrease in the oxidation rate and the quantum efficiency in the case of stable organic molecules.

When there are more H_2O_2 in the system, it can also trap the h^+ as in reaction (51) and quench $\cdot OH$ as in reaction (7) which also lead to decreased rate of degradation.

$$H_2O_2 + 2\ h^+ \rightarrow O_2 + 2H^+ \quad (51)$$

Oxygen plays an important role in photocatalytic degradation reactions in aqueous solutions by scavenging the electrons generated on the photocatalyst thereby inhibiting the recombination of electrons and holes. The formation of highly reactive superoxide radical anion which is responsible for the photocatalytic degradation is the outcome of this reaction.

$$O_2\ (g) + e^- \rightarrow (O_2^{-\cdot}) \quad (52)$$

$O_2^{-\cdot}$ participates in a series of reactions directly or indirectly as in (53) – (60) resulting in the formation of a number of reactive free radicals which interact with and degrade the pollutant.

$$H_2O \rightarrow OH^- + H^+ \quad (53)$$

$$O_2^{-\cdot} + H^+ \rightarrow HO_2^{\cdot} \quad (54)$$

$$2HO_2^{\cdot} \rightarrow H_2O_2 + O_2 \quad (55)$$

$$HO_2^{\cdot} + e^- \rightarrow HO_2^{-\cdot} \quad (56)$$

$$HO_2^{-\cdot} + H^+ \rightarrow H_2O_2 \quad (57)$$

$$H_2O_2 + O_2^{-\cdot} \rightarrow OH^{\cdot} + OH^- + O_2 \quad (58)$$

$$H_2O_2 + e^- \rightarrow OH^{\cdot} + OH^- \quad (59)$$

$$OH^- + h^+ \rightarrow OH^{\cdot} \quad (60)$$

In order to confirm the role of dissolved O_2 in the photocatalytic degradation IC, the reaction system is deaerated with N_2, and the experiments were carried out under otherwise identical conditions. The effect of deaeration is not significant thereby suggesting that the main source of O_2 for the reaction is not the dissolved form. The required O_2 is provided primarily by the surface (adsorbed) and the lattice of MnO_2 which cannot be easily removed by flushing with N_2.

Amorphous MnO_2 is known to release bulk oxygen more easily to the surface which makes it a better catalyst regarding facile activation and regeneration.[32] MnO_2 with multiple oxidation states together with its electron donor-acceptor properties is an excellent oxidation – reduction catalyst. Photolysis of MnO_2 increases the oxygen species on the surface either by oxygen migration to the surface or by Mn migration to the bulk or both. Surface oxygen is consumed faster upon irradiation and oxygen from the bulk moves to the surface. In the case of MnO_2, the loss of oxygen takes place at temperatures as low as 50 ^{0}C. The photo-initiated oxygen release from MnO_2 may be due to movement of O^{2-} (bulk) to the surface and subsequent weakening of MnO_2 bonds.[59] In the re-oxidation of oxides, atmospheric oxygen and/or dissolved O_2 is taken up by the surface of the partially reduced MnO_2 as follows[32]:

$$O_2\ (g) + e^- \rightarrow (O_2^-) \quad (61)$$

$$(O_2^-) + e^- \rightarrow 2(O^-) \rightarrow O^{2-}\ (s) \quad (62)$$

Most of the oxygen radicals are present in the bulk of the catalyst while some of them may remain on the surface for a short period. These highly active oxygen radicals can regenerate reduced manganese species. Under UV irradiation, the bonds in MnO_2 are weakened and O^{2-} is released to the surface. Even though the lifetime of excited state oxygen species is short, they possess adequately high energy and electronegativity to facilitate the reduction or hydrogen abstraction from the substrate. Possible reaction pathways are:

$$O^{2-}\ (s) \xrightarrow[-\ e^-]{h\nu} (O^-) \xrightarrow[-\ e^-]{h\nu} O_2\ (\text{surface}) \quad (63)$$

$$O_2\ (\text{surface}) + RH\ (\text{i.e., IC}) \rightarrow HO_2^{\cdot}\ (\text{surface}) + R^{\cdot} \quad (64)$$

$$O_2\ (\text{surface}) + R \rightarrow \text{Intermediates} \rightarrow$$

$$\rightarrow \text{Mineralization}\ (CO_2 + H_2O) \quad (65)$$

The abstracted $H^{\cdot}$ interacts with the hole and gets oxidized to form acid sites on the surface of MnO_2.

$$H^{\cdot} + h^+ \rightarrow H^+ \quad (66)$$

The regeneration of MnO_2 may be represented as:

$$-Mn^{(3+\text{ or }2+)} \xrightarrow[-\ e^-]{h\nu} -Mn^{(4+\text{ or }3+)} \quad (67)$$

$$n(-Mn^{(4+\text{ or }3+)}-) + O^{2-}(\text{from reaction 62}) \rightarrow MnO_2\ (\text{or } Mn_3O_4) \quad (68)$$

Unless the oxygen is replenished periodically, the activity of the catalyst will be lost faster. This is verified by recycling the catalyst immediately after use by simple filtration followed by quick drying at 120 ^{0}C for 1 h. The degradation of IC (in 30 minutes) decreased steeply from ~75 % in the presence of the fresh catalyst to ~30% in first recycling, ~11 % in second recycling and ~8% in third recycling. This confirms the drastic change in the surface characteristics, loss of adsorption sites and loss of oxygen from the lattice, bulk and/or the surface of MnO_2. This loss is not fully compensated by contact with atmospheric oxygen.

The migration of bulk oxygen to the less energetic surface sites and its consumption by participation in catalytic reactions has been proven experimentally and from ESR studies.[60]

The formation of H_2O_2 during the photocatalytic degradation of IC is verified by analyzing the reaction solution immediately after decolorization and periodically after that. The concentration of in situ formed H_2O_2 increases initially, reaches an optimum and decreases after that. This is consistent with the earlier reports[57] on the oscillation in the concentration of in situ formed H_2O_2 in semiconductor-mediated photocatalytic systems which are attributed to concurrent formation and decomposition [reactions (53)-(60)].

Dyes are known to absorb light efficiently in the visible region. Hence IC can absorb more visible light and act as a sensitizer thereby transferring electrons from the excited dye molecule to the conduction band of MnO_2.

$$Dye_{(ads)} \rightarrow Dye_{(ads)}^{*} \quad (69)$$

$$Dye_{(ads)}^{*} + MnO_2 \rightarrow Dye_{(ads)}^{+\cdot} + MnO_2(e_{CB}^{-}) \quad (70)$$

$$Dye_{(ads)}^{+\cdot} \rightarrow \text{Intermediates} \rightarrow \text{Oxidation/Degradation} \quad (71)$$

The similar pathway was suggested for the degradation of dyes on Ag/TiO_2 catalyst also.[61] However, dye sensitization as a mode of catalyst activation is highly concentration-dependent. At lower concentration of the dye, there will be only monolayer coverage and the energy acquired by light absorption may not be adequate to sensitize the semiconductor. At higher concentration, there will be multilayer adsorption of the dye. Consequently, light absorption and photocatalytic efficiency may not increase significantly because the inner layers will tend to act as insulators with respect to outer layers.

Conclusion

Trace amounts of the toxic dye pollutant Indigo Carmine in water are degraded efficiently by MnO_2 mediated photocatalysis. However, the degradation does not lead to complete mineralization which requires more efficient photocatalyst such as TiO_2 or the combination MnO_2/TiO_2. The degradation does not follow the modified L-H mechanism or pseudo-first order kinetics as in the case of many AOPs probably because of the high adsorption and oxidation capability of MnO_2 and consequent faster degradation. The degradation is faster under acidic conditions. H_2O_2 which is a powerful oxidant for many photocatalytic reactions inhibits the degradation which is attributed to the quenching of the photoproduced holes and reactive ·OH radicals. However, another oxidant persulphate enhances the degradation through the in situ generation of reactive $SO_4^{-\cdot}$ radical anion and ·OH. Salts/anions likely to be present in water influence the degradation differently varying from 'moderate inhibition' to 'no effect' or even 'enhancement' depending on the chemistry of the anion, its concentration, interactions with the substrate, catalyst, intermediates, etc. and other reaction conditions. The surface, bulk as well as lattice oxygen of MnO_2 participates in the photocatalytic degradation of IC, and this results in decreased activity with every recycling.

Acknowledgement

Financial support from the Council of Scientific and Industrial Research (CSIR), India by way of Senior Research Fellowship to KPV is gratefully acknowledged.

References

[1]Hoffmann, M. R., Martin, S. T., Choi, W., Bahnemann, D. W., *Chem. Rev.*, **1995**, *95*, 69, pubs.acs.org/doi/abs/10.1021/cr00033a004

[2]Gaya, U. I., Abdullah, A. H., *J. Photochem. Photobiol. C: Photochem. Rev.*, **2008**, *9*, 1, https://doi.org/10.1016/j.jphotochemrev.2007.12.003

[3]Devipriya, S., SugunaYesodharan., *Solar Energy Materials and Solar Cells*, **2005**, *86*, 309, https://doi.org/10.1016/j.solmat.2004.07.013

[4]Ollis, D., Pichat, P., Serpone, N., *Appl. Catal.B: Environ.*, **2010**, *99*, 377, https://doi.org/10.1016/j.apcatb.2010.06.030

[5]Chong, M. N., Jin, B.,Chow, C. W. K., Saint, C., *Water Res.*, **2010**, *44*, 2997, https://doi.org/10.1016/j.watres.2010.02.039

[6]Sakthivel, S., Neppolean, B., Shankar, M. V., Arabindoo, B., Palanichamy, M., Murugesan,V., *Solar Energy Mater. Sol. Cells*, **2003**, *77*, 65, https://doi.org/10.1016/S0927-0248(02)00255-6

[7]Shibin, O. M., Rajeev, B., Veena, V., Yesodharan, E. P., Yesodharan, S., *J. Adv. Oxid. Technol*, **2014**, *17*, 297, https://doi.org/10.1515/jaots-2014-0215

[8]Fenoll, J., Hellin, C., Martinez, M., Flores, P., Navarro, S., *Appl. Catal. B: Environ.*, **2012**, *115-116*, 31, https://doi.org/10.1016/j.apcatb.2011.12.023

[9]Rao, A. N., Sivasankar, B., Sadasivam, V., *J. Hazard. Mater.*, **2009**, *166*, 1357, **DOI:** 10.1016/j.jhazmat.2008.12.051

[10]Takeuchi, J. P., Cuong, M., Zhang, T-M.,Matsuoka, M., Anpo, M., *Res. Chem. Intermed*., **2010**, *36*, 327, doi:10.1007/s11164-010-0126-5

[11]Pei, D., Luan, J., *Int. J. Photoenergy*, **2012,** article id 262831, 13 pages, http://dx.doi.org/10.1155/2012/262831

[12]Chen, H., Li, W., Liu, H., Zhu, I., *Micropor. Mesopor. Mater.*, **2011**, *138***,** 235, https://doi.org/10.1016/j.micromeso.2010.09.021

[13]Wu, C. G., Chao, C. C., Kuo, F. T., *Catal.Today*,**2004**, *97*, 103, https://doi.org/10.1016/j.cattod.2004.04.055

[14]Bae, E., Choi, W., *Environ Sci. Technol.*, **2003**, *37*, 147, DOI: 10.1021/es025617q

[15]Li, Y., Sun, S., Ma, M., Ouyang, Y., Yan, W., *Chem. Eng. J.*, **2008**, *142*, 147, https://doi.org/10.1016/j.cej.2008.01.009

[16]Anpo, M., Takeuchi, M., *J CataL., 2003,* **216**, 505, https://doi.org/10.1016/S0021-9517(02)00104-5

[17]Zheng, Z., Huang, B., Qin, X., Zhang, X., Dai, Y., Whangbo, M-H., *J. Mater. Chem.*, **2011**, *21*, 9079. https://doi.org/10.1039/c1jm10983a

[18]Sakthivel, S., Shankar, M. V., Palanichamy, M., Arabindoo, A., Bahnemann, D. M., Murugesan, B. V., *Water Res.*, **2004**, *38*, 3001, https://doi.org/10.1016/j.watres.2004.04.046

[19]Chen, H-W., Ku, Y., Kuo, Y-L., *Water Res*., **2007**, *41*, 2069, https://doi.org/10.1016/j.watres.2007.02.021

[20]Jabs, C. F. I., Drutz, H. P., Summit Jr, R. I., *Am. J. Obst. Gynecol*, **2001**, 185, 1368, https://doi.org/10.1067/mob.2001.119072

[21]Jeffords, D. L., Lange, P. H., DeWolf, W. C.,*Urology*, **1977**, *9*, 180, https://doi.org/10.1016/00904295(77)90192-3

[22]Vautier, M., Guillard, C., Hermann, J. M., *J. Catal*., **2001**, *201*, 46, https://doi.org/10.1006/jcat.2001.3232

[23]Galindo, C., Jacques, P., Kalt, A., *J. Photochem. Photobiol A: Chem*., **2001**, *141*, 47, https://doi.org/10.1016/S1010-6030(01)00435-X

[24]Othman, I., Mohamed, R. M., Ibrahem, F. M., *J. Photochem. Photobiol A: Chem*., **2007**, *189*, 80, https://doi.org/10.1016/j.jphotochem.2007.01.010

[25]Vidya Lekshmi, K. P., Gayathri, P. V., Yesodharan, S., Yesodharan, E. P., *IOSR J Appl. Chem*., **2015**, 29.

[26]Vidya Lekshmi, K. P., Yesodharan, S., Yesodharan, E. P., *IOSR J Appl. Chem*., **2016**, 25.

[27]Standard methods for estimation of water and wastewater, American Public Health association, **1999**, 5220A, D1292

[28]Jain, S., Yamgar, R., Jayram, R. V., *Chem. Eng. J*., **2009**, *148*, 342, https://doi.org/10.1016/j.cej.2008.09.006

[29]M. Sayed, M., Pingfeng, F., Khan, H. M., Zhang,P., *Int. J. Photoenergy*, **2014**, Article ID 490264 11 pages, http://dx.doi.org/10.1155/2014/490264

[30]Shibin, O. M., Suguna Yesodharan., Yesodharan, E. P., *J. Env. Chem. Eng*., **2015**, *3*, 1107, https://doi.org/10.1016/j.jece.2015.04.026

[31]Anju, S. G., Jyothi, K. P., Joseph, S., Yesodharan, S., Yesodharan, E. P., *Res. J. Recent Sci*., **2012**, 1, 191

[32]Cao, H., Suib, L., *J Am. Chem. Soc*., **1994**, *116*, 5334, DOI: 10.1021/ja00091a044

[33]Neppolean, B., Choi, H. C., Sakthivel, S., Aurobindo, B. Murugesan, B., *J. Hazard. Mater*., 2002, *89*, 303, https://doi.org/10.1016/S0304-3894(01)00329-6

[34]Shen, Y. F., Zorger, R. P., Suib, S. L., McCurdy, L., Potter, D. I., O'Young, C. L., *J. Chem. Soc. Chem. Comm*., **1992** , *17*, 1213. https://doi.org/10.1039/c39920001213

[35]Anandan, S., Vinu, A., Venkatachalam, N., Arabindoo, B., Murugesan, V., *J Mol. Catal. A:Chem*., **2006**, *256*, 312, https://doi.org/10.1016/j.molcata.2006.05.012

[36]Anju, S. G., Yesodharan, S., Yesodharan, E. P., *Chem. Eng. J*., **2012**, 189-190, 84, https://doi.org/10.1016/j.cej.2012.02.032

[37]Rabindranathan, S., Devipriya, S., Yesodharan, S., *J. Hazard. Mater*., **2003**, *102* , 217, https://doi.org/10.1016/S0304-3894(03)00167-5

[38]Yatmaz, H. C., Akyol, A., Bayramoglu, M., *Ind. Eng. Chem Res*., **2004**, *43*, 6035, **DOI:** 10.1021/ie049921z

[39]O'Shea, K. E., Garcia, I., Aguilar, M., *Res. Chem. Intermed*., **1997**, 23, 325, DOI: 10.1163/156856797X00556

[40]Zhou, S., Ray, A. K., *Ind. Eng. Chem. Res*.,**2003**, *42*, 6020, DOI**:** 10.1021/ie030366v

[41]Saien, J., Soleymani, A. R., *J. Hazard. Mater*.,**2007**, *14*, 507, https://doi.org/10.1016/j.jhazmat.2006.10.065

[42]Cunningham, J., Al-Sayyed, G., *J. Chem. Soc. Faraday Trans*., **1990**, *86*, 3935, DOI:10.1039/FT9908603935

[43]Barka, N., Assabane, A., Nounah, A., Ichou, I. A., *J. Hazard. Mater*., **2008**, *152*, 1054, https://doi.org/10.1016/j.jhazmat.2007.07.080

[44]Kuan, W. H., Chen, C. Y., Hu, C. Y., *Water Sci. Technol*., **2011**, *64*, 899, DOI: 10.2166/wst.2011.262

[45]Gray M. J., Malati, M. A., Rophael, M. W., *J. Electroanal. Chem. Interfacial Electrochem*., **1978**, 89, 135, https://doi.org/10.1016/S0022-0728(78)80038-2

[46]Zhang, H., Chen, W. R., Huang, C. H., *Environ.Sci Technol*., **2008**, *42*, 5548, DOI: 10.1021/es703143g

[47]Berlin, A. A., *Kinet. Catal*., **1986**, *27*, 34.

[48]Guillard, C., Puzenat, E., Lachheb, H., Houas, A., Herrmann, J-M, *Int. J. Photoenergy*, **2005**, 7, 1, http://dx.doi.org/10.1155/S1110662X05000012

[49]Rincon, A-G., Pulgarin, C., *Appl,Catal. B: Environ*, **2004**, *51*, 283, https://doi.org/10.1016/j.apcatb.2004.03.007

[50]Minero, C., Pellizari, P., Maurino, V., Pellizzetti, E., Vione, D., *Appl. Catal. B. Environ*. **2008**, *77*, 308, https://doi.org/10.1016/j.apcatb.2007.08.001

[51]Amalric, L., Guillard, C., Blanc-Brude, E., Pichat, P., *Water Res*., **1996**, 30, 1137, https://doi.org/10.1016/0043-1354(95)00292-8

[52]Peterson, M. W., Turner, J. A., Nozik, A. J., *J. Phys. Chem*., **1991**, *95*, 221, DOI**:** 10.1021/j100154a044

[53]Zepp, R. G., Hogne, J., Bader,H., *Environ Sci. Technol*., **1987**, *21*, 443, DOI**:** 10.1021/es00159a004

[54]Zhu, H., Jiang, R., Xiao, L., Chang, Y., Guan, Y., Li, X., Zeng, G., *J. Hazard. Mater*., **2009**, *169*, 933, https://doi.org/10.1016/j.jhazmat.2009.04.037

[55]Gratzel, M., Frank, A. J., *J Phys Chem*., **1982**, *86*, 2964, DOI: 10.1021/j100212a031

[56]Salvador, P., *J. Electrochem Soc*., **1981**, *128*, 1895, DOI: 10.1149/1.2127760

[57]Jyothi, K. P., Yesodharan, S., Yesodharan,E. P., *Ultrason. Sonochem*., **2014**, *21*, 1782, https://doi.org/10.1016/j.ultsonch.2014.03.019

[58]Gerischer, H., Heller, A., *J Phys Chem*., **1991**,95, 5261, DOI: 10.1021/j100166a063

[59]Kung, H., '*Transition metal oxides: Surface chemistry and catalysis;* Elsevier: Amsterdam, **1989,** pp. 100-120

[60]Kuriacose, J. C., Ramakrishnan, V., Yesodharan, E. P., *Ind. J. Chem*., **1975**, *13*, 1350.

[61]Anandan, S., Sathish Kumar, P.,Pugazhenthiran, N., Madhavan, J., Maruthamuthu, P., *Solar Energy Mater. Sol.Cells*, **2008**, *92*, 929, https://doi.org/10.1016/j.solmat.2008.02.020

Received: 11.05.2017.
Accepted: 10.06.2017.

SYNTHESIS OF GOLD NANOPARTICLES FROM CHLOROAURIC ACID USING RED WINE

T. Pavliashvili[1], T. Kalabegishvili[2,3], M. Janjalia[2], E. Ginturi[2] and G. Tsertsvadze[4]

Keywords: gold nanoparticles, chloroauric acid, red wine, transmission electron microscopy, UV–Visible spectrophotometer.

Gold nanoparticles were synthesized from chloroauric acid using the red wine of two types. The synthesis was carried out at room temperature. The optical absorption spectrum of the obtained gold nanoparticles was studied by using a UV-visible spectrophotometer, and the structure and particle sizes – by a transmission microscope. It was found that the geometric shapes of nanoparticles depended on the concentration of the working solution and the reducing agent. Nanoparticle size distribution histograms were plotted and assessed. The applications of obtained results were defined.

*Corresponding Authors
E-Mail: pavliashvilitamaz@yahoo.com
[a] Institute of Micro- and Nanoelectronics, 13 I. Chavchavadze Ave., Tbilisi, 0179 Georgia
[b] I. Javakhishvili Tbilisi State University, 3 I. Chavchavadze Ave., Tbilisi, 0128 Georgia
[c] Ilia State University, Institute of Applied Physics, 3/5 K. Cholokashvili Ave., Tbilisi 0162, Georgia
[d] Georgian Technical University, 77 M. Kostava Str., Tbilisi 0175 Georgia

Introduction

Recently, gold nanoparticles have found wide application in medicine and biophysical research. They are also promising for designing the devices of a new generation. It is suggested by their unique properties. Unlike bulk gold, the gold nanoparticles possess ferromagnetic, catalytic and tunable optical properties. In particular, the optical properties of gold nanoparticles are determined by their plasmon resonance associated with the excitation of conduction electrons and localized in a wide spectral region, from visible to infrared, depending on the size, shape, and structure of nanoparticles.[1]

The gold nanoparticles are chemically stable and biocompatible. Various physical and chemical methods are used for the synthesis of gold nanoparticles. However, these methods are expensive and involve the use of toxic reducing agents. Hence preference is given to alternative environment-friendly methods of green chemistry. Recently it has been revealed that many biological objects such as plants, bacteria, fungi, etc. can transform the ions of inorganic metals into metal nanoparticles. For this purpose, they more often use plant extracts. Synthesis of nanoparticles with the help of green reducing agents has a number of advantages over other methods. Short synthesis time, low cost of the process, the safety of personnel and the environment, etc. makes this method attractive for production of nanoparticles. The use of plant extracts allows carrying out more convenient monitoring of nanoparticle size and shape and simplifying subsequent purification.[2]

Various plant extracts and dry red wine are used for the synthesis of metal nanoparticles. Healing properties of dry red wines are known since ancient times. The dry red wines have a complex chemical composition and contain ethyl and methyl alcohols, sugars (mainly glucose and fructose), and various organic acids (catechins and anthocyanins). From polyphenols, resveratrol is of special noteworthy. Resveratrol is contained in grape skins and seeds and passes into the wine from there during the process of its production. The content of resveratrol in the red wine varies from 0.2 to 5.8 mg L^{-1}. The content of resveratrol in the white wine is much less. This useful substance possesses antioxidant, anti-inflammatory and cardioprotective properties. It is also effective as a cancer-preventive.

Materials and Methods

In this work, the process of production of gold nanoparticles from chloroauric acid ($HAuCl_4$) by using the red wine Saperavi is discussed. The wine of two types was used: 1. The wine produced by ancient Georgian technology in qvevri (clay vessel) buried in the ground. 2. The wine produced in oak barrels. Red wine Saperavi is produced from the eponymous local grape cultivar in the province of Kakheti. Big clay vessels, so-called qvevri, are buried in such a way that its hole is at the level of the ground. Such a position of qvevri, which first the grape must is fermented and then the wine is aged in, provides the temperature of about 14 °C. This temperature is optimal for long-term storage of wine.

As is well known, the properties and flavor of wine depend on the grape variety, the place of its growth and the production technology. The main difference of the qvevri technology from the European one is that stems and seeds are not separated from grape flesh before fermentation. The European technology involves separation of seeds and stems from grape flesh and then pouring of grape juice into the vessels for fermentation. The wines produced by qvevri technology contain more tannin and polyphenols.

The synthesis was carried out at room temperature. The aqueous solution of $HAuCl_4$ of concentration 10^{-3} M was used. The wine was poured in small portions into the flask with the working solution. The Saperavi wine was used simultaneously as a reducing agent and a stabilizer of the solution. The changed color of the solution pointed to the formation of nanoparticles in it.

The optical transmission spectra of the nanoparticles were studied with the help of UV–Vis Spectrophotometer Sintra 10e. The absorption peak was recorded at 550 nm. The structure and sizes of nanoparticles were determined by using transmission microscope JEM–100SX. The size of nanoparticles varied over the range of 3 – 30 nm. Both types of wine showed good reducing and stabilizing properties.

The presence of gold nanoparticles was also confirmed by the appearance of absorption in the visible region at the wavelength of 550 nm. The optical transmission spectra of the solutions based on these wines were identical (Fig. 1).

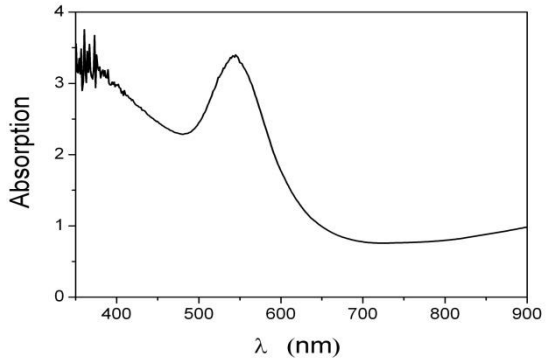

Figure 1. The optical transmission spectra of the red wine.

It was revealed that the geometric shape of nanoparticles depended on the concentration of the working solution, and on the ratio between the concentrations of the working solution and the reducing agent. In diluted solutions of both types of wine, nanorods, and spheroid and ellipsoid nanoparticles were formed (Figs. 2 and 3), while, with the excess of the reducing agent (wine), the nanoparticles of triangle, cubic, hexagons and other geometric shapes were formed (Figs. 4 and 5).

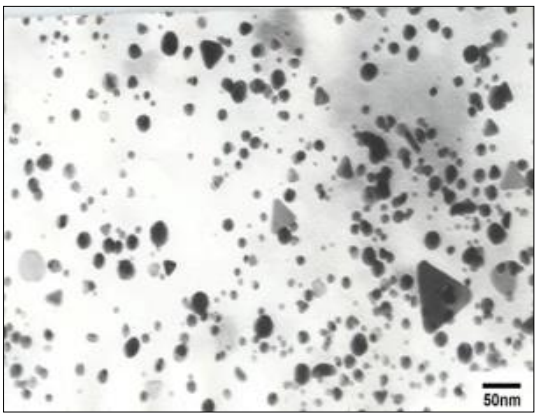

Figure 2. Microphoto of gold nanoparticles synthesized by using the red wine produced by the qvevri method.

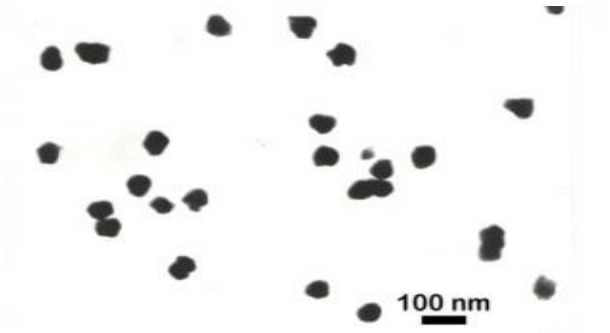

Figure 3. Microphoto of gold nanoparticles produced using the wine produced in oak barrels.

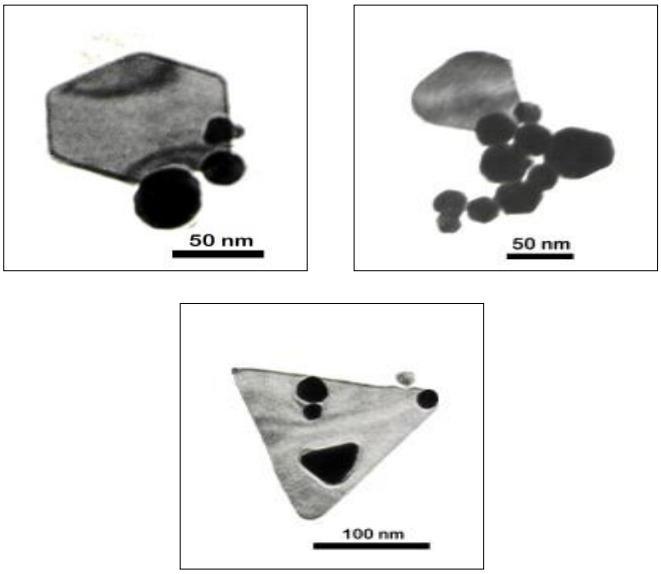

Figure 4. Microphoto of gold nanoparticles synthesized by using the supersaturated solution of the red wine produced by the qvevri method.

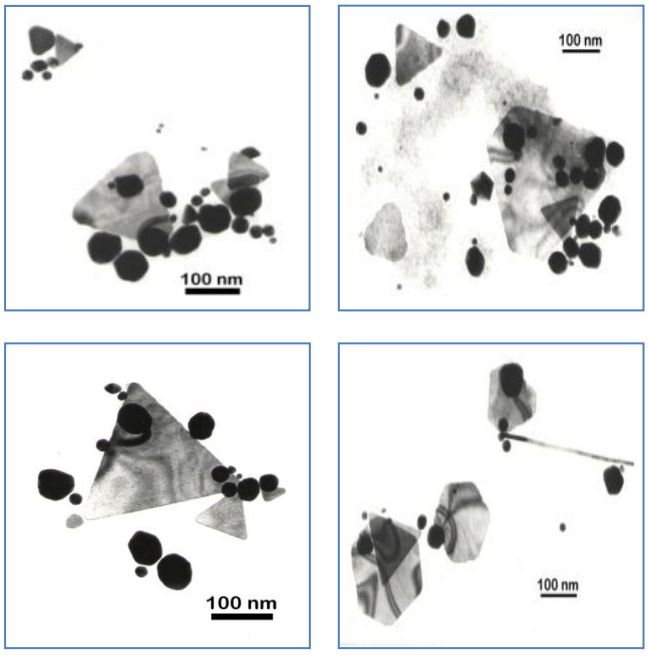

Figure 5 is continued in the next page.

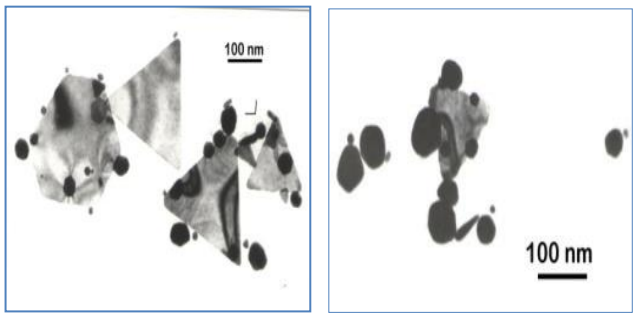

Figure 5. Microphoto of gold nanoparticles synthesized by using the diluted solution of the red wine produced in oak barrels.

To assess the size distribution of nanoparticles, relevant histograms were plotted (Figs. 6 and 7).

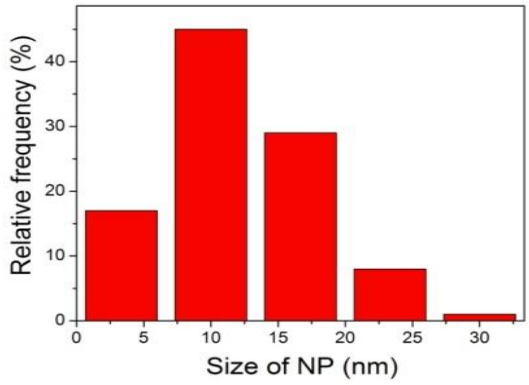

Figure 6. Distribution of gold nanoparticles synthesized by using the diluted solution of the red wine produced by the qvevri method.

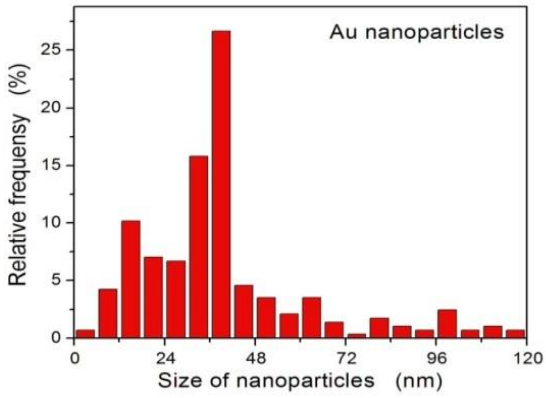

Figure 7. Distribution of gold nanoparticles synthesized by using the diluted solution of the red wine produced in oak barrels.

Conclusion

Gold nanoparticles of different geometric shapes and sizes were synthesized. We obtained interesting preliminary results that could find wide application in the field of biological research and medicine. The range of these applications is quite extensive. Here are given just some of them:

Visualization of cancer cells. Traditionally visualization of nanoobjects is carried out by using highly sensitive fluorescent tags. However, this technique is not devoid of shortcomings, which is expressed in photochemical instability and the need for expensive detectors. Plasmon-resonant gold particles are very bright. The scattering cross section of nanoparticles is by 5 – 7 orders of magnitude higher than the fluorescent molecule cross section. One of the widespread methods of detection of micro- and nano-objects is dark-field microscopy. In dark-field microscopy, only the light scattered by an object under the side lighting enters the lens. In the result, the scattering object glows brightly on the dark background. Besides, the nanoparticles are mainly accumulated on the surfaces of tumors. Due to these properties of nanoparticles, the gold nanoparticles have great opportunities for visualization and diagnostics of oncological diseases by optical microscopy in the dark field mode (resonant scattering optical microscopy). The nanoparticles can be detected by a common digital CCD camera.[3] The fact that the metal nanoparticles have plasmon resonance makes them promising for designing biosensors for diagnostics and treatment of oncological diseases.

Gold nanoparticles as containers for target delivery of medicines. Until recently spherical gold particles were mainly used in biomedicine.[4] With the development of the technology of synthesis of nanoparticles, there emerged the nanoparticles of other shapes. For nanoparticles of different shapes and structure, the desired frequency of plasmon resonance can be achieved by varying the relative sizes. The formation of gold nanoparticles of various shapes during their synthesis with the red wine Saperavi indicates the prospects of their application to target delivery of medicines.

Photothermal therapy. Currently, gold nanoparticles are widely used in photochemical therapy (PCT) of oncological diseases.[5] The surface plasmon resonance of gold nanoballs in water solution is in the vicinity of 520 nm. The wavelength of surface plasmon resonance depends on the shape and size of nanoparticles, the distance between nanoparticles, and the local dielectric environment. The use of lasers in PCT of oncological diseases ensured controlled and targeted impact on cancer tissues. When the gold nanoparticles are used, to heat them up at the plasmon resonance wavelength, the nanoparticles have to be irradiated with laser radiation at 520 nm wavelength. As the radiation with such a wavelength does not pass through a biological tissue, it is an acute problem to synthesize gold nanoparticles with the surface plasmon resonance wavelength in the transparency window of the biological tissue, which is 800 – 900 nm. For this, we could modify the shapes of nanoparticles. In this connection, the synthesis of gold nanoparticles of various geometric shapes with red wine in a single technological cycle is interesting and promising. To clarify the mechanism of the synthesis process, additional studies are needed.

Acknowledgements

This paper has been presented at the 4th International Conference "Nanotechnologies," October 24 – 27, 2016, Tbilisi, Georgia (Nano – 2016).

References

[1]Dicman, L. A., Khebcov, N. G., *Acta Naturae*, **2011**, *3(2)*, 34-55. Cataldo, F., Ursini, O., Angelini, G., *Eur. Chem. Bull*., **2016**, *5(1)*, 1-7, DOI: http://dx.doi.org/10.17628/ecb.2016.5.1-7; Habashi, F., *Eur. Chem. Bull*., **2016,** *5(10)*, 416-419, DOI: http://dx.doi.org/10.17628/ecb.2016.5.416-419; Kalabegishvili, T. L., Murusidze, I. G., Kirkesali, E. I., Rcheulishvili, A. N., Ginturi, E. N., Gelagutashvili, E. S., Kuchava, N. E., Bagdavadze, N. V., Janjalia, M. V., Pataraya, D. T., Gurielidze, M. A., Frontasyeva, M. V., Zinicovscaia, I. I., Pavlov, S. S., Tsertsvadze, G. I., Gabunia, V. N., *Eur. Chem. Bull.*, **2015**, *4(1-3)*, 45-49, http://dx.doi.org/10.17628/ecb.2015.4.43-49;

[2]Yamamoto Y. and Hori. H., *Rev. Mater. Sci*., **2006**, *12*, 23-25.

[3]Makarov, V. V., Love, A. J., Sinitsina, O. V., Makarova, S. S., Yavlinski, I. V., Tal'ianski, M. E., Kalinina N. O., *Acta Naturae*, **2014**, *6(1)*, 35-44

[4]Yegorov, A. M., Gukasov, V. M., Ivanin, A. I., Rubtsova, M. I., Yaminskiy. I. V., The Use of Gold Nanoparticles in Biomedical Applications Utilizing Optical Methods. Innovatics and Expert Examination. *SRI FRCEC (Scientific Research Institute – Federal Research Center for Project Evaluation and Consulting Service*, **2014**, *2(13)*, 243.

[5]Meshalkin, Y. P., Bgatova. N. P., *J. Siberian Fed. Univ., Biol.*, **2008**, *3(1)*, 248-253.

Received: 27.04.2017.
Accepted: 10.06.2017.

SYNTHESIS OF SOME NEW 4-(BENZOTHIAZOLYLAMINO)-PYRAN-2-ONE DERIVATIVES AND THEIR ANTIBACTERIAL ACTIVITY

Ramiz Hoti,[a] Hamit Ismaili,[a]* Naser Troni,[a] Idriz Vehapi,[b] Malesore Pllana,[c] Veprim Thaci[a]

Keywords: Pyran-2-one, benzothiazole, condensation, antibacterial activity, zones of inhibition.

Novel 4-substituted pyran-2-one derivatives were synthesized by condensation of 6-methylpyran-2-ones and corresponding 2-aminobenzothiazoles. Condensation of 4-chloro-6-methyl-2H-pyran-2-one **2a** and 2-aminobenzothiazoles **3(a-c)** afforded corresponding 4-(2-benzothiazolylamino)-6-methyl-2H-pyran-2-one **4a,** 4-(4-methyl-2-benzothiazolylamino)-6-methyl-2H-pyran-2-one **4b** and 4-(5,6-dimethyl-2-benzothiazolylamino)-6-methyl-2H-pyran-2-one **4c**. By condensation of 4-chloro-3-nitro-6-methyl-2H-pyran-2-one **2b** and 2-aminobenzothiazoles 3(a-d)**,** 4-(2-benzothiazolylamino)-3-nitro-6-methyl-2H[1]-pyran-2-one **4d** and 4-(6-ethoxy-2-benzothiazolylamino)-3-nitro-6-methyl-2H[1]-pyran-2-one **4e** were synthesized. The synthesized products were characterized on the basis of IR, ^{1}H-NMR and ^{13}C-NMR spectra. Compounds **4a-4e** were screened for their antibacterial activity against *S. Aureus, E. Coli* and *Klebsiella*. Their antibacterial activity is examined by measuring the zones of inhibition around the disks impregnated with the corresponding product solutions in N,N-DMF concentration 2 mg mL^{-1}, 4 mg mL^{-1} and 6 mg mL^{-1} and results are reported.

* Corresponding Authors
E-Mail: ramizhoti@yahoo.com
[a] Department of Chemistry, Faculty of Nature Sciences, University of Prishtina, 10000 Prishtina, Kosovo
[b] Institute of Public Health of Kosovo, 10000 Prishtina, Kosovo
[c] Faculty of Mining and Metallurgy, University of Mitrovica, 40000 Mitrovica, Kosovo

Introduction

Pyran-2-ones and their derivatives are an important class of compounds and play an important role in many life processes. Many of such derivatives are reported for their synthesis[1] and a wide range of biological activities.[2-4] They were shown to exhibit antimicrobial,[5] antibacterial,[6] antifungal,[7] antimalarial,[8] and anticonvulsant activity.[9] 3-Hydroxypyran-2-one was found to be present in kojic acid derivatives and reported for their significant antimicrobial activity. Some 4-hydroxypyran-2-one derivatives exhibited inhibitory activity in the enzymatic process of HIV protease.[10] Some natural pyrone antibiotics containing hydroxamate or catechole groups are used for lead complexiation in cases of poisoning.[11] Some polycyclic aromatic compounds have been shown to have antitumor activity as they may be inserted between DNA bases. Their selective activation in the tumor may be applied to anticancer chemotherapy with reduced side effects.[12] It has been reported that 3-bromo-6-(4-chlorophenyl)-4-methylthio-2H-pyran-2-one has shown protective action against hepatitis.[13] The biological activity of these derivatives is conditioned by their structure, so the presence of different substituents on the pyrone ring indicates their impact on the type and potency of biological activity.[14] Unfortunately, the relationship between structure and biological activity of these derivatives so far has not yet been sufficiently clarified.

On the other hand, the extraordinary biologically importance of benzothiazole derivatives has generated a constant interest for their synthesis and research. In continuation of our previous studies and in an attempt to synthesize the new derivates[15-17] in this paper we had intended to synthesize some new heterocyclic derivatives by condensation of 4-chloro-6-methyl-2H-pyran-2-one and substituted 2-aminobenzothiazole which could serve as pro-pharmaceutical products.

Methods and materials

The compounds are synthesized under catalytic conditions using commercial reagents of Aldrich company. The reaction flow was monitored by thin layer chromatography using Merck Kieselgel-60 (F-254) as a stationary phase and a mixture of benzene:toluene:glacial acetic acid (v/v/v 85:10:5) as the mobile phase. The synthesized products are purified by crystallization from methanol and ethanol.

Melting points are determined used a paraffin oil bath with the open capillary tube. The IR spectra are recorded in KBr discs on Shimadzu 8400xFT-IR spectrometer with 4cm^{-1} resolution. The ^{1}H-NMR and ^{13}C-NMR spectra are recorded in DMSO on UNITYplus-300"NMR 1" spectrometer. Chemical shifts were reported in ppm downfield fromTMS as internal standard (δ0.00).

Antibacterial activity of the synthesized compounds is examined using standard discs (*d*=5.0mm, maximum capacity10 pg) measuring the zones of inhibition. Standard discs were previously impregnated with 2 mg mL^{-1}, 4 mg mL^{-1} and 6 mg mL^{-1} solutions of respective compounds in N,N-DMF.

Synthesis of 4-heteroarylamino-6-methyl-2H-pyran-2-ones 4(a-c). General procedure

The reaction mixture containing 0.72 g (5 mmol) of 4-chloro-6-methyl-2H-pyran-2-one **2a**, equimolar amounts of corresponding 2-aminobenzothiazole (**3a-3d**) and a catalytic amount of triethylamine were dissolved in 12 mL of acetonitrile. The reaction mixture was refluxed in a water bath for 8-12 hours, then was cooled and crude product was filtered off under vacuum, then was dried and crystallized from ethanol.

4-(-2-Benzothiazolylamino)-6-methyl-2H- pyran-2-one (4a)

White crystalline product, yield was 88 %, m.p. 220 ^{o}C, FTIR (KBr, cm^{-1}): 3420, 3250, 2978, 2923, 1705, 1685, 1680, 1618, 1160, 1130, 760. ^{1}H NMR (300 MHz, DMSO-d_6, ppm) 1,90 (s, 1H), 4,10 (s, 1H), 5,80 (s, 1H), 6,20 (s, 1H), 7,60-8,20 (m, 4H). ^{13}C-NMR (δ, ppm) 23,1, 93,8, 103,2, 123,0, 124,0, 125,4, 126,2, 127,3, 127,9, 145,6, 162,4, 167,8, 175,3.

4-(4-Methyl-2-benzothiazolylamino)-6-methyl-2H-pyran-2-one (4b)

White crystalline product, yield was 82 %, m.p. 228-230 ^{o}C. FTIR (KBr, cm^{-1}): 3440, 3040, 2925, 1695, 1670, 1640, 1080, 770. ^{1}H NMR (300 MHz, DMSO-d_6, ppm; 2,05(s, 3H), 2,40 (s, 3H), 4,35(s, 1H), 5,95(s, 1H), 6,30(s, 1H), 7,40-7,90(m, 3H).

4-(5,6-Dimethyl-2-benzothiazolylamino)-6-methyl-2H-pyran-2-one (4c)

Brown crystalline product, yield was 79 %, m.p. 175-176 ^{o}C.FTIR (KBr, cm^{-1}): 3446, 2975-2925, 1685, 1670, 1140, 1100, 765.

Synthesis of 4-heteroarylamino-6-methyl-3-nitro-2H-pyran-2-ones (4d-4e). General procedure

The reaction mixture containing 0.85 g (5 mmol) of 4-chloro-6-methyl-3-nitro-2H-pyran-2-one **2b** equimolar amounts of 2-aminobenzothiazoles (**3a, 3d)** and a small amount of triethylamine were dissolved in 20 mL of acetonitrile, and the reaction mixture was refluxed in aqueous baths for 6-10 hours. Then the mixture was cooled and crystalline product was filtered off under vacuum, and dried in air, then purified by crystallization from ethanol.

4-(2-Benzothiazolylamino)-3-nitro-6-methyl-2H-pyran-2-one (6a)

Yellow crystalline product, yield was 67.5 %, m.p.=124-126^{o}C.FTIR (KBr, cm^{-1}): 3400, 3050, 2940, 1690, 1630, 1585, 1515, 1340, 1300, 750, 720.

4-(2-Benzothiazolylamino)-3-nitro-6-methyl-2H-pyran-2-one (6d)

Yellow crystalline product, yield was 72.5 %, m.p. 152-154 ^{o}C. FTIR (KBr, cm^{-1}): 3450, 3170, 2930, 1695, 1605cm^{-1}, 1540, 1480, 1290, 1070, 790. ^{1}H NMR (300 MHz, DMSO-d_6, ppm;1,33 (t, 3H), 1,95 (s, 3H), 4,05 (q, 2H), 4,40(s, 1H), 6,28 (s, 1H),7,61-7,92 (m, 3H). ^{13}C-NMR; (δ, ppm):14,8, 22,9, 66,2, 103,2, 108,8, 111,0, 113,3, 123,0, 124,1, 140,2, 144,6, 156,5, 161,9, 167,2, 174,8.

Results and discussion

On the basis of previous research it has been established that 4-chloro-6-methyl-2H-pyran-2-one (**2)** in the reaction with 2-aminobenzothiazoles (**3**) forms corresponding 4-benzothiazolylamino-6-methyl-2H-pyran-2-ones (**4**). Also, 4-chloro-3-nitro-6-methyl-2H-pyran-2-one in reaction with 2-aminobenzothiazoles forms the corresponding nitro derivatives **4d-4e.**

By reaction of 4-hydroxy-6-methyl-2H-pyran-2-one **1** and equimolar amount of phosphorous oxychloride, 4-chloro-6-methyl-2H-pyran-2-one **2a** is synthesized in 85 % yield. The obtained product is condensed with 2-aminobenzothiazoles (**3a-3c**) in acetonitrile, giving the corresponding benzothiazolylamino-6-methyl-2H-pyran-2-ones (**4a-4c**). (Scheme 1). Also by condensation of 4-chloro-3-nitro-6-methyl-2H-pyran-2-one **2b** with 2-aminobenzothiazoles **3a** and **3d**, corresponding nitro derivatives **4d** and **4e** were synthesized.

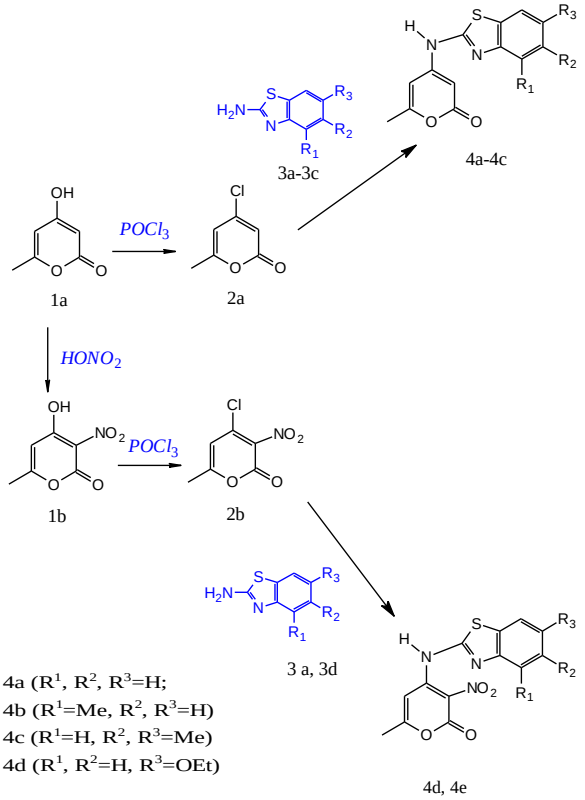

Scheme 1. Synthetic procedures

Table 1. Physical properties of compounds **4a-4e** and their elemental analysis

Nr.	Molecular formulas	Molecular weight	Elemental analysis (%), calcd.(found)	mp/ °C	Yield (%)
4a	$C_{13}H_{10}N_2O_2S$	258.08	C-60.45; H-3.90; N-10.85; O-12.40; S-12.40 (C-60.42; H-3.87; N-10.86); S-12.35	220-222	88.1
4b	$C_{14}H_{12}N_2O_2S$	271.10	C-61.74; H-4.44; N-10.29; O-11.76; S-11.76 (C-61.71; H-4.40; N-10.32); S-11.72	228-230	82.2
4c	$C_{15}H_{14}N_2O_2S$	286.11	C-62.91; H-4.93; N-9.79; O-11.18; S-11.18 (C-62.87; H-4.89; N-9.82; S-11.15)	175-176	79.6
4d	$C_{13}H_9N_3O_4S$	427.41	C-51.47; H-2.99; N-13.85; O-21.12; S-10.56 (C-51.51; H-3.03; N-13.80; S-10.52)	124-126	67.5
4e	$C_{15}H_{13}N_3O_5S$	347.10	C-51.86; H-3.77; N-12.10; O-23.05; S-9.22 (C-51.90; H-3.81; N-12.06; S-9.18)	152-154	72.8

Structural elucidation of the synthesized products is based on spectrometric IR and NMR data. In the IR spectrum of the compound, **4a** appeared an absorption signal absorption at 3420 cm^{-1} which is responsible for $\nu(NH_2)$ stretching vibrations. The characteristic signal at 3250 cm^{-1} appeared due to aromatic ν(CH) stretching vibrations while the absorption signal at 2978 resulted from methyl ν(CH) stretching vibrations. The sharp peak at 1695 cm^{-1} is responsible for ν(C=O) stretching vibrations, while the absorption modes at 1680 and 1618 cm^{-1} result from ν(C=N) and ν(C=C) stretching vibrations. On the other hand, the absorption signal at 1130 cm^{-1} is characteristic for lactonic ν(C-O-C) stretching vibrations while the sharp peak at 750 cm^{-1} resulted from aromatic δ(C-H) oop bending vibrations.

In the ^{1}H-NMR spectrum of compound **4a**, a three proton singlet is appeared at δ1.90 ppm corresponding to the methyl protons, while the singlets at δ5.80 ppm and 6.00 ppm correspond to the pyronic protons. A singlet displayed at δ4.10 ppm results from amine proton, while benzothiazole protons are displayed as multiplets at δ7.60-8.20 ppm. In the ^{13}C-NMR spectrum, the respective signals for 13 carbon atoms are displayed.

In the IR spectrum of compound **4b**, an absorption signal at 3422 cm^{-1}, which results from υ(NH) stretching vibrations is displayed. Also characteristic peaks at 3040 cm^{-1} and 2925 cm^{-1} which respond to the aromatic υ(CH) and methyl υ(CH) stretching vibrations were assigned. The lactone carbonyl vibrations appeared at 1696 cm^{-1} while those υ(C=N) and υ(C=C) of the aromatic system assigned at 1670 cm^{-1} and 1640 cm^{-1}. The sharp peak at 770 cm^{-1} is characteristic for aromatic bending δ(C-H) oop vibrations. The ^{1}H-NMR spectrum of compound **4b**, displayed two singlets at δ2.05 ppm and δ2.40 ppm characteristic for methyl protons, whereas two singlets at δ5.95 ppm and δ6.30 ppm are responsible to the pyronic ring proton and the singlet at δ4.35 ppm results from the amine proton. Benzothiazole protons have been shown as a multiplet at δ7.40-7.90 ppm.

In the IR spectrum of compound **4c**, the absorption signal appeared at 3446 cm^{-1} which is responsible for ν(NH) stretching vibrations of secondary amines.

The absorption band at 2975-2925 cm^{-1} is attributed to υ(CH) stretching vibrations of aromatic and methyl group. The characteristic peak for unsaturated six-membered lactones has appeared in 1705 cm^{-1}. Signals at 1685 cm^{-1} and 1670 cm^{-1} correspond to υ(C=N) and υ(C=C) stretching, while the signal at 765 cm^{-1} responsible for aromatic bending δ(CH) vibrations also is appeared.

The IR spectrum of compound **4d** showed an absorption peak at 3400 cm^{-1} which result from the υ(NH) stretching vibrations. The absorption peaks at 3050 cm^{-1} and 2940 cm^{-1} are responsible for aromatic and methyl υ(CH) stretching vibrations. The intense absorption at 1690 cm^{-1} resulted from υ(C=O) stretching vibrations while aromatic υ(C=N) and υ(C=C) modes are displayed at 1630 cm^{-1} and 1585 cm^{-1}. Two signals at 1515 cm^{-1} and 1340 cm^{-1} are assigned for asymmetric and symmetric $\upsilon(NO_2)$vibrations while the lactone υ(C-O-C) mode appeared at 1300 cm^{-1}. The Peak at 750 cm^{-1} resulted from aromatic δ(CH) bending mode.

In the IR spectrum of the compound **4e** is observed the absorption peak at 3450 cm^{-1} which is responsible for υ(NH) stretching vibrations. The aromatic υ(CH) vibrations are displayed at 3170 cm^{-1} while those of the methyl group at 2930 cm^{-1}. A sharp peak at 1695 cm^{-1} and the peaks at 1605 cm^{-1} and 1540 cm^{-1} are responsible for υ(CO) stretching and aromatic υ(C=N) and υ(C=C) stretching modes. The peaks at 1480 cm^{-1} and 1290 cm^{-1} respond to asymmetric and symmetric $\upsilon(NO_2)$ vibrations. Also in the spectrum is shown the bending absorption δ(CH) (oop) at 790 cm^{-1}.

In the ^{1}H-NMR spectrum of the compound **4e** appeared a three-proton triplet at δ1.40 ppm which corresponds to the methyl group protons, while the singlet at δ1.95 has resulted from the methyl group of the pyronic ring. The two-proton quartet at δ4.05 ppm results from ethylene protons, whereas the signal at δ4.40 ppm is displayed due to amine proton. A singlet at δ1.95 ppm corresponds to the pyronic proton, while the benzothiazole protons are displayed as a multiplet at δ7.61-7.92 ppm. In the ^{13}C-NMR spectrum of **4e**, the respective signals for 15 carbon atoms are displayed.

Table 2. The zones of inhibition (mm) of the discs impregnated with solutions of the synthesized compounds

	***S. aureus*, dose in mg mL^{-1}**			***E. coli*, dose in mg mL^{-1}**			***Klebsiella*, dose in mg mL^{-1}**		
	dose in mg mL^{-1}			**dose in mg mL^{-1}**			**dose in mg mL^{-1}**		
	2	**4**	**6**	**2**	**4**	**6**	**2**	**4**	**6**
4a	8.0	10.0	11.5	20.0	22.5	23.0	24.5	24.0	25.0
4b	10.0	10.5	12.0	21.0	23.0	25.0	16.5	18.5	19.5
4c	10.0	11.0	13.0	18.0	20.0	23.0	16.0	18.0	22.5
4d	9.5	10.0	10.5	22.0	24.0	24.5	20.0	23.0	25.5
4e	10.0	12.5	13.5	24.5	24.5	25.5	20.5	19.0	24.0

Antibacterial activity of the products 4a-e

Following this study compounds **4a-4e** are investigated for their antibacterial activity. Our research has been conducted in terms of testing their activity against bacteria *S. aureus*, *E. coli*, and *Klebsiella*, on the basis of Standard disc method.[18] The discs have previously been impregnated with solutions of the compounds in N,N-DMF with concentrations of 2 mg/mL, 4 mg/mL and 6 mg/mL. After 48 h incubatoin, the zones of inhibition around the standard discs were measured and reported. Results are summarized in table 2.

Compounds of series **4a-4e** showed significant antimicrobial activity against *E. Coli* and *Klebsiella*, while their activity against *S. Aureus* was moderate. Compounds **4e** and **4c** were most active against *S. aureus*, compounds **4b** and **4e** showed the most activity against *E. Coli* whereas **4a** and **4e** were more active against *Klebsiella*.

Antibacterial activity against *E. Coli* and *Klebsiella* displayed in a large-scale. On the other hand, these products expressed both bactericidal and bacteriostatic activity against *S. Aureus*. While bactericidal activity was low, bacteriostatic activity is shown in a large range (+3.0 mm). Compound **4e** expressed considerable activity against these microorganisms. It has been observed that the nitro group of pyronic residue had a significant impact on antibacterial activity. Also, the impact of the methyl and ethoxy group of the benzothiazole moiety was considerable.

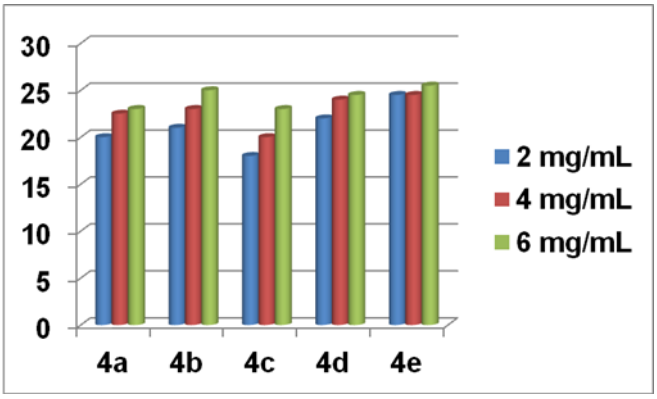

Figure 1. The graphical presentation of zones of inhibition (mm) against *S. aureus*

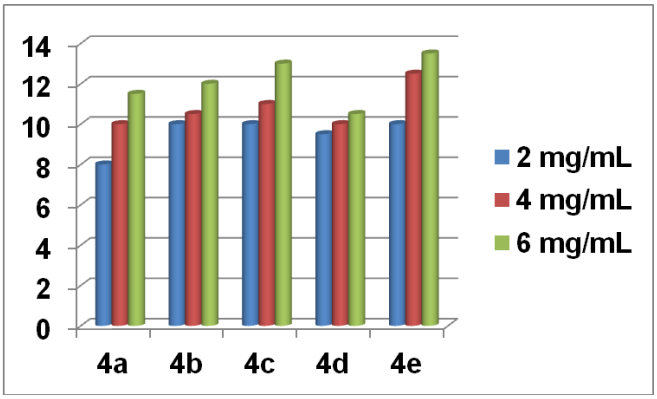

Figure 2. The graphical presentation of zones of inhibition (mm) against *E. coli*

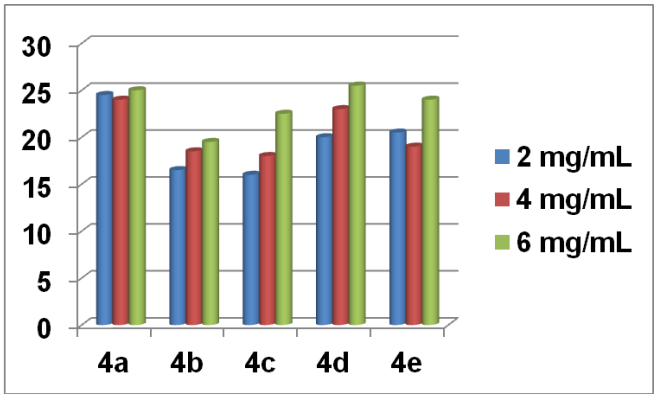

Figure 3. The graphical presentation of zones of inhibition (mm) against *Klebsiella*

We my consider that the antibacterial activity may result as a consequence of the involvement of these products in enzymatic reactions. In any way these products can cause enzymatic inhibition of cell wall construction of the microorganisms, however, mechanism of enzymatic inhibition is not yet fully studied. It was observed that by increasing the concentration of solvents, their antimicrobial activity increased.

Conclusions

Novel 6-methyl-2H-pyran-2-one derivatives 4(a-e) have been synthesized in high yield. Compounds 4e and 4c were more active against *S. Aureus*, compounds 4b and 4e

expressed more antibacterial activity against *E. coli*, while compounds 4a and 4e have been more active against *Klebsiella*. The impact of nitro, methyl and ethoxy groups in antibacterial activity was significant. In general, antibacterial activity is shown to be proportional to the concentration of these compounds.

Acknowledgement

We are grateful to Prof. Dr. Hrvoj Vancik, Department of Organic Chemistry and Biochemistry, University of Zagreb, Croatia, for their support and facilities.

References

[1]Kepe, V., Kocevar, M., Polanc, S., *J. Heterocycl. Chem*.,**1996**, *33(6)*,1996, 1707–1710. http://onlinelibrary.wiley.com/doi/10.1002/jhet.5570330626/abstract

[2]Parker, S. R., Cutler, H. G., Jacyno, J. M., Hill, R. A., *J. Agric. Food Chem.*,**1997**,*45*(7), 2774–2776. http://pubs.acs.org/doi/abs/10.1021/jf960681a

[3]Dong, Y., Nakagawa-Goto, K., Lai C. Y., Morris-Natschke, S. L., Bastow, K. F., Lee, K. H., , *Bioorg. Med. Chem. Lett.*, **2011**, *21(8)*, 2341–2344. https://www.ncbi.nlm.nih.gov/pmc/articles/PMC3072684/

[4]Defant, A., Mancini, I., Tomazolli, R., Balzarini, J., *Arch.Pharm.Chem.LifeSci.*,**2015,***348*, 23-33. doi/10.1002/ardp.201400235/epdf

[5]Aytemir, M. D., Demirerol, D., Hider, C., Ozalp, M., *Turk J Chem.*, **2003***27*, 757–764. http://journals.tubitak.gov.tr/chem/issues/kim-03-27-6/kim-27-6-12-0303-15.pdf

[6]Li, H. H., Qi, F. M., Dong, L. L., Fan, G. X., Che, J. M., Guo, D. D., Zhang, Z. X., Fei, D. Q., *Phytochem. Letters*, **2014,** *10*, 304–308. http://www.sciencedirect.com/science/article/pii/S1874390014001980

[7]Jelen, H., Blaszczyk, L., Chełkowski, J., Rogowicz, K., Strakowska, J.,**2014**, *13(3)*, 589–600. https://link.springer.com/article/10.1007/s11557-013-0942-2

[8]McCracken, S. T., Kaiser, M.,Boshoff, H. I.,Peter D. W. Boyd, P. D. W., Copp, B. R., Bioorg. Med. Chem.,**2012,** 20(4), 1482–1493. https://www.ncbi.nlm.nih.gov/pmc/articles/PMC3276683/

[9]Aytemir, M. D., Calis, U., Ozalp, M., *Arch. Pharm. (Weinheim)*, **2004**, *337*, 281–288. https://www.ncbi.nlm.nih.gov/pubmed/15095421?dopt=Abstract

[10]Vara Parsad, J. V. N., Tummino, P. J., Ferguson, D., Saunders, J., Roest, S. V., McQuade, T. J., Heldsinger, A., Reyner, E. L., Steward, B. H., Guttendorf, R. J., Para, K. S.,*Biochem. Biophysm. Res. Commun.*,**1996**, *221(3)*, 815-820. http://www.sciencedirect.com/science/article/pii/S0006291X96906798

[11]Brtko, J., Rondahl, L., Fickova, M., Hudecov, D., Eybl, V., Uher, M., *Cent. Eur. J. Public Health*, **2004**, *12*, 16–18. https://www.researchgate.net/profile/Julius_Brtko/publication/8564052_Kojic_acid_and_its_derivatives_History_and_present_state_of_art/links/0912f510c021fbb7c6000000.pdf

[12]Dong, Y.,Nakagawa-Goto, K., Lai, C. Y., Morris-Natschke, S. L., Kenneth F. Bastow, K. F., Lee, K. H., *Bioorg. Med. Chem. Lett.*, **2011***21(8)*, 2341–2344. https://www.ncbi.nlm.nih.gov/pmc/articles/PMC3072684/

[13]Konreddy, A., K., Toyama, M., Ito, W., Bal, C., Baba, M., Sharon, A., *ACS Med. Chem. Lett*., **2014**, *5(3)*, 259–263. https://www.ncbi.nlm.nih.gov/pmc/articles/PMC4027742/

[14]Parker, S. R., Cutler, H. G., Jacyno, J. M., Hill, R. A., *J. Agric. Food Chem.*,**1997**,*45(7)*, 2774–2776. http://pubs.acs.org/doi/abs/10.1021/jf960681a

[15]Hoti, R., Nura-Lama, A., Mulliqi-Osmani, G., Troni, N., Gashi, F., Ismaili, H., Thaci, V., *Orbital: E-J. Chem.*, **2014**, *6(3)*, 184-190. http://www.orbital.ufms.br/index.php/Chemistry/article/view/564

[16]Hoti, R., Troni, N., Nura-Lama, A., Mulliqi-Osmani, G., Ismaili, H., Thaci, V., *Eur. Chem. Bull.*,**2017**, 6(2), 83-88. DOI: 10.17628/ecb.2017.6.83-88

[17]Hoti R., Kalaj V., Vehapi I., Ismaili H., Thaçi V., Bicaj M., *FASEB J. Exp. Biol.*, **2010**, lb487, http://www.fasebj.org/content/24/1_Supplement/lb487.short

[18]Bauer, A. W., Kirby, W. M., Sherris, J. C., Turuck M., *Am. J. Clin. Pathol.*,**1966,** 45(4), 493-496. https://www.ncbi.nlm.nih.gov/pubmed/5325707

Received: 18.05.2017.
Accepted: 10.07.2017.

SYNTHESIS AND CHARACTERIZATION OF SOME 4-SUBSTITUTED THIAZOLIDINONE DERIVATIVES

Assala Salam Jebur[a] and Mahmood Shakir Magtoof[a]*

Keywords: Thiazolidinones; imines; synthesis; NMR spectroscopy

This study is concerned with the synthesis and characterization of 4-thiazolidinone derivatives (**3a-3h**). These compounds were prepared by reacting mercaptoacetic acid with the appropriate Schiff bases (imines) by heating at 50-60 °C in chloroform with moderate yields (51-75 %). The structures of these 4-thiazolidinone derivatives were established on the basis of the spectral studies using IR, ^{1}H-NMR, ^{13}C-NMR, ^{13}C-NMR DEPT and MS.

* Corresponding Authors
Tel: 009647813199256
E-Mail: Mahmood672000@yahoo.com
[a] Department of Chemistry, Science, College,Thiqar University, Thiqar, Nasyria, Iraq

Introduction

Thiazolidinones are ketone derivatives of the saturated form of thiazole (called thiazolidine). 1,3-Thiazolidin-4-ones are five-membered heterocycles with one sulfur and one nitrogen atom (Figure 1).

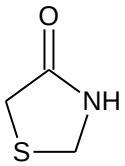

Figure 1. Thiazolidinone ring

1,3-Thiazolidin-4-ones belong to the most intensively investigated classes of five-membered heterocyclic compounds, the biological significance of this class of compounds attracted us to work on the synthesis of new derivatives because numerous 4-Thiazolidinones known for their versatile pharmacological activities[1,2] such as hypnotic,[3] anti-cancer,[4] cardiovascular[5] and antioxidant[6] effect.

Experimental part

The ^{1}H-NMR spectra were recorded using VARIAN spectrophotometer (500 MHz), the ^{13}C-NMR spectra were recorded using VARIAN spectrophotometer (75 MHz).The chemical shift values are expressed in δ(ppm), using tetramethylsilane (TMS) as internal standard and d_6-DMSO as the solvent. The mass spectra were recorded at 70eV using HPLC-LCQ Fleet/Thermo Scientific mass spectrophotometer

General procedure for the preparation of imines (2a-2h)[7-9]
Preparation of mono-imines (2a-2d).

In general, the mono-imines **(2a-2d)** were prepared by the reaction of the mixture of 0.01 mol amine with 0.01 mol aldehyde in 20 ml of methanol or ethanol and 4-6 drops of glacial acetic acid. The reaction mixture was refluxed for 0.5-9 h, and the progress of the reaction was followed by TLC using hexane:ethyl acetate 6:4 as eluent. After completion the reaction, the solvent was evaporated, and the residue was recrystallized from a suitable solvent.

3-(4-Bromophenylimino)indolin-2-one (2a)

The compound was prepared by reacting 1.169 g (0.01 mol) of 4-bromoaniline and 1 g (0.01 mol) of indoline-2,3-dione (isatin). Yield=75 %, M.p.=273-275 ºC, colour orange, IR (KBr disk) 1608 cm^{-1} (C=N).

2-Chloro-N-(4-chlorobenzylidene)aniline (2b)

The compound was prepared by reacting 1.72 g (0.01 mol) of 2-chloroaniline and 1.4 g (0.01 mol) of 4-chlorobenzaldehyde. Yield = 71.7 %, m.p. = 225-228 ºC**,** colour white, IR (KBr disk) 1614 cm^{-1} (C=N).

2-(3-Ethoxy-2-hydroxybenzylideneamino)benzoic acid (2c)

The compound was prepared by reacting 0.825 g (0.01 mol) of 2-aminobenzoic acid and 1 g (0.01 mol) of 3-ethoxy-2-hydroxybenzaldehyde. Yield = 87.5 %, m.p. = 208-209 ºC**,** colour orange, IR (KBr disk) 1625 cm^{-1} (C=N).

4-Bromo-2-(4-bromophenyliminomethyl)phenol (2d)

The compound was prepared by reacting 0.85 g (0.01 mol) of 4-bromoaniline and 1 g (0.01 mol) of 5-bromo-2-hydroxybenzaldehyde. Yield = 87.5 %, m.p. = 108-110 ºC**,** colour yellow, IR (KBr disk) 1618 cm^{-1} (C=N).

Preparation of bis-imines (2e-2h)

In general, the bis-imines **(2e-2h)** were prepared by the reaction of 0.01 mol diamine with 0.02 mol of aldehyde (20 ml) of methanol or ethanol and 4-6 drops of glacial acetic acid. The reaction mixture was refluxed for 1-9 h, with monitoring the progress of the reaction by TLC using hexane:ethyl acetate 6:4 as eluent. After completion the reaction, the solvent was evaporated and the product was recrystallized from a suitable solvent .

2,2'-{Benzene-1,4-diylbis[nitrilomethylylidene]}bis(6-ethoxy-phenol) (2e)

The compound was prepared by reacting 0.324 g (0.01 mol) of benzene-1,4-diamine with 1 g (0.02 mol) of 3-ethoxy-2-hydroxybenzaldehyde. Yield = 85 %, m.p = 187-190 ºC, colour orange, IR (KBr disk) 1624 cm^{-1} (C=N).

2,2'-{Naphthalene-1,5-diylbis[nitrilo(*E*)methylylidene]}bis(6-ethoxyphenol) (2f)

The compound was prepared by reacting 0.452 g (0.01 mol) of naphthalene-1,5-diamine with 0.95g (0.02 mol) of 3-ethoxy-2-hydroxybenzaldehyde. Yield = 96 %, m.p = 133-136ºC, colour chartreuse, IR (KBr disk) 1618 cm^{-1} (C=N).

2-Ethoxy-6-[({4-[(*E*)-(3-ethoxy-2-hydroxybenzylidene)amino]-benzyl}imino)methyl]phenol (2g)

The compound was prepared by reacting 0.595 g (0.01 mol) of 4-(4-aminobenzyl)benzenamine with 1 g (0.02 mol) of 3-ethoxy-2-hydroxybenzaldehyde. Yield = 87.6 %, m.p = 157-158ºC, colour yellow, IR (KBr disk) 1615 cm^{-1} (C=N).

4-bromo-2-[({4-[(*E*)-(5-bromo-2-hydroxybenzylidene)amino]-benzyl}imino)methyl]phenol (2h)

The compound was prepared by reacting 0.595 g (0.01 mol) of 4-(4-aminobenzyl)benzenamine with 1 g (0.02 mol) of 5-bromo-2-hydroxybenzaldehyde. Yield = 84.2 %, m.p = 142-143 ºC, colour yellow, IR (KBr disk) 1623 cm^{-1} (C=N).

General procedures of mono and bis thiazolidinones (3a-3h)[10]
Preparation of mono thiazolidinones (3a-3d)

A mixture of appropriate Schiff bases (0.01 mol) **(2a-2d)** and thioglycolic acid (0.01 mol, 0.20 ml) in a suitable solvent (50) ml was refluxed for 10-30 h. Water formed during the reaction was removed azeotropically by a Dean-Stark apparatus. The progress of the reaction was monitored by TLC using hexane:ethyl acetate 6:4 as eluent. This mixture of reaction are treated with sodium bicarbonate solution to remove unreacted acid. The obtained solids were filtered, washed and purified by recrystallization from dichloromethane to give color powders.

3'-(4-Bromophenyl)spiro[indoline-3,2'-thiazolidine]-2,4'-dione (3a)

The compound was prepared by reaction of 0.5 g (0.01 mol) of 3-((4-bromophenyl)imino)indolin-2-one **(2a)** and 0.153 g (0.115 ml, 0.01 mol) of thioglycolic acid. Yield=55 %, m.p.=180-182ºC, colour: yellow. IR (KBr) 1654 (C=O of thiazolidinone ring); 3024cm^{-1} (Ar-H), 2909 cm^{-1} (C-H aliphatic), 1393 cm^{-1} (C-N), 665 cm^{-1} (C-S). ^{1}H-NMR (500 MHz, DMSO-d_6) δ=4.4 (s, 2H, C_5H); 7.3-8.01 (m, 8H, ArH); 9.27(s, 1H, N-H). ^{13}C NMR (75 MHz, DMSO-d_6) δ=36(s, -CH_2-), 49(s, -C-), 107-139(m, Ar-C); 177(s, CH_2-C=O); 179(s, N-H-C=O).

3-(2-Chlorophenyl)-2-(4-chlorophenyl)thiazolidin-4-one (3b)

The compound was prepared by reaction of 0.8 g (0.01 mol) of 2-chloro-N-(4-chlorobenzylidene)aniline **(2b)** and 0.29 g (0.22 ml, 0.01 mol) of thioglycolic acid. Yield=61 %, m.p.=248-251 ºC, colour: orange. IR (KBr) 1681 (C=O of thiazolidinone ring), 3018 cm^{-1} (Ar-H), 2930 cm^{-1} (C-H aliphatic), 1396 cm^{-1} (C-N), 667 cm^{-1} (C-S). ^{1}H-NMR (500 MHz, DMSO-d_6) δ=4.3(s, 2H,C_5H), 7.2(s, 1H, C_2H), 7.4-8.01(m, 8H, ArH). ^{13}C NMR (75 MHz, DMSO-d_6) δ =36.9(s, -CH_2-), 43(s, -CH-), 111-142(m, Ar-C), 175(s, CH_2-C=O).

2-(2-(3-Ethoxy-2-hydroxyphenyl)-4-oxothiazolidin-3-yl)benzoic acid (3c)

The compound was prepared by reaction of 2-((3-ethoxy-2-hydroxybenzylidene)amino)benzoic acid **(2c)** (0.5 g, 0.01 mol) and thioglycolic acid (0.16 g, 0.12 ml, 0.01 mol). Yield=70 %, m.p.=178-180 ºC, colour: orange. IR (KBr) 1691 cm^{-1} (C=O of thiazolidinone ring); 3010 cm^{-1} (Ar-H), 2945 cm^{-1} (C-H aliphatic); 1399 cm^{-1} (C-N); 637 cm^{-1} (C-S). ^{1}H-NMR (500 MHz, DMSO-d_6) δ=1.9(s, 3H, -CH_3); 4.2 (s, 2H, C_5H); 4.4(s, 2H, -CH_2); 7.20(s, 1H, C_2H); 7.22-8.7 (m, 8H, ArH); 9.59(s, 1H, O=C-OH). ^{13}C NMR (75 MHz, DMSO-d_6), δ=28(s, CH_3); 35(s, -CH_2-); 40(CH_2O); 44(s, -CH-); 116-153 (m, Ar-C); 172(s, CH_2-C=O); 182(COOH).

2-(5-Bromo-2-hydroxyphenyl)-3-(4-bromophenyl)thiazolidin-4-one (3d)

The compound was prepared by reaction of 0.7 g (0.01 mol) of 4-bromo-2-(((4-bromophenyl)imino)methyl)phenol **(2d)** and 0.18 g (0.137 ml, 0.01 mol) of thioglycolic acid. Yield=78 %, m.p.=171-172 ºC, colour: yellow. IR (KBr) 1685 cm^{-1} (C=O of thiazolidinone ring); 3052 cm^{-1} (Ar-H) , 2913 cm^{-1} (C-H aliphatic) ; 1385 cm^{-1} (C-N) ; 681 cm^{-1} (C-S). ^{1}H-NMR (500 MHz, DMSO-d_6) δ =4.48 (s, 2H, C_5H);7.3(s, 1H, C_2H); 7.5-8.01(m, 8H, ArH); 9.62 (s, 1H, Ar-OH). ^{13}C NMR (75 MHz, DMSO-d_6) δ=37(s, -CH_2-); 45(s, -CH-); 120-157(Ar-C); 172(s, CH_2-C=O).

Preparation of bis thiazolidinones (3e-3h)

A mixture of appropriate Schiff bases (0.02 mol) (**2e-2h)** and thioglycolic acid (0.02 mole, 0.40 ml) in a suitable solvent (50 ml) was refluxed for 10-30 h, water formed during the reaction was removed azeotropically by a Dean-Stark apparatus.

The progress of the reaction was checked by TLC using hexane : ethyl acetate 6:4 as eluent . This mixture of reaction was treated with sodium bicarbonate solution to remove unreacted acid. The obtained solid was filtered, washed and purified by recrystallization from dichloromethane to give color powder.

3,3'-(1,4-Phenylene)bis(2-(3-ethoxy-2-hydroxyphenyl)thiazo-lidin-4-one) (3e)

The compound was prepared by reaction of 0.4 g (0.01 mol) of **2e** and 0.18 g (0.139 ml, 0.02 mol) of thioglycolic acid. Yield=71 %, m.p.=155-157 ºC, colour: orange. IR (KBr) 1654 cm^{-1} (C=O of thiazolidinone ring); 3014 cm^{-1} (Ar-H), 2920 cm^{-1} (C-H aliphatic); 1380 cm^{-1} (C-N) ; 671 cm^{-1} (C-S). ^{1}H-NMR (500 MHz, DMSO-d_6) δ = 1.8(s, 6H,-CH_3); 4.0(s, 4H, -CH2); 4.6 (s, 4H, C_5H); 7.2-8.04(m, 12H, Ar-H); 9.5(s, 2H, Ar-OH). ^{13}C NMR (75 MHz, DMSO-d_6) δ =29(d, -CH_3); 38(d, -CH_2); 42(d, CH_2O); 53 (d, -CH-); 113-153(m, Ar-C); 178(d, CH_2-C=O).

3,3'-(Naphthalene-1,5-diyl)bis(2-(3-ethoxy-2-hydroxyphenyl)-thiazolidin-4-one) (3f)

The compound was prepared by reaction of 0.5 g (0.01 mol) of **2f** and 0.1 g (0.153 ml, 0.02 mol) of thioglycolic acid. Yield=59 %, m.p.=154-157 ºC, colour: brown. IR (KBr) 1650 cm^{-1} (C=O of thiazolidinone ring); 3030 cm^{-1} (Ar-H), 2911 cm^{-1} (C-H aliphatic); 1387 cm^{-1} (C-N); 668 cm^{-1} (C-S). ^{1}H NMR (500 MHz, DMSO-d_6), δ=1.9(s, 6H, -CH_3); 4.11(s, 4H, -OCH_2); 4.7 (s, 4H, C_5H); 7.4(s, 2H, -C_2H-); 7.58-8.1(m, 14H, Ar-H); 9.6 (s, 2H, Ar-OH).

2-(3-Ethoxy-2-hydroxyphenyl)-3-(4-(4-(2-(3-ethoxy-2-hydroxy-phenyl)-4-oxothiazolidin-3-yl)benzyl)phenyl)thiazo-lidin-4-one (3g)

The compound was prepared by reaction of 0.5 g (0.01 mol) of **2g** and 0.093 g (0.141 ml, 0.02 mol) of thioglycolic acid. Yield=76 %, m.p.=105-107 ºC, colour: orange. IR (KBr) 1654 cm^{-1} (C=O of thiazolidinone ring); 3027 cm^{-1} (Ar-H), 2915 cm^{-1} (C-H aliphatic); 1390 cm^{-1} (C-N); 672 cm^{-1} (C-S). ^{1}H-NMR (500 MHz, DMSO-d_6), δ=1.87(s, 6H, -CH_3); 2.9(s, 2H, -CH_2-); 4.2(s, 4H, -OCH_2); 4.4 (s, 4H, C_5H); 7.39(s, 2H, -C_2H-); 7.59-8.16(m, 14H, Ar-H); 9.58 (s, 2H, Ar-OH).

2-(5-Bromo-2-hydroxyphenyl)-3-(4-(4-((R)-2-(5-bromo-2-hydr-oxyphenyl)-4-oxothiazolidin-3-yl)benzyl)phenyl) thiazolidin-4-one (3h)

The compound was prepared by reaction of 0.4 g (0.01 mol) of **2h** and 0.18 g (0.139 ml, 0.02 mol) of thioglycolic acid. Yield=73 %, m.p.=246-247 ºC, colour orange. IR (KBr) 1660 cm^{-1} (C=O of thiazolidinone ring); 3032 cm^{-1}. (Ar-H), 2918 cm^{-1} (C-H aliphatic); 1395 cm^{-1} (C-N); 677 cm^{-1} (C-S). ^{1}H-NMR (500 MHz, DMSO-d_6), δ=2.8(s, 2H, -CH_2-); 4.2(s, 4H, C_5H); 7.1(s, 2H, -C_2H-); 7.59-8.16(m, 14H, Ar-H); 9.4 (s, 2H, Ar-OH).

RESULTS AND DISCUSSION

Thiazolidinones **3a-3h** have been prepared by reaction of the appropriate Schiff bases **(2a-2h)** with thioglycolic acid in a suitable solvent (benzene or chloroform).

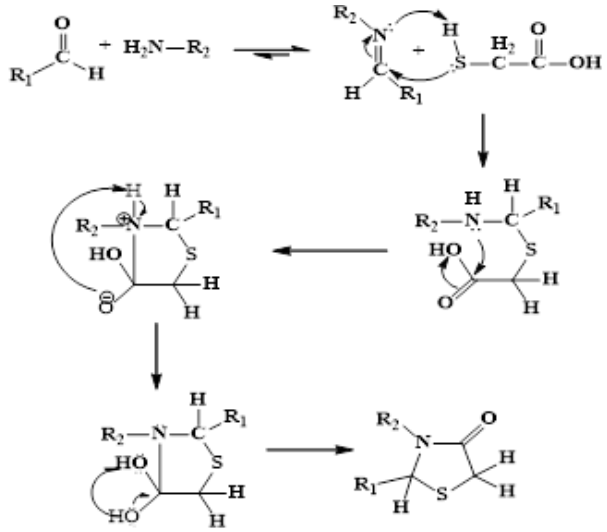

Scheme 1. Mechanism of formation of mono thiazolidinone.

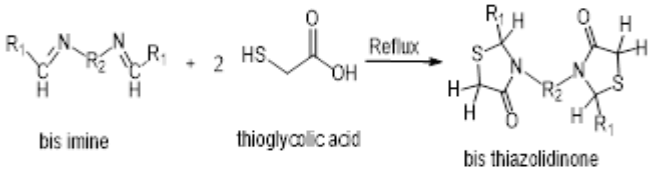

Scheme 2. Synthesis of bis thiazolidinone.

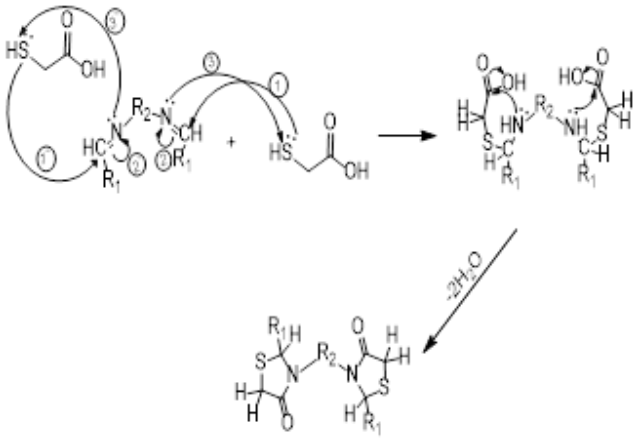

Scheme 3. Probable mechanism of the formation of bis-thiazolidinone

Analysis of infrared spectra

The IR spectra of thiazolidinones 3a-3h in KBr disk show six band groups correspond to the stretching vibration of the aromatic C-H, aliphatic C-H, carbonyl amide group, aromatic C=C, the C-N and bending vibration of S-C bonds, occur within the ranges 3107-2980, 2975-2887, 1691-1654, 1399-1361, 738-654, and 925-617 cm^{-1} respectively.

The absorption frequencies are affected by substitution of the phenyl ring, and the substitution by electron-donating groups (methyl group decreases) while substitution by electron-withdrawing groups (bromo) increase the vibrational frequencies.

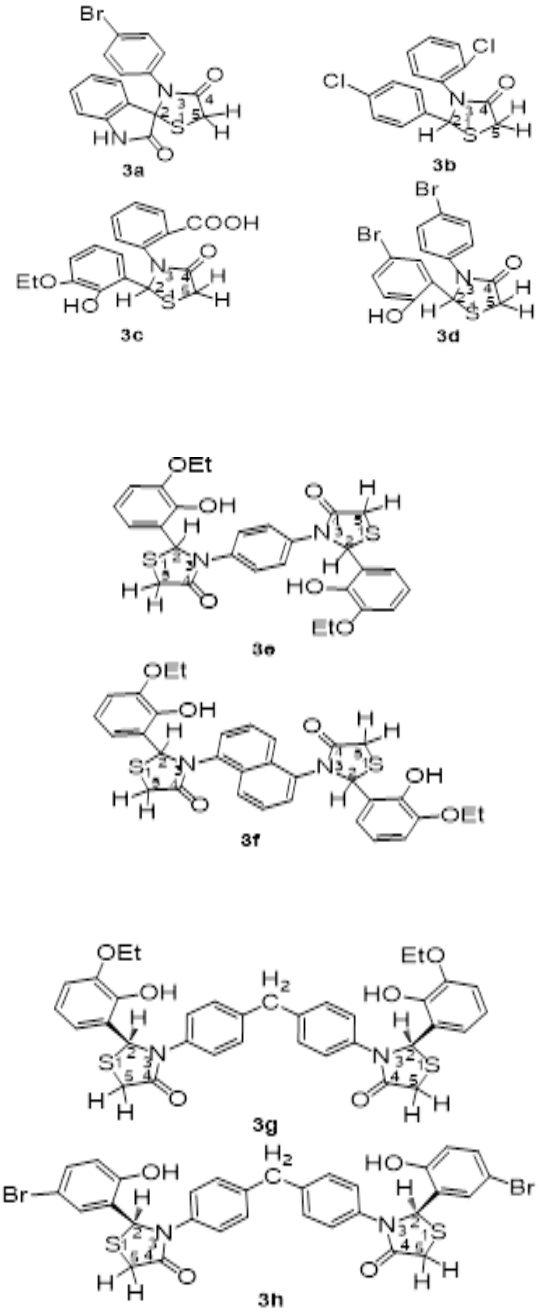

Figure 2. Structures of the compounds **3a-3h**.

^{1}H-NMR spectral analysis

The ^{1}H-NMR spectrum of **3a** shows a singlet signal at δ 4.4ppm for methylene group of thiazolidin-4-one ring, a multiplet signal at δ 7.3-8.01 ppm for aromatic protons (m, 8H, Ar-H), finally a singlet signal at δ 9.2 ppm for amide proton (1H, N-H).

Analysis of ^{13}C-NMR spectra

The ^{13}C NMR spectrum of **3a** showed thiazolidin-4-one ring signals at δ 36 ppm for C5 carbon 5) at δ 49.94 ppm for C2 atom. A multiplet for aromatic carbons at δ 107-139 ppm, a singlet of carbonyl group at δ 177.06 ppm and a signal for C4 carbon of the ring were observed at δ 179.78 ppm.

Analysis of mass spectra

The mass spectrum of **3a** showed the molecular ion peak corresponding to the particular compound at 375 m/z. The fragmentation of **3a** gave the peaks at 301, 283, 273, 205, 156, 117, 76 and 64 m/z which attributed to the fragments of $C_{14}H_9BrN_2O^+$, $C_{15}H_{11}N_2O_2S^+$, $C_{13}H_9BrN_2^+$, $C_{10}H_7NO_2S^+$, $C_6H_4Br^+$, $C_7H_5N_2^+$, $C_6H_4^+$, and $C_5H_4^+$, respectively.

The mass spectrum of **3b** showed the molecular ion peak corresponding to the particular compound at 359 m/z, and the fragmentation of **3b** gave the peaks at 342, 314, 238, 210, 181 and 154 m/z which attributed to the fragments of $C_{18}H_{16}NO_4S^+$, $C_{17}H_{16}NO_3S^+$, $C_{11}H_{12}NO_3S^+$, $C_{10}H_{12}NO_2S^+$, $C_8H_7NO_2S^+$, $C_7H_8NOS^+$, respectively.

The mass spectrum of **3c** showed the molecular ion peak corresponding to the particular compound at 429 m/z, and the fragmentation of **3c** gave the peaks at 355, 183, 172, 156, 76, 64 m/z which attributed to the fragments of $C_{13}H_9Br_2NO^+$, $C_7H_5BrN^+$, $C_6H_4BrO^+$, $C_6H_4Br^+$, $C_6H_4^+$, $C_5H_4^+$, respectively.

Analysis of ^{13}C-NMR DEPT spectra

^{13}C-NMR DEPT spectra of **3a** showed thiazolidin-4-one ring signals at δ 36(negative) 49.94(positive) ppm for C5 carbon C2 carbons, respectively. Multiplet signals for aromatic carbons were observed at δ 107-139 (positive) ppm, while at δ 177.06(positive) and δ 179.78(positive) ppm the carbonyl γ-lactam C4 signals could be observed, respectively.

^{13}C-NMR DEPT spectrum of **3b** showed the following signals: δ 28.67 (positive) ppm for -CH_3**,** δ 35.67(negative) ppm for C5, δ 40.82(positive) ppm for -OCH_2, and δ 44.94 ppm C2, multiplet signals for aromatic carbons at δ 106-153 (positive) ppm, δ 172.90 (positive) ppm for C4 and δ 183.02(positive) ppm for carbonyl of carboxylic group.

Acknowledgements

This work is sponsored by the University of Thi-Qar as a part of research development and higher studies projects.

References

[1]Kato T., Ozaki T., Tamura K., Suzuki Y., Akima M., Ohi N., *J. Med. Chem*. **1999,** *42*, 3134-3146. https://doi.org/10.1021/jm9900927

[2]Solankee, A., Solankee, P., Patel, H., *Int. J. Chem. Sci.*, **2008**, *6(2)*, 1017.

[3]Chaudhary S. K., Verma M., Chaturvedi A. K. and Parmar S. S., *J. Pharm. Sci.*, **1975**, *64*, 614. https://doi.org/10.1002/jps.2600640408

[4]Shah B. R., Desai N. C., Undavia N. K. and Trivedi P. B., *Indian J. Heterocycl. Chem.*, **1993**, *2*, 249.

[5]Nagar S., Singh H. H., Sinha J. N. and Parmar S. S., *J. Med. Chem.*, **1973**, *16*, 178. https://doi.org/10.1021/jm00260a027

[6]Kato T., Ozaki T., Tamura K., Suzuki Y., Akima M., Ohi N., *J. Med. Chem.*, **1998**, *41(22)*, 4309. https://doi.org/10.1021/jm980335f

[7]Hello K .M ., *Iraqi J. Chem*., **2000,** *24*, 266.

[8]Krishnaswamy D., *Tetrahedron*, **2002,** *34*, 4567. https://doi.org/10.1016/s0040-4020(02)00363-0

[9]Abdulrhman Y. K., Mahmood, S. M., *Best Journal.*, **2014,** *2(5)*, 37-48.

[10]Divyesh, P., Premlata, K. and Navin, P., *Arch. Appl. Sci. Res.*, **2010**, *2(6)*, 68-75.

Received: 20.04.2017.
Accepted: 11.07.2017.

THERMODYNAMICS OF ALLOXAN SOLUBILITY IN VARIOUS SOLVENTS AT DIFFERENT TEMPERATURES

S. Baluja,[a]* Divyata Lava,[a] Asmita Hirpara[a] and K. Bhesaniya[a]

Keywords: alloxan; solubility; thermodynamic parameters; Apelblat and Buchowski-Ksiazczak models.

The solubility of Alloxan in methanol, ethanol, ethane-1, 2-diol, water, acetone, and tetrahydrofuran was measured by gravimetric method over a temperature range (293.15 to 323.15) K at atmospheric pressure. The solubility increases non-linearly with temperature in all the studied solvents. Further, in protic solvents, solubility is maximum in methanol and minimum in ethane-1, 2 diol whereas in the selected nonprotic solvents, solubility is greater in tetrahydrofuran than in acetone. The experimental data were correlated with modified Apelblat and Buchowski-Ksiazczak equations. The calculated results show good agreement with the experimental data. Some thermodynamic parameters such as dissolution enthalpy, Gibb's free energy, and entropy of mixing have also been calculated. The evaluated thermodynamic parameters are found to be positive. The positive enthalpy and Gibb's free energy indicate endothermic and spontaneous dissolution of compounds. The positive entropy suggests entropy-driving dissolution process.

*Corresponding Authors
E-Mail: shipra_baluja@rediffmail.com
[a] Physical Chemistry Laboratory, Department of Chemistry, Saurashtra University, Rajkot-360005 (Gujarat), India.

Introduction

Diabetes mellitus has been considered as one of the major health concerns all around the world today.[1,2] One of the most potent methods to induce experimental diabetes mellitus is chemical induction by alloxan which is a well known diabetogenic agent.[3-6]

Alloxan is an oxygenated pyrimidine derivative, and its IUPAC name is 2,4,5,6-pyrimidinetetrone. Figure 1 shows the structure of alloxan.

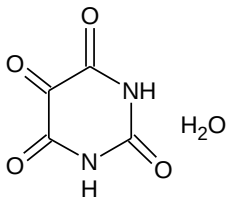

Figure 1. The structure of alloxan

It causes selective necrosis of the β-cells of pancreatic islets. In pharmaceutical industries, the crystallization process is a critical method for both drug intermediates and final drugs. The solubility data is essential for the selection of the proper solvent for the crystallization process and in pre-formulation studies.[7] Further, phenomenological treatment of drug delivery, transport and distribution are dependent on knowledge of solubility.[8] The transportation through membranes and the topical activity of drugs can also be predicted by solubility data.[9]

Various workers have reported solubility of drugs and other compounds in different solvents.[10-12] Thus, in the present work, the solubilities of alloxan have been determined in various solvents; methanol, ethanol, ethane-1,2-diol, water, tetrahydrofuran and acetone over a temperature range 293.15 K to 323.15 K by a gravimetric method. The experimental solubility data were correlated with modified Apelblat and Buchowski-Ksiazczak models. Further, some thermodynamic parameters such as enthalpy of dissolution, Gibb′s energy, and entropy of solutions have been evaluated.

Experimental

Materials

Alloxan was purchased from Loba Chemie Pvt. Ltd. The polymorph used in this study was monohydrate. The melting point of alloxan was determined measured by Differential Scanning Calorimeter (Shimadzu-DSC-60) and was found to be 254 ^{0}C. All of the solvents used for the present study were of analytical grade and supplied by Loba Chemie Pvt. Ltd. These solvents were purified by drying over anhydrous sodium sulfate and were fractionally distilled. The solvents were stored over molecular sieves. The purities of the solvents were confirmed by GC-MS (SHIMADZU-Model No.-QP-2010) equipped with column (DB-5MS, 25 m in length, 0.20 mm internal diameter and 0.33μm film) and were found be greater than 99.8 %.

Solubility measurement

The solubility of alloxan was determined by the gravimetric method. For each measurement, an excess mass of drug was added to a known mass of solvent. The equilibrium cell was heated to a constant temperature with continuous stirring for about 5 hours (the temperature of the water bath approached the constant value, and then the actual value of the temperature was recorded). After 5 hours, stirring was stopped, and the solution was kept for 2 hours to approach equilibrium. The equilibrium time of 2 hours is optimized by checking the concentration of solution at

different intervals of time. After 2 hours, the change in concentration was less than 1 %, so the saturated solution was assumed to be equilibrium. The upper portion of this clear solution was filtered through a membrane (0.22 μm) and was kept in a weighed vial. The vial with the solution was quickly weighed to determine the mass of the sample. When the mass of the residue reached constant value, the final mass was recorded. All of the masses were taken using an electronic balance (Mettler Toledo AB204-S, Switzerland) with an uncertainty of ±0.0001 g. At each temperature, the measurement was conducted three times, and an average value was used to determine the mole fraction solubility. The saturated mole fraction solubility (x_i) of the drug in each solvent can be calculated by using equation (1).

$$x_i = \frac{\frac{m_2}{M_2}}{\frac{m_1}{M_2} + \frac{m_2}{M_2}} \quad (1)$$

where

M_1 is the molar mass of solvent and

M_2 is the molar mass of alloxan.

m_1 and m_2 are the mass of the solvent and solute (alloxan), respectively.

At each temperature, the measurement was conducted three times. By using the average value, mole fraction solubility of alloxan in selected solvents was calculated.

Results and discussion

The mole fraction solubilities x_i of alloxan in the selected solvents are presented in Table 1 at different temperatures (293.15 to 323.15 K) with an uncertainty of ±0.1 K and more visually given in Fig. 2. It is observed that the solubility of alloxan increases nonlinearly with temperature. Further, in protic solvents, solubility is maximum in methanol and minimum in ethane-1,2-diol. The order of solubility is: methanol > water > ethanol > ethane-1,2 diol. In the selected nonprotic solvents, solubility is greater in tetrahydrofuran than in acetone. The results are compared with dielectric constants and dipole moments of the solvents, which was given in Table 2. For protic solvents, solubility was maximum in methanol and minimum in ethane-1,2-diol which is of reverse order of dipole moment. The dipole moment of ethane-1,2-diol is highest among studied protic solvents whereas that of methanol is lowest. In nonprotic solvents, solubility was found to be in higher in tetrahydrofuran (THF) than in acetone. The dipole moment of acetone is higher than that of THF. So, the solubility of alloxan was increasing with decreasing of dipole moment.

The temperature dependence of alloxan solubility in pure solvents was described by the modified Apelblat model.[13]

$$\ln x_{ci}^{a} = A + \frac{B}{T} + C \ln T \quad (2)$$

Table 1. Experimental and calculated mole fraction solubilities (x_i) of alloxan in different studied solvents at different temperatures.

T/K	x_i	x_{cal}[a]	x_{cal}[b]
	Methanol		
293.15	0.1054	0.1055	0.1061
298.15	0.1172	0.1172	0.1170
303.15	0.1291	0.1294	0.1287
308.15	0.1420	0.1420	0.1410
313.15	0.1550	0.1549	0.1541
318.15	0.1681	0.1681	0.1680
323.15	0.1813	0.1815	0.1826
	Ethanol		
293.15	0.0856	0.0856	0.0865
298.15	0.0962	0.0962	0.0963
303.15	0.1069	0.1073	0.1068
308.15	0.1190	0.1189	0.1181
313.15	0.1310	0.1307	0.1301
318.15	0.1426	0.1427	0.1429
323.15	0.1546	0.1548	0.1565
	Ethane-1,2 diol		
293.15	0.0113	0.0114	0.0116
298.15	0.0143	0.0141	0.0141
303.15	0.0172	0.0172	0.0169
308.15	0.0206	0.0206	0.0202
313.15	0.0240	0.0240	0.0240
318.15	0.0283	0.0283	0.0283
323.15	0.0327	0.0327	0.0333
	Water		
293.15	0.0377	0.0378	0.0378
298.15	0.0403	0.0403	0.0404
303.15	0.0429	0.0429	0.0429
308.15	0.0456	0.0455	0.0456
313.15	0.0482	0.0482	0.0483
318.15	0.0510	0.0511	0.0511
323.15	0.0539	0.0539	0.0540
	THF		
293.15	0.0460	0.0461	0.0469
298.15	0.0549	0.0546	0.0546
303.15	0.0638	0.0638	0.0632
308.15	0.0739	0.0739	0.0729
313.15	0.0840	0.0840	0.0836
318.15	0.0954	0.0954	0.0955
323.15	0.1068	0.1067	0.1086
	Acetone		
293.15	0.0128	0.0129	0.0128
298.15	0.0132	0.0132	0.0132
303.15	0.0136	0.0136	0.0135
308.15	0.0140	0.0139	0.0139
313.15	0.0143	0.0143	0.0143
318.15	0.0146	0.0146	0.0146
323.15	0.0150	0.0150	0.0150

[a]Apelblat equation, [b]Buchowski-Ksiazczak equation.

The values of parameters *A*, *B* and *C* were evaluated by nonregression method and are given in Table 3.

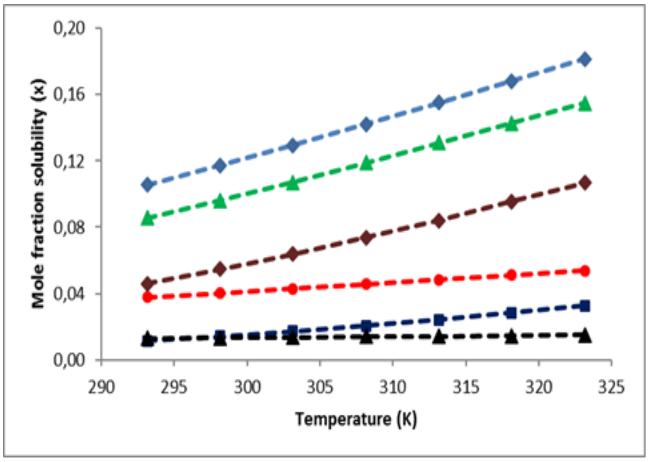

Figure 2. Variation of mole fraction solubilities (x_i) with temperature (T) for alloxan in different studied solvents. Methanol (♦), ethanol (▲), water (●), ethane-1,2-diol (■), THF (♦), acetone (▲). Dashed lines represent calculated mole fraction solubility by Apelblat equation

Using these parameters, mole fraction solubility (x^a_{ci}) was evaluated. These calculated solubilities (x^a_{ci}) are also plotted against temperature along with experimental mole fraction solubility (x_i) as shown in Figure 2. It is observed that these are good agreement between the experimental and calculated solubility values.

The Buchowski-Ksiazczak (λh) equation was first introduced by Buchowski *et al.* to describe solid-liquid equilibrium. In the present study, solubility data was also correlated with temperature by the following Buchowski-Ksiazczak (λh) model.[14]

$$\ln\left(1+\frac{\lambda\left(1-x^{b}_{ci}\right)}{x^{b}_{ci}}\right)=\lambda h\left[\frac{1}{T}-\frac{1}{T_m}\right] \qquad (3)$$

where

T and T_m are the experimental and melting temperature of alloxan

λ and h are two adjustable parameters.

Table 2. Dipole moments and Dielectric constants of the studied solvents

Solvent	Dipole moment	Dielectric constant
Methanol	1.70	32.70
Ethanol	1.69	24.55
Ethane-1,2 diol	2.28	38.66
Water	1.80	80.00
THF	1.55	5.61
Acetone	2.88	20.70

The values of λ and h are evaluated using experimental solubility data and are reported in Table 4. Using these values of adjustable parameters, solubility (x^b_{ci}) is calculated using equation (3).These values are also plotted against temperature along with experimental mole fraction solubility (x_i) as shown in Figure 3. It is observed that the calculated solubilities by Buchowski-Ksiazczak (λh) model are in good agreement with experimental solubility in all the solvents.

The root-mean-square deviations (RMSD) and average relative deviations (ARD) are also calculated for both Apelblat and Buchowski–Ksiazczak models using following equations:

$$RMSD=\left[\sum_{i=1}^{N}\frac{\left(x^{a/b}_{ci}-x_i\right)^2}{N-1}\right]^{1/2} \qquad (4)$$

$$ARD=\frac{1}{N}\sum_{i}^{N}\frac{x_i-x^{a/b}_{ci}}{x_i} \qquad (5)$$

where N is the number of experimental points.

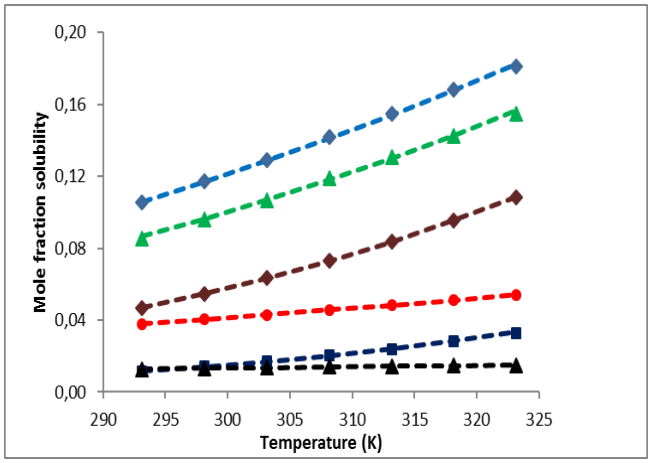

Figure 3. Variation of mole fraction solubilities (x_i) with temperature (T) for alloxan in different studied solvents. Methanol (♦), ethanol (▲), water (●), ethane-1, 2-diol (■), THF (♦), acetone (▲). Dashed lines represent calculated mole fraction solubilities by Buchowski-Ksiazczak equation

These values are listed in Tables 3 and 4 for Apelblat and Buchowski–Ksiazczak models respectively.

From these solubility data, some thermodynamic parameters such as enthalpies of solution (ΔH_{sol}), Gibb's energy of dissolution (ΔG_{sol}) and entropy of solutions (ΔS_{sol}) have also been evaluated. The enthalpies of solution (ΔH_{sol}) was calculated by modified van't Hoff equation, i.e., from the slope of the plot of ln$x$ versus ($1/T$ - $1/T_{hm}$).

Table 3. Parameters *A*, *B* and *C* of Apelblat model in studied solvents

Parameters	*A*	*B*	*C*	10^2 *RMSD*	10^2 *ARD*
Methanol	76.1403	-5030.5957	-10.7785	0.0146	-0.0533
Ethanol	106.5523	-6563.97	-15.2482	0.0233	-0.0003
Ethane-1,2-diol	241.2325	-14029.2250	-34.8287	0.0085	0.0734
Water	-2.2895	-992.8372	0.4225	0.0065	-0.0346
THF	180.4289	-10624.1830	-25.9236	0.0125	0.0604
Acetone	-3.4772	-450.6254	0.1161	0.0053	-0.0096

**ARD*=average relative deviation, *RMSD*=root mean square deviation

Table 4. Parameters of Buchowski-Ksiazczak λ*h* equation in the studied solvents

Parameters	λ	*h*	10^2*RMSD*	10^2*ARD*
Methanol	1.4234	1204.997	0.0762	-0.0084
Ethanol	1.4710	1272.619	0.0955	-0.0017
Ethane-1,2 diol	1.7522	1890.145	0.0326	-0.0562
Water	0.2071	5423.384	0.0115	-0.2255
THF	2.5826	1025.290	0.0897	-0.0345
Acetone	0.0270	18197.910	0.0039	-0.0929

**ARD*=average relative deviation, *RMSD*=root mean square deviation

$$\left[\frac{\partial \ln x_i}{\partial\left[\frac{1}{T}-\frac{1}{T_m}\right]}\right]_p = -\frac{\Delta H_{sol}}{R} \qquad (6)$$

where

T is the experimental temperature, and

R is gas constant.

T_{hm} is the mean harmonic temperature

T_{hm} is is given as

$$T_{hm} = \frac{n}{\sum_{i=1}^{n}\frac{1}{T}} \qquad (7)$$

where n is the number of experimental temperatures.

In the present case, the T_{hm} value obtained is only 307.83 K. From the intercepts of these plots, Gibbs energy change (ΔG_{sol}) for the solubility process was evaluated by the following relation:

$$\Delta G_{sol} = -RT_{hm}\ \text{intercept} \qquad (8)$$

Using these evaluated ΔH_{sol} and ΔG_{sol} values, the entropies of solutions (ΔS_{sol}) were obtained from the following equation:

$$\Delta S_{sol} = \frac{\left(\Delta H_{sol} - \Delta G_{sol}\right)}{T_{hm}} \qquad (9)$$

Table 5 summarizes these thermodynamic parameters. It is found that enthalpy of dissolution (ΔH_{sol}) is positive for all the solvents indicating the thereby endothermic behavior of dissolution.

Table 5. Thermodynamic parameters: Enthalpy of dissolution (ΔH_{sol}), Gibbs's Energy (ΔG_{sol}) and Entropy (ΔS_{sol}) of dissolution of alloxan in different studied solvents

Solvent	ΔH_{sol} kJ mol^{-1}	ΔG_{sol} kJ mol^{-1}	ΔS_{sol} J mol^{-1} K^{-1}
Methanol	14.2502	5.0260	29.9640
Ethanol	15.5638	9.8789	47.3505
Ethane-1,2 diol	27.5526	10.0150	56.9030
Water	9.3283	7.9160	4.5880
THF	22.0155	6.7260	49.6690
Acetone	4.0431	10.9410	22.4080

This suggests that there may be strong interactions between drug and solvent molecules that those between the solvent molecules and the newly formed bond energy between drug and solvent molecule is not powerful enough to compensate the energy needed for breaking the original association bond in various solvents.[15] The Gibbs energy of dissolution (ΔG_{sol}) is positive for the studied solvents suggesting that the dissolution process is spontaneous. Further, the order of ΔG_{sol} values is the reverse of solubility data. The Gibb's energy of dissolution is minimum for methanol and maximum for acetone whereas solubility is maximum for methanol and minimum for acetone. Further, the entropy of dissolution (ΔS_{sol}) is found to be positive in all the solvents. The positive entropy change indicates that the entropy of solubilization is unfavorable for the solute in solution.[14] The entropy depends on the functional groups present in the drug as well as in the solvent. Owing to the Alloxan molecule containing groups of different nature like –NH-, -C=O, there may exist various forces such as electrostatic force, hydrogen bond, hydrophobic interaction and stereoscopic effect in the dissolving process.

Conclusion

In protic solvents, solubility is maximum in methanol and minimum in ethane-1,2-diol. The order of solubility is: methanol > ethanol >water > ethane-1,2-diol. In the selected nonprotic solvents, solubility is greater in THF than in acetone. The positive Gibb's energy and enthalpy of dissolution suggest dissolution process be endothermic and spontaneous.

References

[1]Abdel-Barry, J. L., Abdel-Hassan, I. A., Al-Hakiem, M. H.: Hypoglycemic and anti-hyperglycemic effects of Trigonella foenumgraecum leaf in normal and alloxan induced diabetic rats. *J. Ethnopharmacol*., **1997**, *58*, 149-155. https://doi.org/10.1016/S0378-8741(97)00101-3

[2]Beach, E. F., Turner, J. J., An enzymatic method for glucose determination in body fluids. *Clin. Chem*. **1958**, *4*, 462-465.

[3]El-Mekkawy, S., Meselhy, M.,Nakamura, N., Tezuka, Y., Hattori, M., Kakiuchi, N., Shimotohno, K., Kawahata, T., Otake, T., Anti-HIV-1 and anti-HIV-1-protease substances from Garnoderma lucidum. *Phytochemistry*. **1998**, *49*, 1651-1657 (1998). https://doi.org/10.1016/S0031-9422(98)00254-4

[4]Obiudu, I. K., Okolie, A. C., Agbafor, N. K., Obiudu, C. V., Anti-Diabetic Property and Phytochemical Composition of Aqueous and Methanol Extracts of Buchholzia coriacea Seeds in Alloxan-Induced Diabetic Rats, *J. Med. Sci.*, **2015**, *15*, 241-245. https://doi.org/10.3923/jms.2015.241.245

[5]Eo, S. K., Kim, Y. S., Lee, C. K., Han, S. S., Possible mode of antiviral activity of acidic protein bound polysaccharide isolated from Ganoderma lucidum on herpes simplex viruses, *J. Ethnopharmacol*., **2000**, *72*, 475-481. https://doi.org/10.1016/S0378-8741(00)00266-X

[6]Lenzen, S., The mechanisms of alloxan- and streptozotocin-induced diabetes, *Diabetologia*, **2008**, *51*, 216–226. https://doi.org/10.1007/s00125-007-0886-7

[7]Lipinski, A. C., Lombardo, F., Dominy, B.W., Feeney, J. P., Experimental and computational approaches to estimate solubility and permeability in drug discovery and development settings. *Adv. Drug Delivery Rev.*, **2012**, *64*, 4-17. https://doi.org/10.1016/j.addr.2012.09.019

[8]Bodor, N., Harget, A., Huang, M.: Neural network studies: I Estimation of the Aqueous solubility of organic compounds. *J. Am. Chem. Soc*., **1991**, *113*, 9480-9483. https://doi.org/10.1021/ja00025a009

[9]Pico, Y., Andreu, V., *Anal. Bioanal. Chem*., 2007, 387, 1287-1299. https://doi.org/10.1007/s00216-006-0843-1

[10]Baluja, S., Bhalodia, R., Gajera, R., Vekariya, N., Bhatt, M., Solubility of difloxacin in acetone, methanol, and ethanol from (293.15 to 313.15) K. *J. Chem. Eng. Data*., **2009**, *54*, 1091-1093. https://doi.org/10.1021/je800742d

[11]Zhao, Y., Wang, Y., Measurement and correlation of solubility of tetracycline hydrochloride in six organic solvents. *J. Chem. Thermodyn.*, **2013**, *57*, 9-13. https://doi.org/10.1016/j.jct.2012.08.007

[12]Bhesaniya, K. D., Chavda, K. V., Sadhu, C. H., Baluja, S., Thermodynamic characteristics of solutions of ornidazole in different organic solvents at different temperatures. *J. Mol. Liq.*, **2014**, *191*, 124–127. https://doi.org/10.1016/j.molliq.2013.12.001

[13]Apelblat, A., Manzurola, E., Solubility of oxalic, malonic, succinic, adipic, maleic, malic, citric, and tartaric acids in water from 278.15 to 338.15 K. *J. Chem. Thermodyn*., **1987**, *19*, 317-320. https://doi.org/10.1016/0021-9614(87)90139-X

[14]Buchowski, H., Ksiazczak, A., Pietrzyk, S.: Solvent activity along a saturation line and solubility of hydrogen-bonding solids. *J. Phys. Chem*., **1980**, *84*, 975-979. https://doi.org/10.1021/j100446a008

[15]Panteli, E. K., Voutsas, E. K., Solubilities of cinnamic acid esters in ionic liquids. *J. Chem. Eng. Data*, **2009**, *54*, 812-818. https://doi.org/10.1021/je800596c

Received: 02.04.2017.
Accepted: 11.06.2017.

SYNTHESIS OF TETRAHYDROBENZO[*b*]PYRAN DERIVATIVES USING THIAMINE HYDROCHLORIDE (VB_1) AS A GREEN CATALYST

Devidas S. Bhagat,[a] Jagadish L. Wawre,[b] Ashok R. Yadav,[b] Pintu G. Pathare,[b] Laszlo Kotai[c] and Rajendra P. Pawar[b]*

Keywords: Thiamine hydrochloride (VB_1), green approach, tetrahydrobenzo[*b*]pyran derivatives.

An environmentally safer synthesis of 2-amino-tetrahydro-4H-chromenes derivatives using vitamin B_1 was achieved by one pot synthesis. In this reaction condensation of various aromatic aldehydes, malononitrile and dimedone at room temperature without addition of any other catalyst has been done. The desired products can be separated directly from the reaction mixture with high purity. This synthetic method is inexpensive, efficient, as well as eco-friendly.

*Corresponding Authors
Tel: +91 0240 2334577; Fax: +91 0240- 2334430.
E-Mail: rppawar@yahoo.com
[a] Department of Forensic Chemistry Government institute of forensic science, Aurangabad-431001, Maharashtra, India
[b] Department of Chemistry, Deogiri College, Station Road, Aurangabad-431005, Maharashtra, India
[c] Research Centre for Natural Sciences, Hungarian Academy of Sciences, P. O. Box 17, HU-1525, Budapest, Hungary

Introduction

Multi-component reactions (MCRs) is an important tool for efficient synthesis of wide variety of heterocycle's such as tetrahydrobenzo[*b*]pyran as its derivatives belong to a major class of natural products. In recent decades tetrahydrobenzo[*b*]pyran and their derivatives have attain considerable attention of scientist community due to their wide range of biological and pharmacological properties such as HA 14-1, MX58151 and rhodomyrtone.

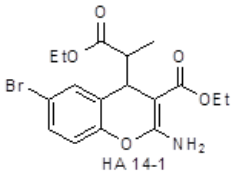

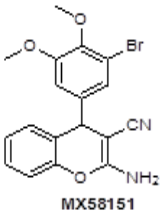

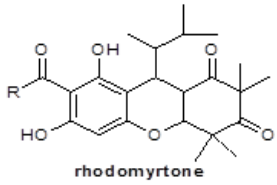

Tetrahydrobenzo[*b*]pyran constitutes the structural unit of a series of natural products. These derivatives can be employed as potent antibacterial such as rhodomyrtone pigments, photoactive materials, etc.[1] The derivatives of tetrahydrobenzo[*b*]pyran showing biological properties as antioxidant[2] spasmolytic and anti-HIV,[3] anticancer,[4] diuretic[5] and anti-anaphylactic activities[6] also widely used in cosmetics, pigments and utilized as potential biodegradable agrochemicals,[7] antibacterial,[8] molluscicidal[9] anti-coagulant and Parkinsons disease,[10] photoactive materials,[11] etc. Several techniques have been reported for the synthesis of 2-aminotetrahydro-4H-chromene derivatives, such as microwave,[12] reflux,[13] ultrasonication,[14] electrochemical synthesis[15] and green synthesis.[16] Realizing the importance of 4H-pyran derivatives, in recent decades various methods has been reported for the synthesis of 4H-benzo[*b*]pyran with the aim of obtaining more biologically potent heterocyclic systems using different catalysts via three-component condensations including the use of amino functionalized silica gel,[17] ionic liquids,[18] Nano-ZnO,[19] hexadecyltrimethyl ammonium bromide,[20] iodine,[21] 2,2,2-trifluoroethanol,[22] $BF_3.OEt_2$,[23] 4-amino-1-(2,3-dihydroxy-propyl)pyridinium salts,[24] SiO_2 NPs,[25] NaBr,[26] triethylene-tetraammonium trifluoroacetate[27] and $PhB(OH)_2$,[28] etc. Herein we synthesized tetrahydrobenzo[*b*]pyran derivatives by condensing various aromatic aldehydes, malononitrile and dimedone at room temperature in presence of vitamin B_1 as catalyst.

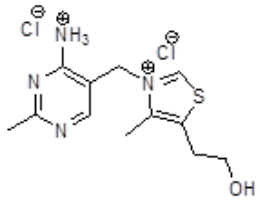

Thiamine hydrochloride (VB_1)

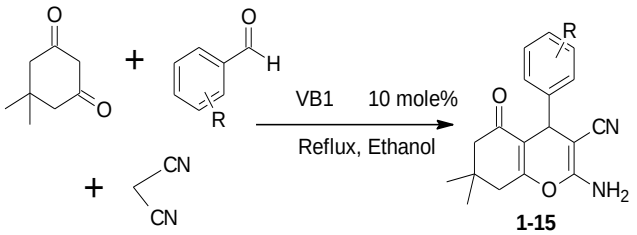

Scheme 1. Synthesis of tetrahydrobenzo[*b*]pyran derivatives by using thiamine hydrochloride (VB_1)

 DOI: 10.17628/ecb.2017.6.211-214

Table 1. Synthesized of 2-amino-5,6,7,8-tetrahydro-7,7-dimethyl-5-oxo-4-phenyl-4H-chromene-3-carbonitrile derivatives

Entry	Aldehydes	Time , min	Yield, %	Melting point, ^{O}C	Ref. No.
1	4-Chlorobenzaldehyde	15	90	211-213	[22]
2	4-Hydroxybenzaldehyde	20	85	205-207	[25]
3	Furan-2-carboxaldehyde	15	92	228-230	[27,28]
4	4-Nitrobenzaldehyde	10	96	193-195	[22]
5	4-Bromobenzaldehyde	10	94	193-195	[22,27,29]
6	4-Methoxybenzaldehyde	20	88	197-199	[25,29]
7	2-Nitrobenzaldehyde	10	91	225-228	[1]
8	4-Methylbenzaldehyde	15	88	208-210	[22,29]
9	4-Cyanobenzaldehyde	10	95	220-222	[24]
10	Benzaldehyde	15	90	220-222	[24,28]
11	3,4-dimethoxybenzaldehyde	15	85	168-170	[25]
12	3-Nitrobemzaldehyde	10	94	206-209	[25,28,29]
13	4-(trifluoromethyl)benzaldehyde	10	92	235-237	[29]
14	3-Bromobenzaldehyde	20	92	225-227	[25]

Table No. 2: Study of effect of catalyst and solvents on yield of product

	Catalyst	Temperature	Solvent	Time	Yield (%)	Reference
1	2,2,2-Trifluoroethanol	Reflux	--	5 h	90	[Khaksar S., *et al.* (2012)][22]
2	BF_3OEt_2	Reflux	Ethanol	2 h	85-90	[Sethukumar A., *et al.* (2012)][23]
3	4-Amino-1-(2,3-dihydroxy propyl) pyridinium hydroxide [ADPPY] [OH]	60-65 °C	Ethanol	48 h	87	[Salvi P. P., *et al.* (2011)]][24]
4	Triethylenetetraammonium-trifluoro acetate	Reflux	Ethanol	10 min	57-90	[Zheng J., et al. (2011)]][27]
5	$PhB(OH)_2$	Reflux	Ethanol-water	10-60 min	42-95	[Nemouchi S., *et al.* (2012)]][28]
6	Thiamine hydrochloride	Reflux	Ethanol	10-30 min	87-96	Present work

Materials and methods

All the chemicals were of commercial grade reagent; purchased from Spectrochem and Sigma aldrich chemical companies in high purity, used without further purification. Melting points were determined in open capillaries visual melting point apparatus. Infrared (IR) spectra in KBr were recorded using a Perkin-Elmer FT-IR spectrometer 65. ^{1}H NMR spectra were recorded on 400 MHz FT-NMR spectrometer in $CDCl_3$ as a solvent and chemical shift values are recorded in units δ (ppm) relative to tetramethylsilane (Me_4Si) as an internal standard. The progress of reactions was monitored on TLC (Thin Layer Chromatography).

General procedure for the synthesis of tetrahydrobenzo[*b*]pyran derivatives

In 25 mL round bottom flask a mixture of appropriated amount of aromatic aldehydes (1 mmol), malononitrile (1.3 mmol), dimedone (1 mmol) and catalyst VB_1 10 mol %, in ethanol (5 mL) was refluxed for appropriated time. The progress of reaction was monitored on TLC. On completion of reaction, the mixture was cooled to room temperature; the crude product was filtered off and washed with water to remove (the catalyst because it is water soluble).

The resulting solid was recrystalized in ethanol to obtain pure tetrahydrobenzo[*b*]pyran derivative. Similarly other derivatives were also prepared as mentioned in Table1.

Spectral analysis of some tetrahydrobenzo[*b*]pyran derivatives:

3e: 2-amino-4-(4-bromophenyl)-5,6,7,8-tetrahydro-7,7-dimethyl-5-oxo-4H-chromene-3-carbonitrile

White solid; yield 95%; mp 220-222°C; Recrystallised from ethanol; IR (KBr) 1422, 2193, 2231.2, 2967, 3224, 3382 cm^{-1}: H1 NMR (CDCl3) 1.00-1.20 (s, 6H), 2.5 (s, 2H), 3.50 (s, 2H), 4.3 (s, 1H), 6.2 (d, 2H), 7.3 (d, 2H), 8.02 (s, 2H) ∂ (ppm).

3j: 2-amino-4-(4-cyanophenyl)-5,6,7,8-tetrahydro-7,7-dimethyl-5-oxo-4H-chromene-3-carbonitrile

White solid; yield 95%; m.p. 220-222°C; Recrystallised from ethanol; IR (KBr) 1422, 2193, 2231.2, 2967, 3224, 3382 cm^{-1}: H^1 NMR ($CDCl_3$) 1.00-1.20 (s, 6H), 2.5 (s, 2H), 3.50 (s, 2H), 4.3 (s, 1H), 6.2 (d, 2H), 7.3 (d, 2H), 8.02 (s, 2H) ∂ (ppm)

Results and discussion

In order to optimize the reaction condition for solvents temperature and yield; the reaction was carried out under various conditions and the results are listed in Table 2. In an optimized reaction conditions, a mixture of dimedone **a** (1 mmol), malononitrile **c** (1.3 mmol), and 4-nitrobenz aldehyde **b** (1 mmol) in ethanol (5 mL) was mixed with 10 mol % thiamine hydrochloride and refluxed for 30 minutes. The reaction proceeds very cleanly at 50-60 ^{0}C temperature and was free of side products. After completion of the reaction as monitored on TLC and simple workup it affords the products in excellent yields (Scheme 1). Among the solvents tested, the reaction in DCM, acetonitrile, chloroform, DMF, DMSO, methanol and ethanol in catalyst free condition gaves poor yield of products. Whereas, in ethanol it affords quite good yield of product **(**Table2 entry 1 to 7); but the reaction required 120 minutes time for completion under reflux condition. In evaluation of catalyst concentration using ethanol as a solvent, 10 mol % of catalyst affords excellent yield of products (Table 2, entry 8 to 13). Further increase in catalyst concentration and temperature does not affect the yield and reaction time of completion. Optimization of temperature of reaction, the reaction was reflux at room temperature, 30, 40, 50, 60 and 70 ^{0}C using 10 mol % of the catalyst gave excellent yield at 50-60 ^{0}C of the desired product (Table 2 entry 14-15).

In order to show generality and scope of this new protocol, we used various substituted aromatic aldehydes and the results obtained are summarized in Table 1. The electron donating aromatic aldehydes gives low yield of products as compared to electron withdrawing substituted aldehydes. The electron withdrawing aldehydes required less time for completion of reactions (Table 1).

Optimization of several conditions like solvent, catalyst concentration and temperature has been also studied as reported in **(**Table 3**)**.

Plausible reaction mechanism

The thiamine hydrochloride (VB_1) was acts as Bronsted-Lowry acid (proton donor)[29]. Malanonitrile and dimedone undergo tautomerism **1** to **2** and **3** to **4**. The dimedone **4** on cross Aldol condensation with aromatic aldehydes **5** gives intermediate **6**, which on E_1cb elimination gives intermediate **7**. The intermediate **7** on Michael addition with **2** gives intermediate **9**. The intermediate **9** on rearrangement and cyclization gives desired product 2-amino-5,6,7,8-tetrahydro-7,7-dimethyl-5-oxo-4-phenyl-4H-chromene-3-carbonitrile **10**.

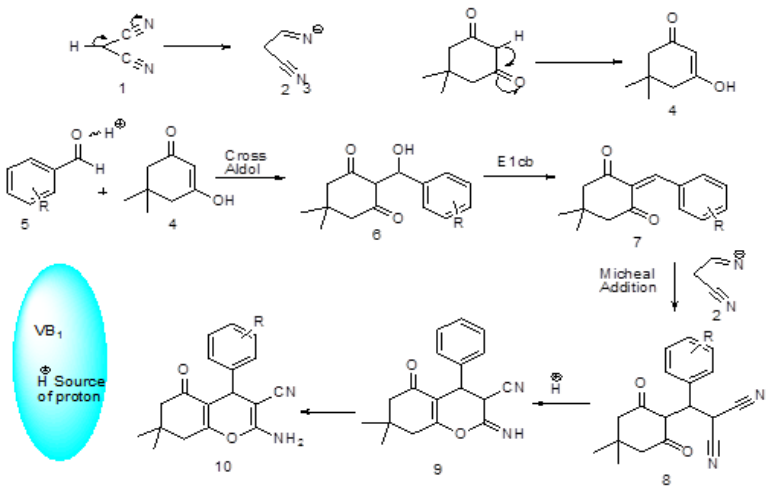

Conclusion

In conclusion, thiamine hydrochloride (VB_1) has been used as an efficient and eco-friendly catalyst for the synthesis of 2-amino-5,6,7,8-tetrahydro-7,7-dimethyl-5-oxo-4-phenyl-4H-chromene-3-carbonitrile derivatives. As the catalyst (VB_1) is water soluble; it can be easily separated and reused after evaporation of water. Simple work-up procedure, shorter reaction time, mild reaction condition and excellent yields makes this methodology to be efficient.

Acknowledgment

We are great thankful to the Department of Chemistry, Deogiri College, Aurangabad for providing laboratory facilities and the permission to use facility the Central Research Laboratories. Council of Science and Industrial Research (CSIR), New Delhi (110012) for financial support under Junior Research Fellowship

References

[1]Boumoud, B., Yahiaoui, A.A., Boumoud, T., Debache, A., *J. Chem. Pharm. Res.*, **2012**, *4*, 795.

[2]Bonsignore, L., Loy , G., Secci, D., Calignano, A., *Eur. J. Med. Chem.*, **1993,** *28,* 517.https://doi.org/10.1016/0223-5234(93)90020-F

[3]Deng, J.Z., Sun, D.A., Starck, S.R., Hecht, S.M., Cerny, R. L., Engen, J. R., *J. Chem. Soc*., **1999**, 1147.

[4]Singh, K., Singh H., Singh, J., *Tetrahedron*, **1996**, *52*, 14273. https://doi.org/10.1016/0040-4020(96)00879-4

[5]Abd El-Rahman N. M., Borik, R. M., *World Appl. Sci. J.*, **2014**, *31*, 01.

[6]Pore D. M., Undale, K.A., Dongare, B.B., Desai, U.V., *Catal. Lett*., **2009**, *132*, 104.https://doi.org/10.1007/s10562-009-0074-0

[7]Sabitha, G., Arundhathi, K., Sudhakar, K., Sastry, B.S., Yadav, J.S., *Synth. Comm*., **2009**, *39*, 433. https://doi.org/10.1080/00397910802378399

[8]Kumar, R. R., Perumal, S., Senthilkumar, P., Yogeeswari, P., Sriram, D., *Bioorg. Med. Chem. Lett*., **2007**, *17*, 6459. https://doi.org/10.1016/j.bmcl.2007.09.095

[9]Abdelrazek, F. M., Metz, P., Kataeva, O., Jager, A., El-Mahrouky, S. F., *Arch. Pharm.*, **2007,** *340*, 543. https://doi.org/10.1002/ardp.200700157

[10]Bonsignore, L., Loy, G., Secci, D., Calignano, A., *Eur. J. Med. Chem.*, **1993**, *28*, 517-520. https://doi.org/10.1016/0223-5234(93)90020-F

[11]Armesto, D., Horspool, W.M., Martin, N., Ramos, A., Seoane, C., *J. Org. Chem*., **1989**, *54*, 3069. https://doi.org/10.1021/jo00274a021

[12]Hoz, D.L., Antonio, A., Diaz-Ortiz, Moreno, A., Sanchez-Migallon, A., Prieto, P., Jose, C. R., Vazquez, E., Gomez, M. V., Herrero, M.A., *Comb. Chem. High Throughput Screen*. **2007**, *10*, 877.https://doi.org/10.2174/138620707783220347

[13]Ziarani, G.M., Abbasi, A., Badiei, A., Aslani, Z., *E-J. Chem*., **2011**, *8*, 293.https://doi.org/10.1155/2011/367613

[14]Shujiang, T., Hong, J., Qiya, Z., Chunbao, M., Daqing, S., Xiangshan, W., Yuan, G., *Chin. J. Org. Chem*., **2003**, *23*, 488.

[15]Makarem, S., Mohammadi, A.A., Fakhari, A.R., *Tetrahedron Lett*., **2008**, *49*, 7194. https://doi.org/10.1016/j.tetlet.2008.10.006

[16]Zhao-Qin, J., Shun-Jun, J., Jun, L., *Chin. J. Chem*., **2005**, *23*, 1085. https://doi.org/10.1002/cjoc.200591085

[17]Joshi V. M., Magar R. L., Throat P. B., Tekale S. U., Patil B. R., Kale M. P. and**,** Pawar R. P., *Chin. Chem. Lett.*, **2014,** *25(3)*, 455, https://doi.org/10.1016/j.cclet.2013.12.016.

[18]Lian, X.Z., Huang, Y., Li, Y.Q., Zheng, W.J., *Monatsh. Chem*., **2008**, *139*, 129.https://doi.org/10.1007/s00706-007-0706-2

[19]Tekale S., Kauthale S., Jadhav K. and Pawar R., *J. Chem.*, **2013,** http://dx.doi.org/10.1155/2013/840954

[20]Jin, T.S., Liu, L.B., Zhao, Y., Li, T.S., *Synth. Comm*., **2005**, *35*, 1859. https://doi.org/10.1081/SCC-200064898

[21]Bhosale R. S., Magar C. V., Solanke K. S., Mane S. B., Choudhary S. S. and Pawar R. P., *Synth. Commun.*, **2007,** *37*, 4353. http://dx.doi.org/10.1080/00397910701578578.

[22]Khaksar, S., Rouhollahpour, A., Talesh, S. M., *J. Fluorine Chem*., **2012**, *141*, 11.https://doi.org/10.1016/j.jfluchem.2012.05.014

[23]Sethukumar, A., Vithya, V., Udhaya Kumar, C., Arul Prakasam, B., *J. Mol. Struct*., **2012**, *1008*, 8. https://doi.org/10.1016/j.molstruc.2011.11.003

[24]Salvi P.P., Mandhare A.M., Sartape A.S., Pawar D.K., Han H.S., Kolekar S.S., *C. R. Chim.*, **2011**, *14*, 878–882.

[25]Banerjee, S., Horn, A., Khatri, H., Sereda, G., *Tetrahedron Lett*., **2011**, *52*, 1878.https://doi.org/10.1016/j.tetlet.2011.02.031

[26]Devi, I., Bhuyan, P.J., *Tetrahedron Lett*., **2004**, *45*, 8625. https://doi.org/10.1016/j.tetlet.2004.09.158

[27]Zheng, J., Li, Y., *Mendeleev Commun*., **2011**, *21*, 280.https://doi.org/10.1016/j.mencom.2011.09.017

[28]Nemouchi, S., Boulcina, R., Carboni, B., Debache, A., *Compt. Rend., Chimie*, **2012**, *15*, 394. https://doi.org/10.1016/j.crci.2012.01.003

[29]Lei, M., Ma, L., Hu, L., *Tetrahedron Lett*., **2010**, *51*, 4186.https://doi.org/10.1016/j.tetlet.2010.06.005

Received: 15.05.2117.
Accepted: 16.06.2017.

IMPROVED SYNTHESIS OF 5-ARYL-2-THIOXOIMIDAZOLIDIN-4-ONES FROM ARYLGLYOXAL HYDRATES

Vasiliy Georgievich Shtamburg,[a]Andrey Alexandrovich Anishchenko,[b]Victor Vasilievich Shtamburg,[a]Alexander Vladimirovich Mazepa,[c] Svetlana Vladimirovna Kravchenko[d] and Evgeniy Alexandrovich Klots[e]

Keywords:arylglyoxals, thiourea,5-aryl-2-thioxoimidazolidin-4-ones, synthesis, condensation.

A new kind of 5-aryl-2-thioxoimidazolidin-4-ones synthesis by condensation of arylglyoxal hydrates with thiourea in acetic acid solution at room temperatures has been developed.

*Corresponding Authors
Tel: +380-68-410-41-79
E-Mail: koloxai@gmail.com
[a] 49038 Ukraine, Dnepr, Mostovayast., 2/6. UkrainianStateUniversityof Chemical Technology
[b] 49010 Ukraine, Dnepr, Armeyskayast. 22b. O. GoncharDnepropetrovskNational University
[c] 65063 Odessa, Armeyskayast. 21 .107. A.V. BogatskyPhysiko-Chemical Institute of NAS ofUkraine
[d] 49038 Ukraine, Dnepr, Efremovast., 25. DnepropetrovskStateAgrarian-Ecomomic University
[e] 25006 Ukraine, Kropivnitsky, Shevchenko st., 1. V. VinnichenkoKirovograd State Pedagogical University

INTRODUCTION

Firstly 5-phenyl-2-thioxoimidazolidin-4-one (**1a)** had been synthesized from phenylglyoxal hydrate by interaction with thiourea in aqueous solution at room temperatures.[1] But in this work 5-phenyl-2-thiohydantoin (**1a)** structure of the condensation product no had been established by the author, only it has relevant of the data of the elemental analysis.[1] Only recently the strictly evidence that phenylglyoxal hydrate interaction with thiourea acetic acid solution at 100ºC yielded **1a** had been done[2] (Scheme 1). A structure of compound **1a** is consistent with data of ^{1}H and ^{13}C NMR spectra and mass-spectrum.[2] Also, it was shown that phenylglyoxal hydrate condensed with N-arylthioureas and N-arylureas yielding 1-aryl-5-phenylthiohydantoins (**2a)** and 1-aryl-5-phenylhydantoins (**2b)** (1,5-diarylimidazolidine-2,4-diones),[3,4] respectively, in the presence of polyphosphoric acid at microwave irradiation in the absence of solvent (Scheme 1). But this method needs using of large amounts of polyphosphoric acid (or "polyphosphoric ester"[3]) and is appreciable only for synthesis of small amounts of 1-aryl-5-phenylthiohydantoins.

It must be noted that arylglyoxals hydrates condense with N-arylthioureas (boiling acetic acid, 4 h) and N,N'-bisarylthioureas (boiling acetic acid, 6 h) in hydrochloric acid presence yielding 1,5-diarylthiohydantoins (**2a)** and 1,3,5-triarylthiohydantoins (**3a),**[4,5] respectively (Scheme 1).

In the same conditions, arylglyoxals react with N-arylureas and N,N'-bisarylureas yielding 1,5-diarylhydantoins (**2b)** and 1,3,5-triarylhydantoins (**3b),**[5] respectively.

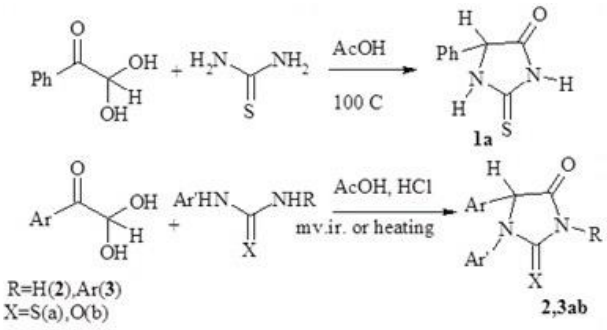

Scheme 1.

Also, it must be noted that 1,5-diarylhydantoins (**2b)** had also been prepared by arylglyoxals condensation with N-arylureas in the presence of hydrochloric acid and acetic acid in boiling ethanol for 4 h.[6]

It is obviously that 1-aryl-5-arylthiohydantoins formation from arylglyoxals hydrates and thiourea takes place in the presence of strong acid[3-5] or in boiling acetic acid solution.[2] But the course of this reaction in acetic acid media at room temperatures has not been studied.

Recently we had shown that arylglyoxals hydrates reacted with N-hydroxyurea in neutral aqueous solution in three stages (Scheme 2) yielding 3-hydroxy-5-arylimidazolidine-2,4-diones (**6)** as final products.[7] Some intermediate products, **4** and **5a-5b** of stages I and II had also been isolated. But in acetic acid media arylglyoxals condense with N-hydroxyurea and N-alkoxyureas selectively forming 5-aryl-3-hydroxyimidazolidine-2,4-diones (**6)** and 3-alkoxy-5-arylimidazolidine-2,4-diones (**7),** respectively at room temperatures[8] (Scheme 3).

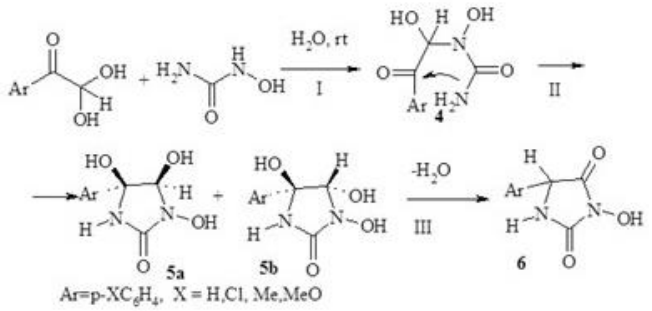

Scheme 2.

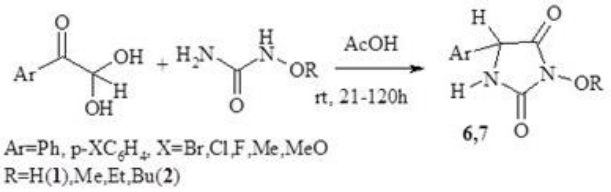

Scheme 3.

Phenylglyoxal hydrate reacts with N-tert-butyl-thiadiazol-2-yl-N'-metylurea in EtOH–H_2O solution in the presence of NaOH yielding cis- and trans-diastereomer 4,5-dihydroxyimidazolidin-2-ones (**8a,b**)[9] (Scheme 4). In the presence of TsOH or oxalic acid compounds **8a,b** transform in hydantoin **9** in boiling MeCN.

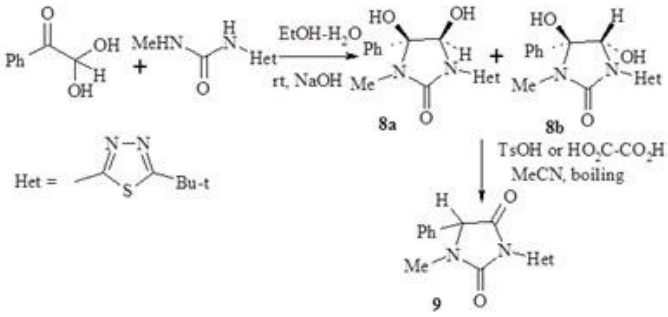

Scheme 4.

It might be possible that arylglyoxals hydrates could react with thiourea yielding proper 5-aryl-2-thioxoimidazolidin-4-one (5-aryl-2-thiohydantoins) in mild conditions. Heating of reaction mixture, the presence of strong acids or microwave irradiation are not conditions for 5-aryl-2-thiohydantoins forming from arylglyoxals hydrates and thiourea.

This work aim is devoted to further exploration of arylglyoxals hydrates interaction with thiourea in media of acetic acid at room temperatures.

EXPERIMENTAL

^{1}H and ^{13}C NMR spectra were recorded on VARIAN JEMINI 400 spectrometer (400 and 100 MHz, respectively); solvent: $(CD_3)_2SO$, with TMS as internal standard. Mass spectra were recorded on VG 70-70EQ mass spectrometer in fast atom bombardment (FAB) mode. The solvents were purified and dried according to standard procedures. Used acetic acid was glacial.

5-Phenyl-2-thioxoimidazolidin-4-one (1a).

A mixture of phenylglyoxal hydrate (405 mg, 2.661 mmol), thiourea (253 mg, 3.326 mmol) and AcOH (10 mL) was stirred at 18-19°C for 10 min, maintained 18-19°C for 112 h, then formed crystal precipitate was filtered off, washed by AcOH (3 mL) and dried under vacuum 3 Torr, yielding (198 mg, 38.7%) 5-phenyl-2-thioxoimidazolidin-4-one (**1a)**, white crystals, m.p. 217 – 219 °C, after crystallization m.p. 218 – 219 °C (THF – C_6H_{14})(cf. m.p. 225°C (EtOH)[1], 188 – 189[2]). ^{1}H NMR spectrum, 400 MHz, $(CD_3)_2SO$, δ, ppm, (*J*, Hz): δ = 5.40 (1H, s, CH); 7.28 (2H, d, ^3J = 7.2, $H^{2,6}$ Ph); 7.36 – 7.40 (1H, m, H^4Ph); 7.41 – 7.45 (2H, m, $H^{3,5}$Ph); 10.51 (1H, s, NH); 11.88 (1H, s, NHC(O)), cf.[2]. ^{13}C NMR spectrum, 100 MHz, $(CD_3)_2SO$, δ, ppm: δ = 63.8 (CH Hydantoin); 126.6 (C-3, C-5 Ph); 128.5 (C-4 Ph) 128.8 (C-2, C-6 Ph); 134.4 (C-1, Ph); 174.7 (C=O); 182.8 (C=S) cf.[2]. Mass spectrum, *m/z*, (I_{rel}%): 193 $[M+H]^+$ (100). Anal. Calcd. for $C_9H_8N_2OS$ in %: C 56.23, H 4.19 , N 14.57. Found: C 56.08, H 4.32, N 14.37. Combined AcOH-filtrate was evaporated under vacuum 4 Torr at 25-30 °C, the residue was washed by cold water (8 ml), crystallized from THF – C_6H_{14}, dried under vacuum 4 Torr at 15 °C, additionally yielding (257 mg, 50.2%) **1a**.

5-(4'-Bromophenyl)-2-thioxoimidazolidin-4-one (1b).

A solution of 4-bromophenylglyoxal hydrate (352 mg, 1.522 mmol) in AcOH (15 mL) was added to mixture of thiourea (145 mg, 1.902 mmol) and AcOH (10 mL) at 18°C, the reaction mixture was stirred 1 h, then it was maintained at 18°C for 20 h, the solvent was evaporated under vacuum 3 Torr at 25–30 °C. The residue was washed by cold water (10 mL), dried under vacuum 3 Torr, yielding (365 mg, 88%) 5-(4'-bromophenyl)-2-thioxoimidazolidin-4-one (**1b)**, white crystals, mp. 204 – 205 °C (THF–C_6H_{14}). ^{1}H NMR spectrum, 400 MHz, $(CD_3)_2SO$, δ, ppm, (*J*, Hz): δ = 5.42 (1H, s, CH); 7.24 (2H, d, ^3J = 8.4, $H^{2,6}C_6H_4$); 7.64 (2H, d, ^3J = 8.4, $H^{3,5}C_6H_4$); 10.51 (1H, s, NH); 11.91 (1H, s, NHC(O)). ^{13}C NMR (100 MHz, $(CD_3)_2SO$,) δ = 63.2 (CH Hydantoin), 121.7 (C-4, C_6H_4Br), 128.7, 131.7 (C-2, C-6, C-3, C-5, C_6H_4Br), 133.8 (C-1, C_6H_4Br), 174.3 (C=O), 182.9 (C=S). Mass spectrum, *m/z*, (I_{rel}, %): 273 $[M+H]^+$ (57), 271 $[M+H]^+$ (53), 91 (69), 72 (100). Anal. Calcd. for $C_9H_7BrN_2OS$ in %: C 39.87, H 2.60 , N 10.33. Found: C 39.89, H 2.95, N 10.24.

5-(4'-Chlorophenyl)-2-thioxoimidazolidin-4-one (1c)

A solution of 4-chlorophenylglyoxal hydrate (158 mg, 0.846 mmol) in AcOH (12 mL) was added to mixture of thiourea (80 mg, 1.048 mmol) and AcOH (5 mL) at 17°C, the reaction mixture was stirred for 30 min, then it was maintained at 17°C for 46 h, the solvent was evaporated under vacuum 3 Torr at 25 – 27°C. The residue was washed by cold water (8 mL), dried under vacuum 3 Torr, yielding (180 mg, 94%) 5-(4'-chlorophenyl)-2-thioxoimidazolidin-4-one (**1c)**, yellow crystals, m.p. 209 – 211 °C (with decomp.) (THF – C_6H_{14}). ^{1}H NMR spectrum, 400 MHz, $(CD_3)_2SO$, δ, ppm, (*J*, Hz): δ = 5.44 (1H, s, CH); 7.30 (2H, d, ^3J = 8.4,

$H^{2,6}C_6H_4$); 7.51 (2H, d, ^3J = 8.4, $H^{3,5}C_6H_4$); 10.51 (1H, s, NH); 11.91 (1H, s, NHC(O)). ^{13}C NMR (100 MHz, $(CD_3)_2SO$,) δ = 63.2 (CH Hydantoin), 128.5, 128.8 (C-2, C-6, C-3, C-5, C_6H_4Cl), 133.1, 133.4 (C-1, C-4, C_6H_4Cl), 174.3 (C=O), 182.9 (C=S). Mass spectrum, *m/z*, (I_{rel}%): 229 $[M+H]^+$ (34), 227 $[M+H]^+$ (100). Anal. Calcd. for $C_9H_7ClN_2OS$ in %: C 40.53, H 2.65 , N 10.50. Found: C 40.46 , H 2.87, N 10.25 .

5-(4'-Fluorophenyl)-2-thioxoimidazolidin-4-one (1d)

A mixture of 4-fluorophenylglyoxal hydrate (164 mg, 0.962 mmol), thiourea (92 mg, 1.202 mmol) and AcOH (9 mL) was stirred at 19°C for 10 min, maintained 18-19°C for 111 h, then the solvent was evaporated under vacuum 4 Torr at 15°C, the residue was washed by cold water (5 ml), dried under vacuum 4 Torr at 16°C, yielding (181 mg, 89%) 5-(4'-fluorophenyl)-2-thioxoimidazolidin-4-one (**1d)**, white crystals, m.p. 169 – 171°C (with decomp.).^{1}H NMR spectrum, 400 MHz, $(CD_3)_2SO$, δ, ppm, (*J*, Hz): δ = 5.42 (1H, s, CH); 7.24 – 7.29 (2H, m, $H^{2,6}C_6H_4F$); 7.29 – 7.34 (2H, m, C_6H_4F); 10.49 (1H, s, NH); 11.88 (1H, s, NHC(O)). ^{13}C NMR (100 MHz, $(CD_3)_2SO$, (*J*, Hz)) δ = 63.15 (CH Hydantoin); 115.59 and 115.81, d, ^{C-F}J = 22 (C-3, C-5, C_6H_4F); 128.72 and 128.81, d, ^{C-F}J = 9 (C-2, C-6 C_6H_4F); 130.65 (C-1, C_6H_4F); 160.73 and 163.17, d, ^{C-F}J = 244 (C-4, C_6H_4F); 174.56 (C=O), 182.76 (C=S). Mass spectrum, *m/z*, (I_{rel}%): 211 $[M+H]^+$ (100), 166(14), 152 (16), 124 (64), 95 (14). Anal. Calcd. for $C_9H_7FN_2OS$: C 51.42, H 3.36 , N 13.33. Found: C 51.36, H 3.24, N 13.45.

5-(4'-Nitrophenyl)-2-thioxoimidazolidin-4-one (1e)

A mixture of 4-nitrophenylglyoxal hydrate (146 mg, 1.463 mmol), thiourea (71 mg, 0.928 mmol) and AcOH (6 mL) was stirred at 15°C for 10 min, maintained 18-19°C for 161 h, then the solvent was evaporated under vacuum 4 Torr at 25-30°C, the residue was washed by cold water (8 ml), dried under vacuum 4 Torr at 16°C, yielding (163 mg, 92%) 5-(4'-nitrophenyl)-2-thioxoimidazolidin-4-one (**1e)**, yellow crystals, m.decomp. 245 – 246°C (THF – PhH – C_6H_{14}).^{1}H NMR spectrum, 400 MHz, $(CD_3)_2SO$, δ, ppm, (*J*, Hz): δ = 5.66 (1H, s, CH); 7.58 (2H, d, ^3J = 8.4, $H^{2,6}C_6H_4$); 8.30 (2H, d, ^3J = 8.4 $H^{3,5}C_6H_4$); 10.64 (1H, s, NH); 12.03 (1H, s, NHC(O)). Mass spectrum, *m/z*, (I_{rel}%): 238 $[M+H]^+$ (40), 222 (11), 91 (100).). Anal. Calcd. for $C_9H_7N_3O_3S$: C 45.57, H 2.97, N 17.71. Found: C 45.22, H 3.12, N 17.43.

5-(4'-Methylphenyl)-2-thioxoimidazolidin-4-one (1f)

A mixture of 4-methylphenylglyoxal hydrate (256 mg, 1.542 mmol), thiourea (147 mg, 1.928 mmol) and AcOH (14 mL) was stirred at 15°C for 15 min, maintained 20°C for 65 h, then the solvent was evaporated under vacuum 4 Torr at 25-30°C, the residue was washed by cold water (11 ml), dried under vacuum 4 Torr at 15°C, yielding (310 mg, 97%) 5-(4'-methylphenyl)-2-thioxoimidazolidin-4-one 1f, white crystals, m.p. 226 – 228°C (with decomp.).^{1}H NMR spectrum, 400 MHz, $(CD_3)_2SO$, δ, ppm, (*J*, Hz): δ = 2.31 (3H, s, Me); 5.33 (1H, s, CH); 7.15 (2H, d, ^3J = 8.0, $H^{2,6}C_6H_4$); 7.23 (2H, d, ^3J = 8.0, $H^{3,5}C_6H_4$); 10.43 (1H, s, NH); 11.80 (1H, s, NHC(O)). Mass spectrum, *m/z*, (I_{rel}%): 207 $[M+H]^+$ (90), 119 (100). Anal. Calcd. for $C_{10}H_{10}N_2OS$ in %: C 58.23, H 4.89 , N 13.58. Found: C 58.35. , H 5.11, N .13.46.

5-(4'-Methoxylphenyl)-2-thioxoimidazolidin-4-one (1g).

A mixture of 4-methoxyphenylglyoxal hydrate (259 mg, 1.421 mmol), thiourea (119 mg, 1.563 mmol) and AcOH (14 mL) was stirred at 21– 23°C for 1 h, maintained at 19°C for 47 h, then the solvent was evaporated under vacuum 3 Torr at 20°C. The residue was extracted by CH_2Cl_2 (15 mL), the white precipitate was filtered off, washed by water (5 mL), dried under vacuum 4 Torr yielding (103 mg, 32.7%) 5-(4'-methoxylphenyl)-2-thioxoimidazolidin-4-one (**1g)**, white crystals, mp. 220 – 221°C (with decomp). ^{1}H NMR spectrum (400 MHz, $(CD_3)_2SO$, δ, ppm, (*J*, Hz): δ = 3.75 (3H, s, OMe); 5.32 (1H, s, CH); 6.98 (2H, d, ^3J = 8.4, $H^{3,5}C_6H_4$); 7.18 (2H, d, ^3J = 8.4, $H^{2,6}C_6H_4$); 10.43 (1H, s, NH); 11.80 (1H, s, NHC(O)). ^{13}C NMR (100 MHz, $(CD_3)_2SO$,) δ = 55.2 (OMe), 63.5 (CH Hydantoin), 114.2 (C-3, C-5 , C_6H_4O), 126.3 (C-1, C_6H_4O), 128.0 (C-2, C-6, C_6H_4O), 159.3 (C-4, C_6H_4O), 175.0 (C=O), 182.6 (C=S). Mass spectrum, *m/z*, (I_{rel}%): 223 $[M+H]^+$ (100). Anal. Cald. for $C_{10}H_{10}N_2O_2S$ in %: C 54.04, H 4.53, N 12.60. Found: C 53.86, H 4.82, N 12.35. To CH_2Cl_2-extract C_6H_{14} (10 ml) was added, the precipitated viscous white oil was isolated, dried under vacuum 3 Torr, after storing at 4°C crystallized additionally yielding (123 mg, 38.8%) thiohydantoin **1g**.

RESULTS AND DISCUSSION

We have found that arylglyoxals hydrates reacted with thiourea in acetic acid solution at room temperatures range 17 – 23°C selectively yielding 5-aryl-2-thioxoimidazolidin-4-ones (**1a–1g**), respectively (Scheme 5). The reaction readily occurs under mild conditions in the absence of heating, microwave irradiation or presence of strong acids.

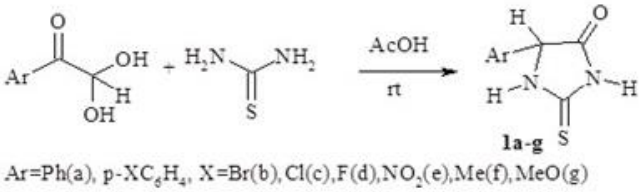

Scheme 5.

Evidently, this reaction occurs in three stage (Scheme 6) by analogy arylglyoxals reaction with N-hydroxyurea and N-alkoxyureas.[7,8] Acetic acid as prevents alternative thiazolidines formation[2] as promotes the third stage of this reaction (Scheme 6). It was regarded[2] that the lone pair electron on the sulfur atom of the thiourea would combine with the acidic proton of acetic acid and the nucleophilic affinity of the sulfur atom would be reduced with acetic acid as the solvent[2]. Thus at first stage thiourea reacts with arylglyoxal by the nitrogen atom yielding substituted thiourea **10,** which cyclizes in 5-aryl-4,5-dihydroxyimidazolidin-2-thione (**11)** at the second stage. Then intermediate **11** is protonated by acetic acid on the

oxygen atom of 5-HO group at the third stage. Further, the water molecule elimination yields "benzylic" cation **11B**, which by 1,2-hydride shift and the proton elimination transforms in thiohydantoin **1**.

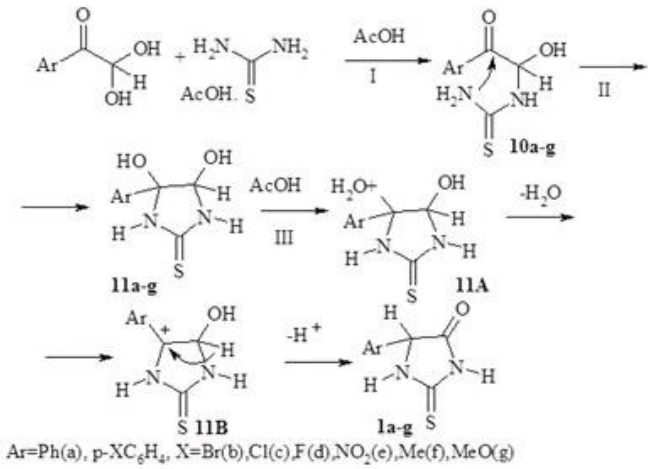

Scheme 6.

It was found that the yields of 5-aryl-2-thioxoimidazolidin-4-ones (**1a–1g)** became sufficient after 1–4 days maintaining of the reaction mixture at room temperature. The structure of obtained **1a–1g** was proved by the data of ^{1}H and ^{13}CNMR and mass spectra. In ^{1}H NMR spectra in 5-aryl-2-thiohydantoins (**1a-1g)** "benzylic" C-H chemical shift lies within the range 5.32 – 5.66 ppm, N^{1}H shift lies over the range 10.43 – 10.51 ppm, N^{3}HC(O) shift lies within the range 11.80 – 12.03 ppm. In their ^{13}CNMR spectra hydantoin "benzylic" C(H) carbon shift lies within the range 63.2 – 63.8 ppm, C=O carbon shift lies over the range 174.3– 175.0 ppm, C=S carbon shift lies within the range 182.6 – 182.9 ppm.

Conclusion

A new improved synthesis of 5-aryl-2-thioxoimidazolidin-4-ones (5-aryl-2-thiohydantoins) by interaction of arylglyoxals hydrates with thiourea in media of acetic acid at room temperature has been developed.

Acknowledgement

This work was supported by Department of Education and Science of Ukraine (grants no 0115U003159 and 0116U001722).

References

[1]Schubert, M.P. *J. Biol. Chem.*,**1935**, *111(3)*, 671-678.

[2]Cai, Qun, Jia, Feng-Cheng, Li, Deng-Kui, Xu, Gheng, Ding, Ke-Rong, Wu, An-Xin,*Tetrahedron*, **2015**, *71*(36), 6104 – 6111.https://doi.org/10.1016/j.tet.2015.06.104

[3]Paul, S., Gupta, M., Gupta, R.,Loupy, A.,*Synthesis*, **2002(1),** 75 – 78. https://doi.org/10.1055/s-2002-19308

[4]Eftekhari-Sis, B.,Zirak, M., Akrabi, A.,*Chem. Rev.*, **2013**, *113*, 2958 – 3043. https://doi.org/10.1021/cr300176g

[5]Muccioli, G.G.,Wouters, J.,Charlier, C., Scriba, G.K.E., Pizza, T., Di Place, P., De Martino, P.,Poppitz, W.,Poupaert, J.H., Lambert, D.M.,*J. Med. Chem.*, **2006**, *49(3)*, 872 – 882.https://doi.org/10.1021/jm050484f

[6]Joshi, K.C., Pathak, V., Goyal, M.K.,*J. Heterocycl. Chem.*, **1981**, *18*, 1651 – 1653.https://doi.org/10.1002/jhet.5570180836

[7]Shtamburg, V.G.,; Anishchenko, A.A.,Shtamburg, V.V.,Shishkin, O.V.;Zubatyuk, R.I.,Mazepa, A.V.,Rakipov, I.M.,Kostyanovsky, R.G., *MendeleevCommun*., **2008**, *18*(2), 102 – 104.https://doi.org/10.1016/j.mencom.2008.03.018

[8]Shtamburg, V.G.,Shtamburg, V.V.,Anishchenko, A.A.,Zubatyuk, R.I.,Mazepa, A.V.,Klots, E.A., Kravchenko, S.V.,Kostyanovsky, R.G.,*Chem. Heterocycl. Comp.*, **2015**, *51(6)*, 553 – 559.https://doi.org/10.1007/s10593-015-1735-0

[9]Hough, T.L.; Hough, I.R.; Pannell, R.W. *J. Heterocycl.Chem.*, **1986**, *23(4)*, 1125–1130. https://doi.org/10.1002/jhet.5570230433

Received: 10.05.2017.
Accepted: 17.06.2017.

HYDROGEN BOND BETWEEN HALOFORMS AND CHLORIDES OF SILICON AND GERMANIUM IN LOW - TEMPERATURE FILMS

I. I. Grinvald,[a] I. Yu. Kalagaev,[a] A. V. Vorotyntsev,[a] A. N. Petukhov[a] A. I. Grushevskaya[a] R. V. Kapustin[a] and I. V. Vorotyntsev[a]

Keywords: FTIR spectroscopy; low temperatures; hydrogen bond; haloforms; silicon; germanium tetrachloride; trichlorosilane.

The FTIR study allowed to reveal that a hydrogen bond can arise in low - temperature films at 20K between chloroform, bromoform and tetrachlorides of silicon and germanium, as well as a dihydrogen bond between chloroform and trichlorosilane. The general scheme of molecular interaction was simulated by *ab initio* calculation in terms of the DFT method. It was shown that the hydrogen atom of methane halides bound with the negatively charged chlorine atom of silicon or germanium tetrachloride, accompanied by transformation of their geometry from molecular symmetry $\mathbf{T_d}$ to $\mathbf{C_{3v}}$.

* Corresponding Authors
Fax: +7 (831) 436 0351
E-Mail: grinwald@mts-nn.ru
[a] R. E. Alekseev Nizhny Novgorod State Technical University, 24 Minin street, 603950 Nizhny Novgorod, Russian Federation.

Introduction

There is a big number of experimental and theoretical works devoted to different aspects of the hydrogen bond IR manifestation in the condensed phase (see for example[1-3]). However, most of them consider the interaction in solution of binary systems. The investigation in solid state relates basically either to the arising of a hydrogen bond in molecular crystals or the matrix isolated at low temperatures unstable species.[4-6] At the same time, the complex formation of the hydrogen bond in homogeneous low-temperature films remained beyond attention. Meanwhile, similar films can simulate the structure of many intermediates arising in chemical reactions. It seems that for the study of this problem the low-temperature IR study of frozen mixture, containing interacted components, is a perspective approach.

The haloforms (trichloro- and tribromomethane) are typical proton donors at hydrogen bond formation with suitable proton acceptors.[7-9] The silicon and germanium chlorides have a strong charge separation on the bond between the central element and the halogen atom. That can lead to the hydrogen bond formation between the negatively charged center (halogen atom) of Si- and Ge-halides and the positively charged hydrogen atom of haloforms.[10] On the other hand, we might expect the arising of the hydrogen bond between $SiHCl_3$ and haloforms owing the interaction of oppositely charged hydrogen atoms in these compounds.[11] However, mentioned types of hydrogen bond were not studied up to date.

In the recent paper, we have presented the IR findings for hydrogen bonded structures in low-temperature films, containing binary mixtures of trichloromethane or tribromomethane with tetrachlorosilane, tetrachlorogermane or trichlorosilane in the 20-200K interval. *Ab initio* calculation of the modeled complexes in terms of density functional theory (DFT) was carried out as well.

Experimental

For the preparation of the low-temperature films, the closed cycle optical refrigerator Displex CSE-202A (Advanced Research System Co. Inc.) with the equipment for depositing of liquid samples vapor on the cooled optical window was used. The operating procedure includes the following steps:

-The refrigerator was vacuumed up to about 10^{-6} Pa and the films of haloform ($CHCl_3$, $CDCl_3$ and $CHBr_3$) were deposited on a cooled optical window (NaCl).

-The samples of silicone or germanium chlorides were injected from a sealed volume, connected to the refrigerator, and deposited on the cooled haloform films.

-The ratio of components was chosen in such a way that the obtained sample had a minimal background and optimal absorption in the recorded spectral interval.

-The film was heated up to 150 K. The optical window was cooled after heating up to 20 K again.

This procedure was repeated 3 times to exclude the IR manifestation of non-equilibrium species. The refrigerator was placed in a spectrometer and the IR spectra were recorded in the 3600 – 2000 cm^{-1} range. The purity of samples was controlled by chromato-mass spectrometer GCMS - QP2010 Plus (Shimadzu Co. Inc.) with a vacuum samples inlet system (Valco Instruments Co. Inc.) and was not less 99 %.

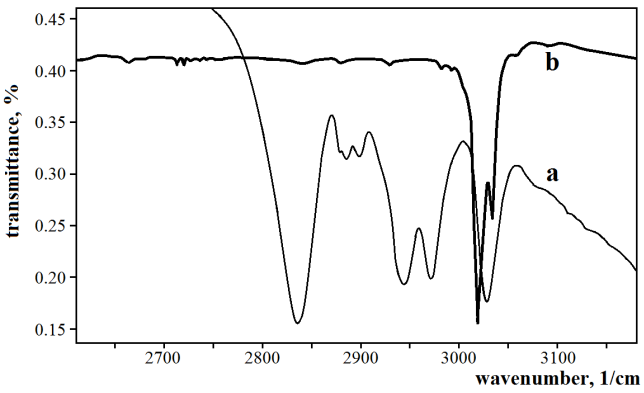

Figure 1a. The spectra of $SiCl_4/CHCl_3$ film at 20 K (a) and pure $CHCl_3$ film at 20K (b)

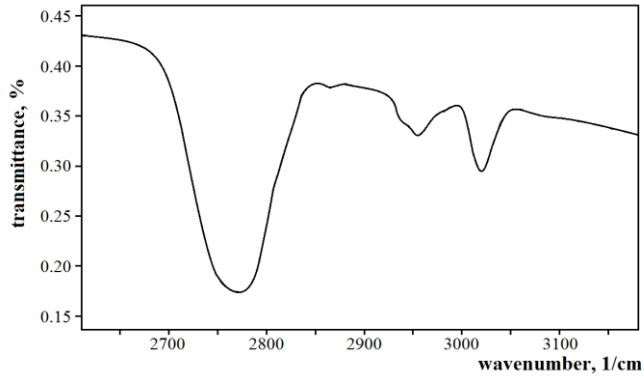

Figure 1b. The spectrum of $GeCl_4/CHCl_3$ film at 20K.

In the spectra of films $CHCl_3/GeCl_4$ recorded at the same conditions the new bands at 2954 cm^{-1} (strong band) and 2772 cm^{-1} (weak band) were detected (Figure 1b).

The band at 3023 cm^{-1} in both cases belongs to CH stretching of non-bonded chloroform. These bands remained in the spectra at film heating up to 200 K, i.e. the temperature of film destruction. Besides, the spectra did not change at reversible heating of films up to 150 K and cooling to 20 K.

In the spectra of tetrachloride films deposited on the deuterated chloroform, the new bands having the expected isotopic shift were shown (Figure 2a and b). Therefore the mentioned above new bands in the spectra of $SiCl_4/CHCl_3$ and $GeCl_4/CHCl_3$ films were assigned to the manifestation of hydrogen bond arising between haloforms and tetrachlorides.

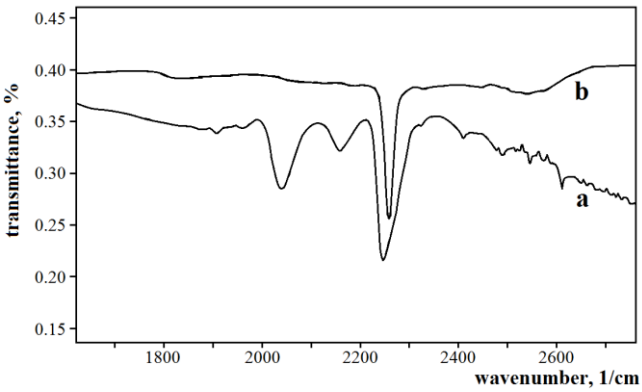

Figure 2a. The spectra of $SiCl_4/CDCl_3$ film at 20K (a) and pure CDCl3 film at 20K (b)

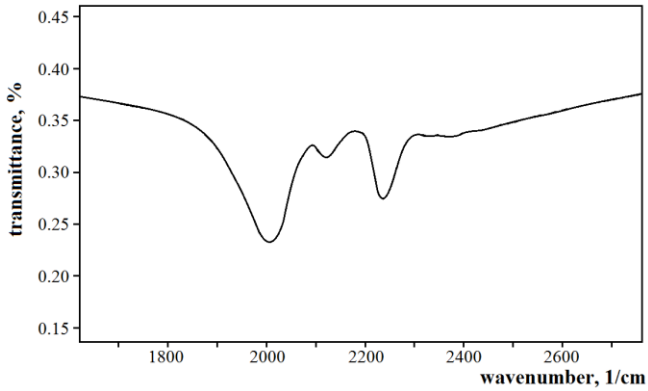

Figure 2b. The spectrum of $GeCl_4/CDCl_3$ film at 20K.

In the case of $CHBr_3/SiCl_4$ film the typical spectral picture of hydrogen bond was observed: along with the CH stretching band of non-bonded bromoform at 3013 cm^{-1} the wide band shifted to the lower frequencies ("red shift"[2]) relative to the CH stretching at 2871 cm^{-1} was found (Figure 3a). For films $CHBr_3/GeCl_4$ the similar IR manifestation of hydrogen bond was revealed, but the weak band at 2691 cm^{-1} could be seen additionally (Figure 3b). As well as for $CHCl_3$ films the appearing bands remain in the spectra at reversible heating 20-150-20K. The band at 3013 cm^{-1}

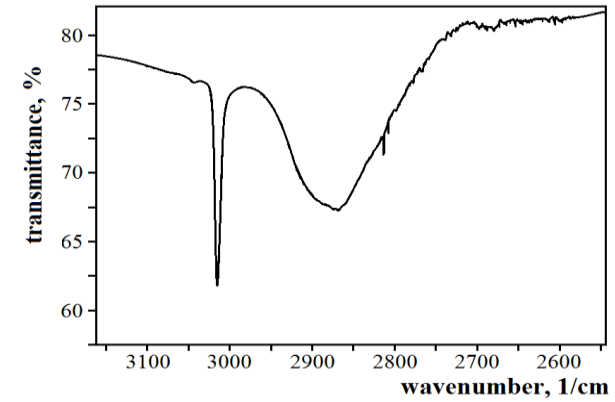

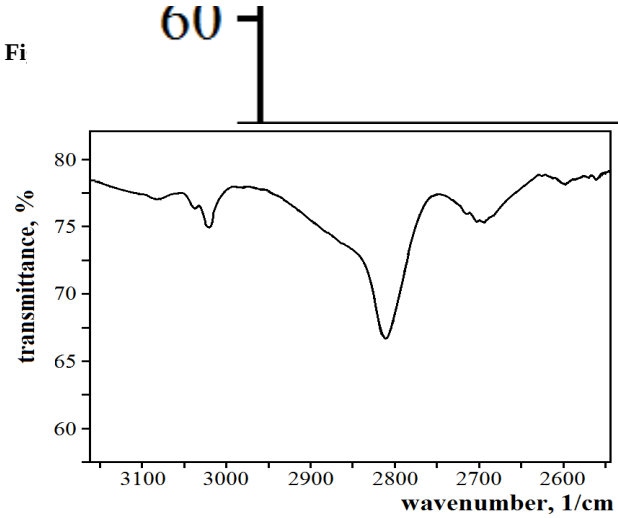

Figure 3b. The spectrum of $GeCl_4/CHBr_3$ film at 20K.

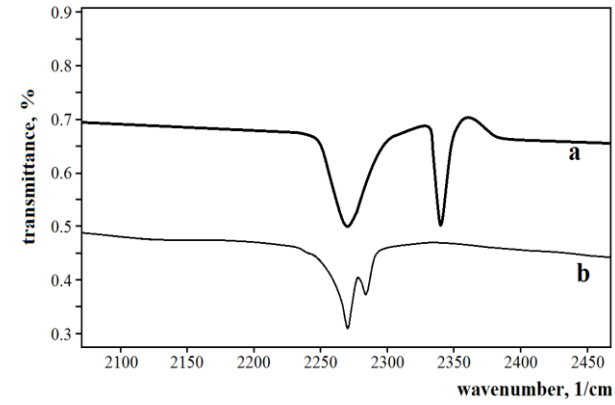

Figure 4. The spectra of $SiHCl_3/CHCl_3$ film at 20K (a) and pure $SiHCl_3$ film at 20K (b).

The arising of the hydrogen bond in the $SiHCl_3/CHCl_3$ film causes another display in IR spectra of films deposited at 20 K (Figure 4). The new band at 2341 cm^{-1} locates close to the SiH stretching vibration in pure $SiHCl_3$ (2271 cm^{-1}) and has a "blue shift"[2] relatives to this one. In the case of interaction between tetrachlorides and haloforms, the hydrogen bond can exist between negatively charged chlorine atom of tetrachloride and the positively charged hydrogen atom of haloforms only.

The trichlorosilane has at least two acceptor centers for the hydrogen atom of the chloroform binding: the chlorine atom and the negatively charged hydrogen atom of trichlorosilane.[10] The position of the new band and its shift relative to SiH stretching corresponds to the mixed ($CH^{\delta+}\cdots{}^{\delta-}HSi$) stretching vibration of the dihydrogen bond.[2]

DFT study

Ab initio calculation was carried out in terms of density functional theory (DFT),[12] realized in the computer program GAUSSIAN 09.[13] The main molecular characteristics were obtained using the B3LYP functional and the 6-311++G(2d,2p) basis set.[14] The DFT calculation for the interacting molecules in the condensed phase should be taken as an approximate model only, in the first regard, because a single electron approximation is not suitable for similar systems.[14] Therefore the quantitative agreement between the calculated and experimental data can hardly be expected. It is particularly true for the theoretically predicted geometry and electronic parameters as well as for the vibration frequencies of hydrogen bonded complexes to be investigated. Hopefully, this calculation allows imagining the general scheme of hydrogen bond formation in low-temperature films.

The computational procedure predicts the light transition of tetrachlorides geometry from $\mathbf{T_d}$ molecular symmetry to C_{3v} shape. This transformation needs energy less than 12.5 kJ mol^{-1}. Therefore the most stable state of intermediates in the case of tetrachlorides and haloforms interaction corresponds to the structure, presented in Figure 5a

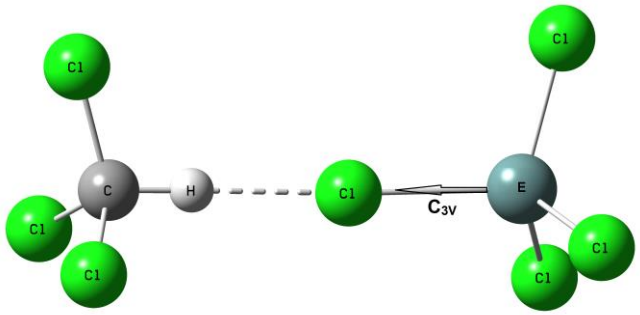

Figure 5a. The calculated geometry and charges of atoms for tetraclorides (E=Si or Ge) - chloroform complexes.

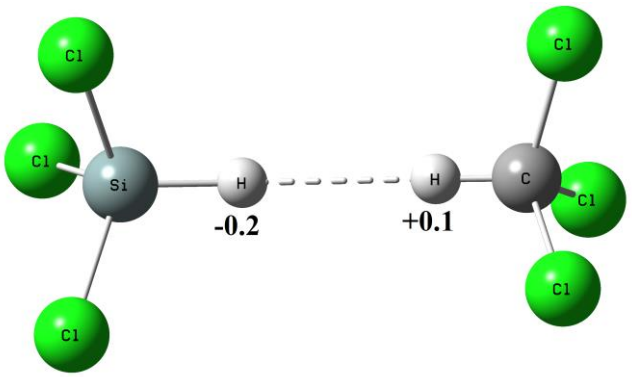

Figure 5b The calculated geometry and charges of atoms for trichlorosilane – chloroform hydrogen bonded complex.

In the case of $SiHCl_3/CHCl_3$ system the hydrogen bond forms between oppositely charged hydrogen atoms of components. The structure of this complex, as well as the charges of the interacting hydrogen atoms, are shown in Figure 5b.

On the whole FTIR and DFT study confirm the arising of a hydrogen bond between haloforms and chlorides of silicon and germanium. The DFT calculation predicts a linear geometry of molecular coordination. The halogen atom of tetrachloride or hydrogen atom of trichlorosilane locates on the $\mathbf{C_{3v}}$ axis of complexes. The few bands, which were revealed in low-temperature films of investigated species, can be considered as the manifestation of less stable hydrogen-bonded structures with another geometry.

References

[1]*The Hydrogen Bond. Recent Developments in Theory and Experiments*. Eds. Schuster, P., Zundel, G., Sandorfy, C., Volume 2, North-Holland, **1976**.

[2]Bakhmutov, V. I., *Dihydrogen Bonds*, John Wiley & Sons, **2008**.

[3]Iogansen, A. V., *Spectrochimica Acta*, **1999A**, *55*, 1585. DOI: 10.1016/S1386-1425(98)00348-5

[4]Gavezotti, A., *Molecular Aggregation: Structure Analysis and Molecular Simulation of Crystals and Liquids*, Oxford University Press, **2009**.

[5]Cradock, S., Hinchcliffe, A. J., *Matrix Isolation: A Technique for the Study of Reactive Inorganic Species*, Cambridge University Press, **1975**.

[6]Baev, A. K., *Specific Intermolecular Interactions of Organic Compounds*, Springer-Verlag, **2012**.

[7]Chandra, A. K., Zeegers-Huyskens, Th., *J. Phys. Chem.*, **2005A**, *109*, 12006. DOI: 10.1021/jp054123n

[8]Favero, L. B., Giuliano, B. M., Melandri, S., Maris, A., Ottaviani, P., Velino, B., Caminati, W., *J. Phys. Chem.*, **2005A**, *109*, 7402. DOI: 10.1021/jp0527599

[9]Kalagaev, I. Yu., Grinvald, I. I., *Pure Appl. Chem.*, **2013**, *85*, 135. DOI: https://doi.org/10.1351/PAC-CON-12-03-06

[10]Grinvald, I., Kalagaev, I., Vorotyntsev, A., Sutyagina, E., *J. Mater. Sci. Eng.*, **2013A**, *3*, 274.

[11]Grinvald, I. I., Kalagaev, I. Yu., Vorotyntsev, A. V., Vorotyntsev, I. V., Sutyagina, E. A. Spirin, I. A., *J. Mater. Sci. Eng.*, **2013A**, *3*, 554.

[12]Parr, R. G., Yang, W., *Density Functional Theory of Atoms and Molecules*, Oxford University Press, **1995**.

[13]Frisch, M. J., Trucks, G. W., Schlegel, H. B., Scuseria, G. E., Robb, M. A., Cheeseman, J. R., Scalmani, G., Barone, V., Mennucci, B., Petersson, G. A., Nakatsuji, H., Caricato, M., Hratchian, X. Li, H. P., Izmaylov, A. F., Bloino, J., Zheng, R., Sonnenberg, G., Hada, J. L., Ehara, M., Toyota, K., Fukuda, R., Hasegawa, J., Ishida, M., Nakajima, T., Honda, Y., Kitao, O., Nakai, H., Vreven, T., Montgomery, J. A. Jr., Peralta, J. E., Ogliaro, F., Bearpark, M., Heyd, J. J., Brothers, E., Kudin, K. N., Staroverov, V. N., Kobayashi, R., Normand, J., Raghavachari, K., Rendell, A., Burant, J. C., Iyengar, S. S., Tomasi, J., Cossi, M., Rega, N., Millam, J. M., Klene, M., Knox, J. E., Cross, J. B., Bakken, V., Adamo, C., Jaramillo, J., Gomperts, R., Stratmann, R. E., Yazyev, O., Austin, A. J., Cammi, R., Pomelli, C., Ochterski, J. W., Martin, R. L., Morokuma, K., Zakrzewski, V. G., Voth, G. A., Salvador, P., Dannenberg, J. J., Dapprich, S., Daniels, A. D., Farkas, Ö., Foresman, J. B., Ortiz, J. V., Cioslowski, J., Fox, D. J., *Gaussian 09, Revision E.01*, Gaussian, Inc., **2009**.

[14]Baranovsky, V. I., *Quantum Mechanics and Quantum Chemistry*, Academy, **2008**.

Received: 29.04.2017.
Accepted: 19.06.2017.